Characterization of Prothoracic Neck Motor Neurons in the Blowfly *Calliphora vicina*

Isabella Katharina Kauer

Dissertation der Fakultät für Biologie
der Ludwig-Maximilians-Universität München

Angefertigt am Max-Planck-Institut für Neurobiologie

vorgelegt von
Isabella Katharina Kauer

München, den 05.09.2016

Erstgutachter: Prof. Dr. Alexander Borst

Zweitgutachter: Prof. Dr. Rainer Uhl

Tag der Abgabe: 05. 09. 2016

Tag der mündlichen Prüfung: 07. 12. 2016

Table of contents

Table of figures

List of abbreviations

ADN	Anterior dorsal nerve
ADNMN	Anterior dorsal nerve motor neuron
cHIN	Contralateral haltere interneuron
CC	Cervical connective
CN	Cervical nerve
CNMN	Cervical nerve motor neuron
DN	Descending neuron
DNOVS	Descending neuron of the ocellar and vertical system
FN	Frontal nerve
FNMN	Frontal nerve motor neuron
H1	Horizontal 1
H2	Horizontal 2
HN	Haltere nerve
HS	Horizontal system
HSE	Horizontal system equatorial
HSN	Horizontal system rorthern
HSS	Horizontal system southern
LPTC	Lobula plate tangential cell
NMN	Neck motor neuron
PN	Prosternal nerve
SOG	Suboesophageal ganglion
V2	Vertical 2
VCN	Ventral cervical nerve
VCNMN	Ventral cervical nerve motor neuron
VS	Vertical system
WN	Wing nerve

In previous studies, neck motor neurons are called "(X)NM" (see *Strausfeld et al. 1987*) or "(X)N NMN" (*Huston and Krapp 2008*). In the present account they are named "(X)NMN" but when referring to the previous literature, the respective original nomenclature is kept.

Summary

Blowflies rely heavily on optic flow for visual orientation and course stabilization. The optic flow perceived during flight triggers an optomotor response of the head in order to keep the visual image of the environment stable on the retina. Visual motion information is processed by large tangential cells in the lobula plate of the fly optic lobe (lobula plate tangential cells, LPTCs), motor action of the head is carried out by 21 pairs of neck muscles innervated by four paired neck nerves (ventral cervical nerve, VCN; cervical nerve, CN; anterior dorsal nerve, ADN; frontal nerve, FN) housing 21 pairs of neck motor neurons. The LPTCs convey visual information directly onto the neck motor neurons of the VCN and CN, which originate from the brain, and indirectly via descending neurons onto the neck motor neurons of the ADN and FN, which originate from the prothoracic ganglion.

Although the patterns of connectivity between LPTCs and neck motor neurons of the VCN and CN have already been studied successfully, it is still unclear which LPTCs provide visual input to the two nerves originating from the thorax, the ADN and FN. The aim of the present study was to functionally characterize the prothoracic neck motor neurons of the ADN and FN and compare their sensitivity for visual motion with the motion sensitivity of well-known LPTCs. Functionally bringing together direction selective lobula plate tangential cells and neck motor neurons that steer muscles to execute movements in response to visual input will enable us to discuss the role of LPTC motion tuning in visually guided head turning behavior.

The first part of the results reports the characterization of ADN motor neurons by means of extracellular nerve suction recording and simultaneous intracellular recording from single LPTCs. The motion tuning of the motor neurons was measured and compared with the motion tuning of particular LPTCs. In addition, dual recordings involving current injections into LPTCs were carried out to check for synaptic connectivity with ADN motor neurons. The second part of the results describes the characterization of FN motor neurons by means of intracellular recording from single motor neurons and simultaneous injection of Neurobiotin into the recorded cells. The motion tuning of the motor neurons was measured, while simultaneous dye filling of the cells allowed for their post-hoc anatomical reconstruction.

The motor neurons of both prothoracic neck nerves showed a clear preference for global over local optic flow and responded more vigorously to rotations than to translations, which is in line with the assumption that they need to extract rotational motion information for compensatory head movements. While the two motor neurons of the ADN were most strongly tuned to mainly horizontal rotations, the five described motor neurons of the FN were tuned to roll-like optic flow. The tuning to different optic flow fields optimally matches the pulling planes of the muscles they innervate. In ADN motor neurons no clear connection with LPTCs could be demonstrated by simultaneous recordings but striking similarities in receptive field size and structure with two cells of the horizontal system corroborate the hypothesis that they play a major role in forming the neck motor neuron response. Five different anatomical cell types were found in FN motor neuron stainings that could each be attributed a distinct motion tuning.

1. Introduction

1.1. Fly vision and gaze stabilization

Flies rely heavily on optic flow for visual orientation and gaze stabilization (*Frye and Dickinson 2001; Srinivasan and Zhang 2004*). When a fly moves, an image of its environment travels across its retina: this visual motion, induced by relative movement between the animal and its surrounding is termed optic flow. Each movement leads to a particular pattern of otic flow: a head turn to the left for example will lead to horizontal motion vectors pointing from left to right on both eyes, a clockwise head roll around the longitudinal axis will lead to motion vectors pointing downward on the left eye and pointing upward on the right eye. These distinctive patterns allow the animal to estimate its own movement.

Calliphora is well known for its aerobatic flight behavior: it moves through three-dimensional space at velocities up to 2.5 m/s and maximal turning rates in excess of 1700°/s (*Bomphrey et al. 2009*). Thus, a visual system is needed that can integrate fast changing information and compensate for body turns to keep vision of spatial detail stable and minimize motion blur. Optic flow elicits a compensatory turning response of the head, termed “optomotor response”, which aims at maintaining a stable gaze by minimizing retinal image slip also when perturbations are present (*Hengstenberg 1991; Land 1999; Kern et al. 2006*). This head turning response is equivalent to eye movements, since flies cannot move their eyes independently of their body: the head is connected to the thorax by non-sclerotized structures that allow it to be moved by neck muscles (Figure 1). Maximum head turning amplitudes in *Calliphora* differ in regard to the axis of movement: yaw and pitch movements of the head can be executed at up to ±20°, while roll movements reach amplitudes of ±90° (*Hengstenberg 1984 and 1991; Hengstenberg et al. 1986*).

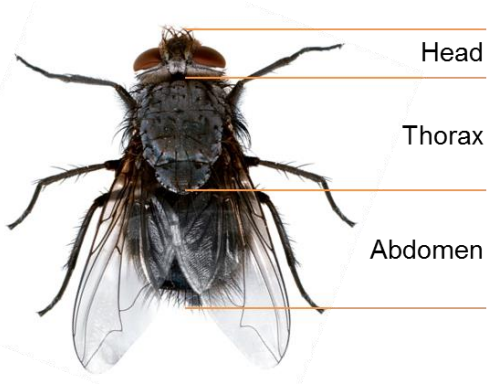

Figure 1: Anatomy of a dipteran fly. The body is divided into head, thorax and abdomen. The head is connected to the thorax by non-sclerotized structures.

Large parts of the fly brain are dedicated to vision. Visual signals are picked up by photoreceptors in the retina which is built of approximately 5000 ommatidia (*Hardie 1984*). Each ommatidium contains 8 photoreceptors (R1-R8) oriented along 7 different optical axes. Photoreceptors with parallel optical axes from neighboring ommatidia synapse onto the same postsynaptic cell, forming a so-called cartridge. This organization is called neural superposition. It leads to an increase in sensitivity without loss of acuity (*Kirschfeld 1967*).

Visual signals are further processed in a set of ganglia that are organized in retinotopic columnar arrays in the optic lobes: the lamina, the medulla and the lobula complex consisting of lobula and lobula plate (Figure 2). Output signals from photoreceptors R1-R6 are sent to the lamina, while R7 and R8 project to the medulla (*Hardie 1984*). In the lamina, the laminar monopolar cells L1 and L2 have been found to be necessary and sufficient for motion detection (*Rister et al. 2007*). In each lamina column R1–R6 synapse onto L1 and L2, building parallel processing pathways. The output signals of these two pathways converge on the dendrites of the lobula plate tangential cells (LPTCs) in the lobula plate via T4 and T5 cells. The large LPTCs are selective for motion in different directions (*Hausen 1982a,b; Hengstenberg 1982*). Recently, subpopulations of T4 and T5 cells have been found to be direction selective and to project to the four different layers in the lobula plate depending on their directional preference: T4/T5 cells responding to horizontal stimuli terminate in layer 1 (anterior) and layer 2, cells responding to vertical stimuli terminate in layer 3 and layer 4 (posterior) of the lobula plate (*Maisak et al. 2013*).

1.2. Lobula plate tangential cells

Visual motion signals are spatially integrated by the giant direction-selective LPTCs in the optic lobes of the fly brain (*Hausen 1982 and 1984; Hengstenberg 1982*). There are about 60 LPTCs in total (*Hausen 1984*), the anatomically most prominent being the ten cells of the vertical system (VS-cells) and the three cells of the horizontal system (HS-cells). They function as matched filters for particular optic flow fields generated during self-motion of the animal (*Krapp and Hengstenberg 1996; Krapp et al. 1998; Franz and Krapp 2000; Haag and Borst 2004*).

1.2.1. VS-cells

In each brain hemisphere, the ten cells of the vertical system extend their dorsal and ventral main dendrites along the dorsoventral axis in the posterior layer of the lobula plate, one next to the other (Figure 2, Figure 3 A). The VS-cells are numbered according to the location of their dendrite from VS1 (most lateral) to VS10 (most proximal). As reflected by the shape of their main dendrites bifurcating from the axon in opposite directions, they are sensitive to vertical motion, responding maximally to downward motion presented at a particular position in the visual field (Figure 3 C).

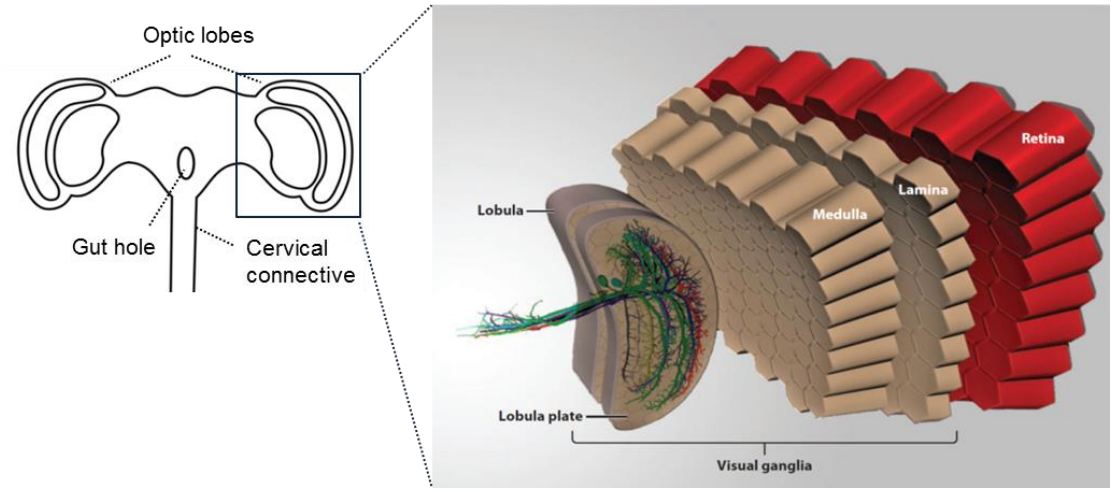

Figure 2: Schematic of the fly optic lobe. Visual signals are taken up by the retina and further processed in retinotopic layers of neuropil: the lamina, medulla and lobula complex, which consists of lobula and lobula plate. The lobula plate houses the giant LPTCs, which respond to visual motion in a direction selective manner. Here, the ten cells of the vertical system (VS-cells) are depicted. From *Borst, Haag and Reiff (2010)*.

They respond to motion with graded de- and hyperpolarizations of their membrane potential: in response to visual motion in their preferred direction (PD) they depolarize, while hyperpolarizing in response to visual motion in their anti-preferred or null direction (ND) (*Hengstenberg 1982*). Detailed mapping of their receptive fields using local small field stimuli and drawing an arrow at each tested location in visual space with the length corresponding to the response strength and the direction indicating the preferred direction of motion at that particular location, showed that their peak sensitivity is not for a pure upward or downward shift of the visual surround but rather composed of areas with different preferred directions (*Krapp et al. 1998*).

As a result, they resemble curled vector fields, which makes them ideal matched filters for different optic flow fields resulting from rotations of the fly around different body axes during certain flight maneuvers (**Figure 3 B**). Each VS-cell is optimally tuned to respond maximally to a rotation around a particular body axis (**Figure 3 B and C**). They are electrically coupled in a chain-like manner, so that the VS-cell network can linearly interpolate between output signals of single VS-cells for a robust representation of the axis of rotation (*Cuntz et al. 2007*).

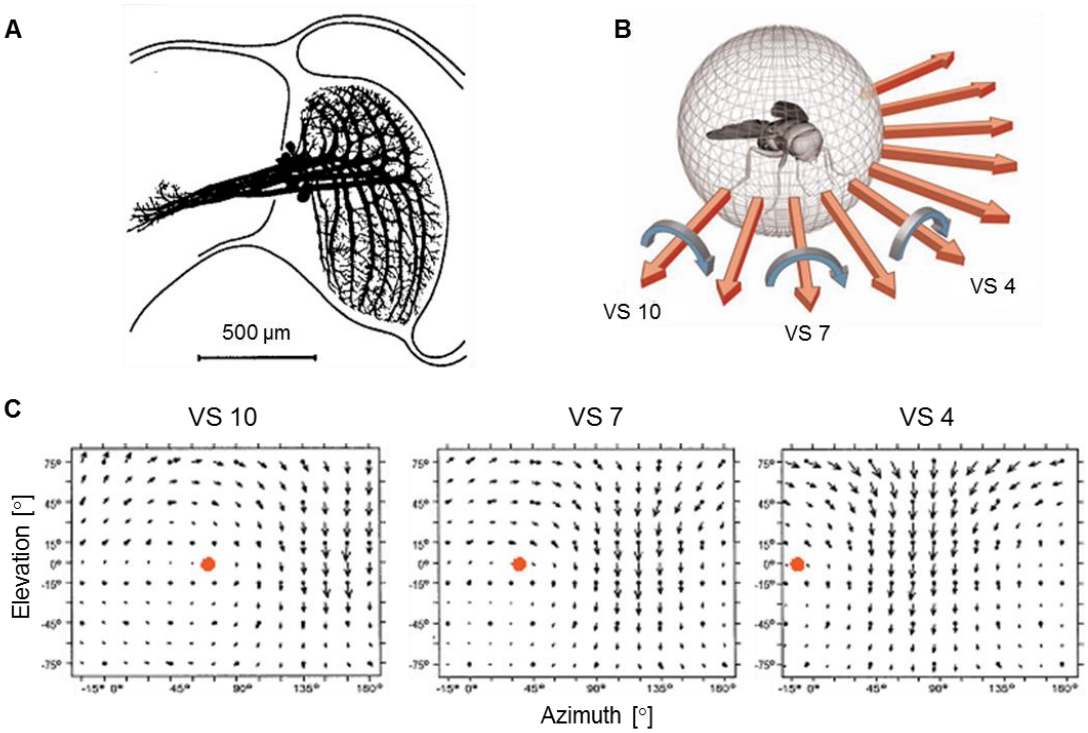

Figure 3: VS-cells. A: Position and anatomy of the VS-cells VS2 (most distal) to VS10 (most proximal) within the right lobula plate, obtained from cobalt fills. Their dendritic fields are vertically oriented stripes, stacked from the distal to the proximal margin of the lobula plate. Together they cover the whole extent of the lobula plate. **B**: A shematic fly with different axes of rotations indicated by the red arrows. The VS-cells work as matched filters for optic flow as generated by rotations around certain axes **C**: Receptive fields of the three example VS-cells from **B**, in the right brain hemisphere. Each receptive field corresponds to a particular axis of rotation as marked by the red dot. Modified from *Borst and Haag (2007).*

1.2.2. HS-cells

The three horizontally sensitive HS-cells of the lobula plate extend their dendritic fields across the northern (HSN), equatorial (HSE) and southern (HSS) part of the lobula plate (**Figure 4 A**). Accordingly, they are sensitive to motion in the dorsal, middle or ventral part of the visual field (*Hausen 1982a, 1982b; Krapp et al. 2001*).

They respond to their preferred stimulus, which is horizontal front-to-back motion in the ipsilateral visual field, with graded membrane potential depolarization (**Figure 4 B**). HSN is most sensitive to front-to-back motion in the dorsal part of the visual field, HSE in the middle and HSS in the ventral part of the visual field, which is reflected in their receptive field structure (**Figure 4 B**). When back-to-front motion stimuli are presented in front of the contralateral eye, EPSPs are generated in HSN and HSE that derive from synaptic coupling of these two cells with the H2 cell. The H2 cell is a spiking LPTC that projects across the midline and provides excitatory input from the contralateral hemisphere. Coupling of HSN and HSE with H2 thus broadens their receptive fields and makes them binocular (*Farrow et al. 2006*).

HSN and HSE project to the protocerebrum where they are electrically coupled to the motor neurons of the ventral cervical nerve (VCN), which are also tuned to horizontal optic flow (*Haag et al. 2010*). HSS is electrically coupled to a motor neuron of the contralateral cervical nerve (CN), which is tuned to vertical optic flow in the frontal visual field (Wertz et al. 2012).

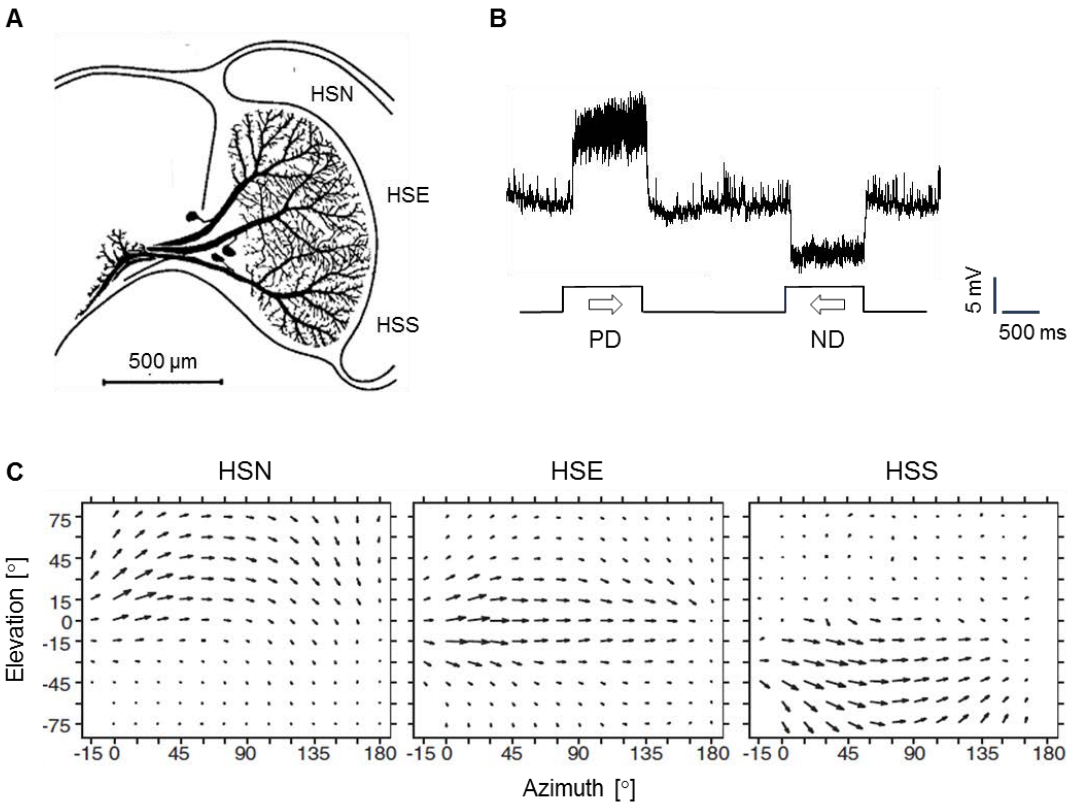

Figure 4: HS-cells. A: Position and anatomy of the three HS-cells within the right optic lobe, as obtained by cobalt staining. Together they cover the full extent of the lobula plate neuropil. Modified from *Hengstenberg (1982)*. **B:** Graded response of an HSE cell of the right side of the brain. A grating moving in the preferred direction (PD) of the cell depolarizes the membrane potential, while the response to a grating moving into the null direction (ND) of the cell is a hyperpolarization of its membrane potential. **C:** Receptive fields of the three HS-cells of the right side of the brain. All three of them are maximally sensitive to a front-to-back rotational optic flow in the part of the visual field that corresponds to their retinotopic position. Modified from *Taylor and Krapp (2007)*.

1.3. Neck motor neurons

The purpose of neck motor neurons is to steer muscles that turn the fly's head. The neck motor system plays a key role in gaze stabilization and controls compensatory head movements to keep the image of the environment stable on the fly's retina when its body rotates (*Hengstenberg 1991*). Thus, the motor system must be precisely informed about visual input in order to generate the appropriate compensatory output.

The VS- and HS-cells of the lobula plate represent the major output elements of the visual system. To generate an optomotor response or to actively track moving objects, they relay signals to the neck motor system. At the level of the neck motor neurons, visual information is combined with information from other sensory organs, *e.g.* the halteres monitoring angular velocity, the prosternal organs monitoring head position (*Milde et al. 1987; Preuss and Hengstenberg 1992*) and the ocelli detecting overall brightness (*Schuppe and Hengstenberg 1993; Krapp 2009*) for steering head position. The present study focuses on the visual components of the optomotor response: the direction-selective LPTCs of the lobula plate, descending neurons that convey their output onto prothoracic neck motor neurons, and the neck motor neurons themselves, innervating the muscles to steer the head.

The neck motor system consists of four paired neck nerves: the cervical nerve (CN), the ventral cervical nerve (VCN), the frontal nerve (FN) and the anterior dorsal nerve (ADN) (Figure 5 B and C). Together, they house 21 pairs of neck motor neurons, each innervating a single neck muscle, with the exception of one CN motor neuron branching to innervate two muscles (OH1 and OH2) and one muscle being supplied by two motor neurons from different nerves (TH2) (*Strausfeld et al. 1987*). As the LPTCs, all neck motor neurons are mirror symmetric on both sides of the nervous system.

The 21 paired motor neurons are divided into two groups: those with their cell bodies in the brain that receive direct synaptic input from LPTCs and originate from the brain (CN and VCN), and those with their cell bodies in the thoracic ganglion that receive LPTC input indirectly via descending neurons and emerge from prothoracic neuropil (ADN and FN) (*Sandeman and Markl 1980; Strausfeld et al. 1987; Haag et al. 2010; Wertz et al. 2012;* Figure 5 B and C).

Some neck motor neurons were found to be visually sensitive. They are tuned to panoramic optic flow that occurs when the fly rotates around particular body axes, similar to VS- and HS-cells. Their receptive fields and panoramic motion tuning are very similar to the tuning of LPTCs *(Huston and Krapp 2008; Haag et al. 2010; Wertz et al. 2012; Kauer et al. 2015). Huston and Krapp (2008)* postulated that the receptive fields of neck motor neurons are more binocular than those of LPTCs, enabling the system to distinguish more accurately between rotational and translational optic flow to govern compensatory head rotations.

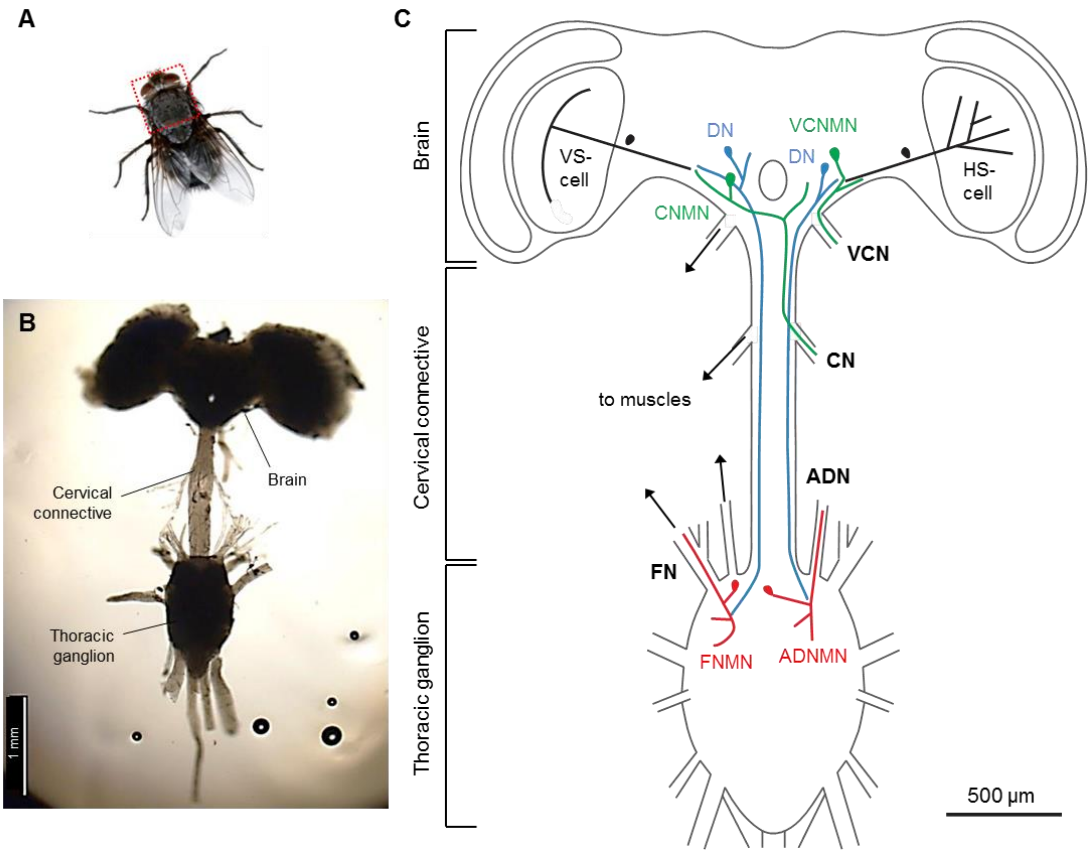

Figure 5: The neck motor system of *Calliphora*. **A:** A dorsal view of a fly, the red square indicating the extent of the nervous system shown in **B**. **B:** Light microscopic image of a *Calliphora vicina* nervous system showing brain, cervical connective and thoracic ganglion. Nerves emerging from the brain and cervical connective are neck nerves, nerves emerging from the thoracic part of the nervous system include neck, wing, leg and haltere nerves. **C:** Schematic drawing of the nervous system as depicted in **B**. HS-and VS-cells are the major output elements of the lobula plate. They relay signals to neck motor neurons that innervate muscles to control head movements. Motor neurons of the ventral cervical nerve (VCN) receive direct synaptic input from HS-cells, motor neurons of the cervical nerve (CN) are directly postsynaptic to VS-cells. Cervical nerve motor neurons (CNMNs) and ventral cervical nerve motor neurons (VCNMNs) have their cell bodies located in the brain, while frontal nerve motor neurons (FNMNs) and anterior dorsal nerve motor neurons (ADNMNs) have their cell bodies in the anterior part of the thoracic ganglion. Brain and thoracic ganglion are connected by the cervical connective that runs through the fly's neck. Descending interneurons from the brain (DNs) that project through the cervical connective integrate signals from LPTCs and relay them onto the prothoracic neck motor neurons of the frontal nerve (FN) and anterior dorsal nerve (ADN).

1.3.1. The cervical nerve (CN) and ventral cervical nerve (VCN)

From detailed anatomical dye-coupling experiments it is known that the CN and VCN are directly postsynaptic to LPTCs (*Strausfeld and Seyan 1985; Strausfeld et al. 1987*). The CN houses eight motor neuron axons which innervate muscles that are proposed to control head declination (pitch) according to their anatomical pulling planes (*Strausfeld et al. 1987*).

Functional coupling between LPTCs and CN motor neurons (CNMNs) has been found in a more recent study by *Wertz et al. (2012)*: The authors showed that a subset of CNMNs (CNMN6 and

CNMN7) receives direct synaptic input from VS- and HS-cells of both hemispheres via gap junctions, by passing current of both polarities between the LPTCs and the neck motor neurons (Figure 6). This can explain the binocular nature of their receptive fields as suggested by *Huston and Krapp (2008)*.

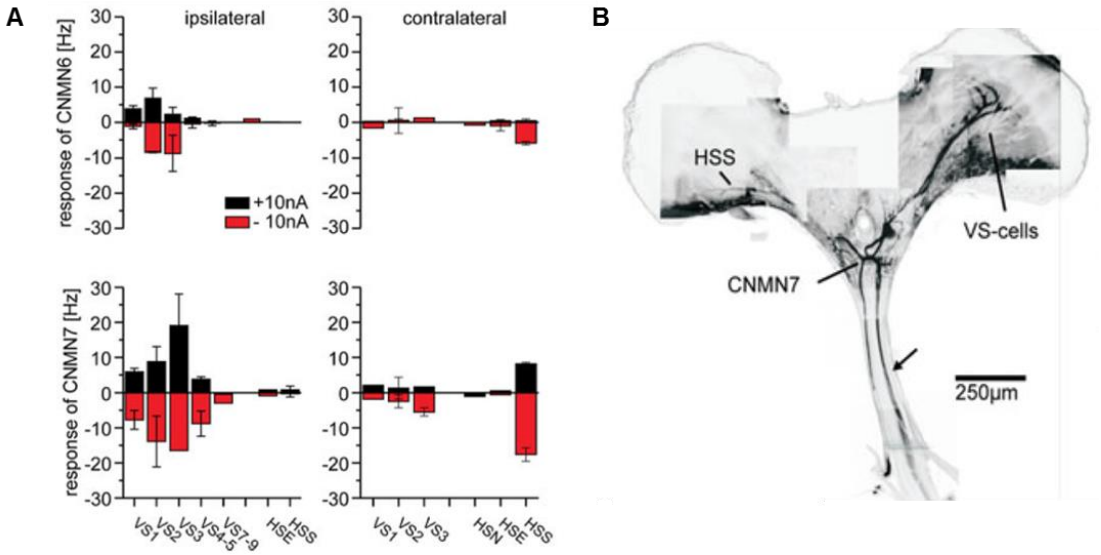

Figure 6: Connectivity between LPTCs and CNMNs. A: CNMN6 (upper panel) and CNMN7 (lower panel) were recorded intracellularly, while different LPTCs of both hemispheres were de- and hyperpolarized. Functional connection could be demonstrated between the two CNMNs and ipsilateral VS2 and VS3 as well as contralateral HSS. Dye coupling experiments suggest that only CNMN7 gets direct input from the LPTCs while CNMN6 is electrically coupled to CNMN7 and gets the LPTC input indirectly. **B:** Injection of Neurobiotin into CNMN7 led to co-staining of ipsilateral VS-cells and contralateral HSS, as well as to the contralateral CNMN7 (arrow) and the ipsilateral CNMN6 (not shown*). From Wertz et al. (2012)*.

The VCN houses three motor neurons that innervate muscles which pull the head sideward (yaw) (*Strausfeld et al. 1987*). Dye-coupling with ipsilateral HS-cells indicates that these motor neurons are sensitive for horizontal motion, which would fit the pulling planes of the muscles. *Haag et al. (2010)* were able to functionally verify this: one investigated VCNM is directly postsynaptic to the ipsilateral HSN- and HSE-cell (Figure 7).

Taking anatomy and physiology together, both *Haag et al. (2010)* and *Wertz et al. (2012)* could demonstrate that the receptive fields of the LPTCs providing synaptic input add up linearly to form the receptive field of the motor neuron. In both studies, dual electrophysiological recording was employed to prove connectivity between neighboring cells. The large diameter axons of VS- and HS-cells in the lobula plate were targeted with one sharp intracellular electrode and a second sharp intracellular electrode was inserted into the dendrite of a CN or VCN motor neuron. These are located in close vicinity of the oesophageal foramen (gut hole) in the deutocerebrum and are thus relatively easy to access and record from (see Figure 5 C). Connectivity between two cells was demonstrated by hyperpolarizing and depolarizing one cell with current injections through the

electrode tip and simultaneously measuring the membrane potential deflection of the second cell with the second electrode.

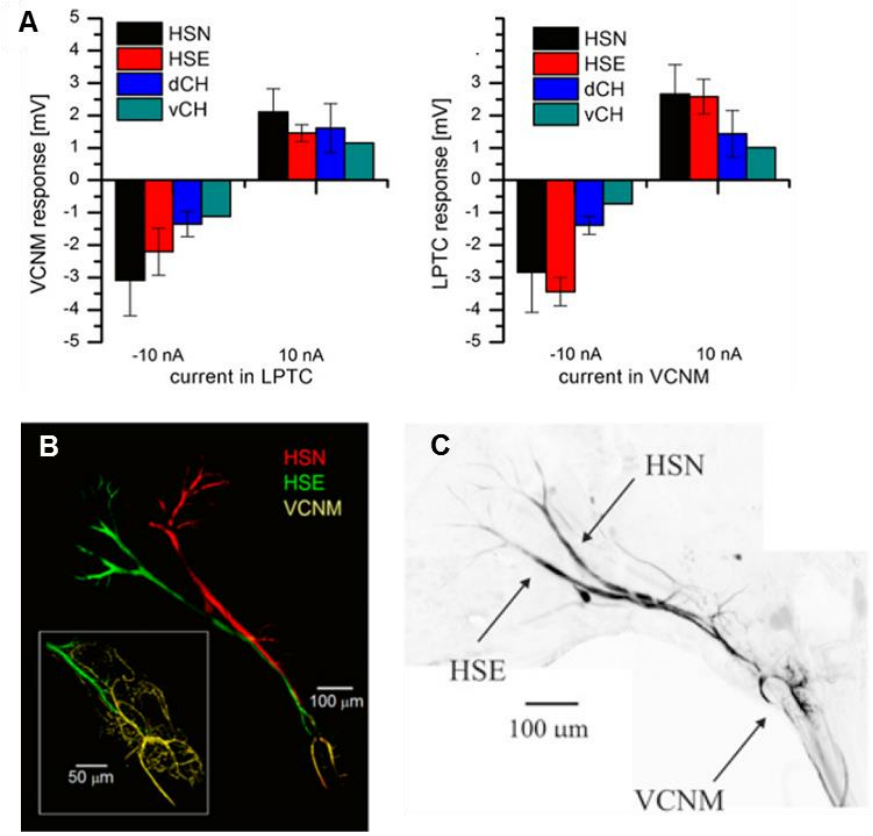

Figure 7: Connectivity between LPTCs and VCNMN. A: One VCNM was recorded intracellularly while different LPTCs were de- and hyperpolarized and vice versa. Current of both polarities passed through both directions and revealed a functional connection between the motor neuron and HSN, HSE, dCH and vCH. **B**: Two-photon images of the VCNMN and HS-cells after injection of Alexa 568 into HSN, Alexa 488 into HSE and amixture of the two dyes into the VCNMN. **C:** Injection of Neurobiotin into the VCNMN led to costaining of HSN and HSE, confirming synaptic coupling. From *Haag et al. 2010*.

While the response characteristics, motion tuning and LPTC-connectivity of VCN and CN motor neurons have been studied in detail, the ADN and FN are less well described. The neck motor neurons of these two nerves receive visual input via descending interneurons that project from the brain through the cervical connective into prothoracic neuropil, where the large and extensively arborized dendritic trees of the FNMNs and ADNMNs are situated (**Figure 5**).

1.3.2. The anterior dorsal nerve (ADN)

1.3.2.1. Muscle innervation and ADNMN anatomy

The ADN contains the axons of two motion-sensitive and direction-selective motor neurons that innervate two neighboring muscles controlling a sideward deflection of the head (*Strausfeld and*

Seyan 1985; Strausfeld et al. 1987; Gilbert et al. 1995) (Figure 8 A). ADNM1 innervates the large strap-shaped transverse horizontal muscle TH1, ADNM2 innervates the smaller spindle-shaped transverse horizontal muscle TH2 that is co-innervated by the cervical nerve motor neuron CNMN3 (Figure 8 B). TH2 is the only muscle that is innervated by two motor neurons, one deriving from the brain, the other from the thoracic ganglion (*Strausfeld et al. 1987*).

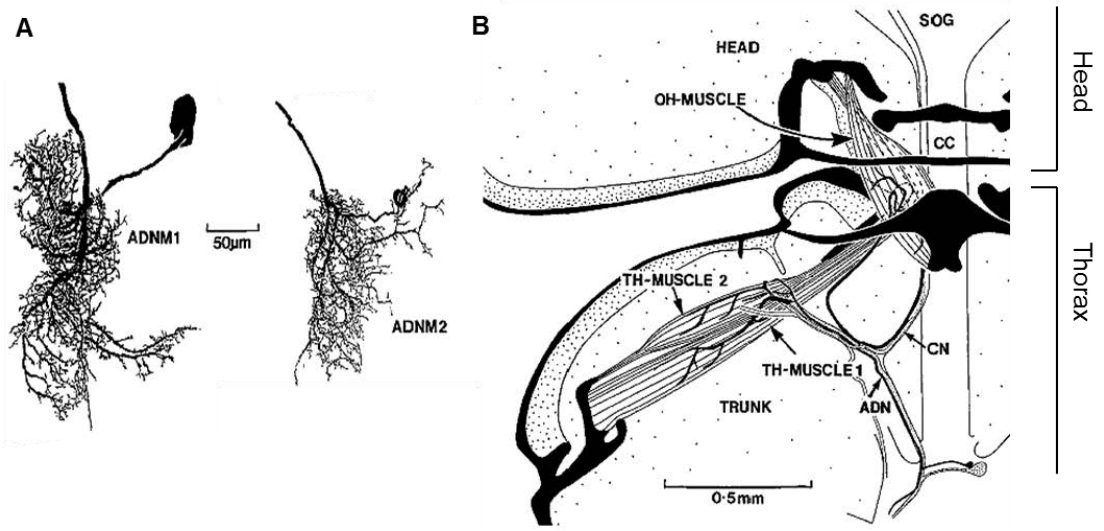

Figure 8: The two motor neurons of the anterior dorsal nerve ADNM1 and ADNM2. A: The two motor neurons differ greatly in size. Both arise from contralateral cell bodies in the prothoracic ganglion and their axons project through the ADN. B: They innervate the transverse horizontal muscles TH1 (ADNM1) and TH2 (ADNM2) that control yaw-movement of the head. TH2 is co-innervated by a CN motor neuron projecting down from the brain. The cross section shows a dorsal view of the left side of the fly's head-trunk-articulation. SOG = suboesophageal ganglion, CC = cervical connective. From *Strausfeld et al. 1987*.

Electrical stimulation of the ADN generates a yaw movement of the head towards the stimulated side, which corroborates the prediction based on the pulling planes of the TH1 and TH2 muscle, that the muscles innervated by the ADN motor neurons control movements in the horizontal plane (*Gilbert et al. 1995*).

1.3.2.2. ADNMN physiology

In a first pioneering study, the physiological characteristics of the two ADNMNs were described by *Milde et al. (1987),* who found the two motor neurons to be most sensitive to a grating moving from front to back in front of the ipsilateral eye. Two motor neurons were easily distinguishable by their spike amplitude and response characteristics: a large unit exhibited no spontaneous activity and responded phasically to stimulation, a small unit was usually spontaneously active and responded tonically.

Huston and Krapp (2008) followed up on this study by not only testing for the principal preferred direction of motion of the motor neurons but by mapping the receptive fields of the cells in more detail. They displayed a square wave grating of 62.2° edge length moving in 16 different directions

in different parts of the visual field and found different responses in the two ADN motor neurons: While one motor neuron is only sensitive for a front-to-back movement right in front of the animal [0,0], within the region of binocular overlap, the other motor neuron has a larger receptive field, responding to a broader range of stimulus positions. Both are most sensitive at the equator of the visual field (0° elevation) (Figure 9). The region of binocular overlap in female *Calliphora* roughly measures between 10° and 25°, depending on the elevation (*Beersma et al. 1977*).

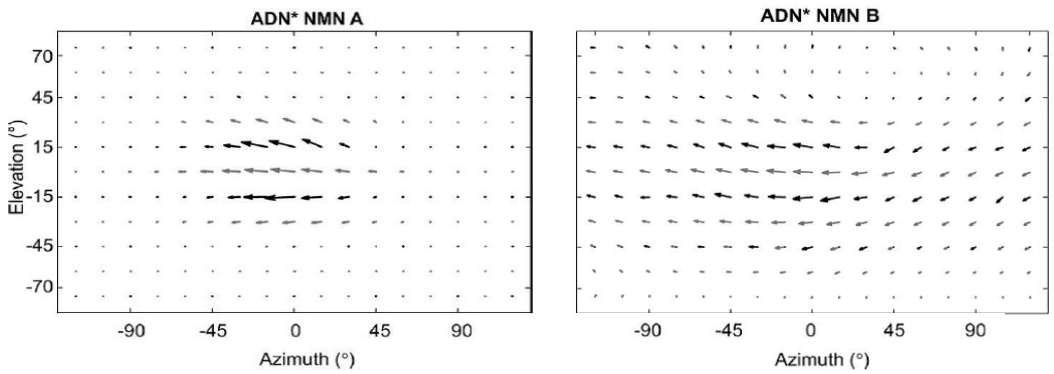

Figure 9: Receptive fields of the two visually sensitive ADN motor neurons. The motor neurons' activity was recorded on the left side of the nervous system while presenting a grating moving in 16 different directions at different positions of the fly's visual field. Both motor neurons are tuned to horizontal front-to-back motion but their receptive fields differ in extent. Arrow length indicates the relative strength of the response (action potential frequency [Hz]) at that particular position, the direction of the arrowhead indicates the preferred direction of the motor neuron at that particular position. Black arrows represent measured data, grey arrows are interpolated. Note that the motor neuron depicted in the right panel responds to contralateral stimuli (0° to 120°) as strongly as to ipsilateral stimuli (-120° to 0°). From *Huston and Krapp (2008)*.

1.3.2.3. Dye coupling

Due to its very small molecular size, cobalt chloride can cross electrical synapses between neurons and be used to visualize their connectivity (*Strausfeld and Obermayer 1976*). Cobalt-coupling thus serves as an indicator for functional synaptic connectivity between two neurons via gap junctions. Chemical synapses on the contrary cannot be resolved by this method. Numerous neuroanatomical studies have used the cobalt-coupling-method to describe the relationship between neck motor neurons and their sensory input anatomically and deduce from this a functional connection between these cells (*Strausfeld and Bassemir 1985a; Strausfeld and Seyan 1985; Milde et al. 1986; Strausfeld et al. 1987; Strausfeld and Gronenberg 1990; Strausfeld et al. 1995*).

For the motor neurons of the ADN, cobalt backfills of the whole nerve did not lead to co-staining (*Strausfeld et al. 1987*). Being visually sensitive, the ADNMNs must get some sort of visual input. Thus the absence of dye-coupling indicates the existence of chemical synapses between the motor neurons and their input elements of the visual pathway. The dendritic trees of ADNM1 and ADNMN2 are located in the dorsalmost neuropil of the prothoracic ganglion, in close proximity to axon collaterals of descending neurons (Figure 10). Hence, even though direct anatomical evidence for a connection between descending neurons and ADNMNs is missing, the location of

their terminals suggests an interaction site. These descending neurons are termed “descending neurons of the lobula columnar and horizontal cell system” (DNColHS) (*Strausfeld and Bassemir 1985b*) (**Figure 10**). They originate in the brain, where their dendrites are cobalt-coupled to all three HS-cells. DNColHS are a group of descending neurons, but not the only ones receiving input from HS-cells. *Strausfeld and Bassemir (1985b)* report that light and electron microscopy exhibit an extensive HS-DN relationship with each HS-collateral being invested by the dendrites of many descending neurons.

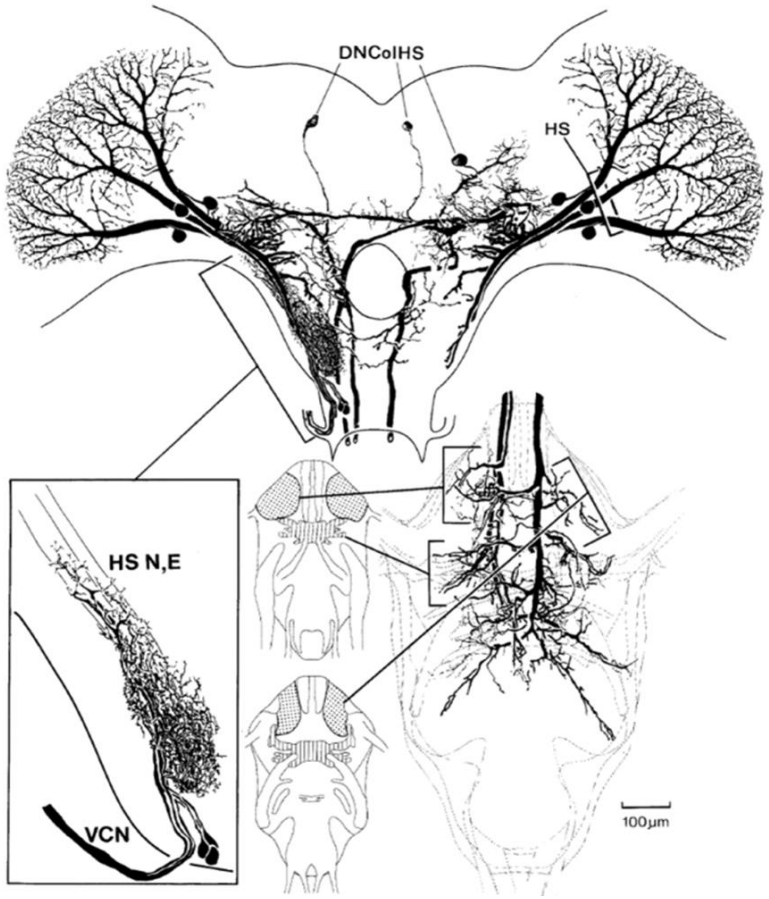

Figure 10: Descending neurons from HS-cells. DNColHS are cobalt-coupled to the axon collaterals of the three HS neurons. DNColHS project through the cervical connective into the thoracic ganglion and terminate there in several neuropils including dorsal neuropil containing the ADNMN dendritic trees (stippled in center diagrams) and the flight neuropil (striped). The axon terminals of HSN and HSE are closely enwrapped by VCN dendrites which receive their direct synaptic input (left inset, see also **Figure 7**). Modified from *Strausfeld et al. (1987)*.

The coupling pattern between HS-cells and descending neurons is more complex than the coupling between VS-cells and descending neurons (*Strausfeld and Bassemir 1985b*). While the VS-cells were shown to functionally synapse onto the large DNOVS interneurons that are relatively easy to record from (*Haag et al. 2007; Wertz et al. 2008*), no recordings from descending interneurons postsynaptic to horizontally sensitive LPTCs have succeeded to date.

Based on neuroanatomical studies (*Strausfeld et al. 1987,* Figure 10) and on the fact that ADNMNs innervate muscles to steer yaw muscles that deflect the head sideward (Figure 8), the horizontally sensitive HS-cells are prime candidates for providing direction-selective visual information onto the ADNMNs via DNColHS neurons.

1.3.3. The frontal nerve (FN)

1.3.3.1. Muscle innervation

The frontal nerve is the largest of the four neck nerves. Mass cobalt fills into its cut stump show at least 13 cell bodies, eight of which belong to neck motor neurons with a large axon diameter (FNM1-FNM8) (*Strausfeld and Seyan 1985; Strausfeld et al. 1987*).

The neck motor neurons FNM1-8 innervate eight "indirect" muscles that do not move the head itself upon contraction, but move a scoop-shaped cuticular structure of the prothorax, termed "cervical sclerite" (Figure 11). The handle-shaped front of the cervical sclerite fits into the concave underside of a cuticular protrusion of the head: the so-called "occipital condyle". Both the occipital condyle and the cervical sclerite are paired structures, i.e. there is one on each side of the neck. These two paired structures build the support for the head. Internal muscles that arise from the lip of the slerite's scoop and taper as tendons towards the head provide rigidity for this articulation. Due to their different pulling planes, the indirect muscles of the frontal nerve can move the sclerite in different directions upon contraction. The pronotal and sternal apodeme are fixed structures and serve as anchor points for the muscles (Figure 11).

According to single cell stainings from *Strausfeld et al. (1987)*, the motor neurons of the frontal nerve innervate indirect neck muscles as follows:
FNM1 innervates the sclerite levator muscle that originates at the pronotal apodeme, a thickened part of anterodorsal cuticle of the pronotum, and tapers to a narrow attachment point at the caudal margin of the cervical sclerite (Figure 11). Contraction of the levator muscle pulls the lower margin of the sclerite upward, declining the structure's upper margin that articulates with the condyle of the rear head and by doing so pushing the head upwards on that side. Unilateral activation of the levator muscle would thus lead to roll-like movements of the head while simultaneous contraction of both levators would push the head up in a pitch-like movement.

FNM2 innervates the sclerite adductor muscle. Similar to the levator, it stretches from the pronotal apodeme to the lower margin of the cervical sclerite and pushes the head both upwards and inwards when contracting (Figure 11).
A downward head movement is controlled by the two massive segments of the sclerite depressor muscle, which are innervated by FNM3 and FNM4. The sclerite depressors link the caudal end of the cervical sclerite to the sternal apodeme (Figure 11). Pulling the caudal margin of the sclerite downwards upon contraction, the frontal margin is pushed upward inside the sclerite-condyle-joint and thereby pushes the head downwards. Unilateral depressor contraction results in a roll-

like-movement of the head, while simultaneous contraction of depressors on both sides of the neck will pull the head downwards (pitch).

FNM5, FNM6, FNM7 and FNM8 innervate a group of internal muscles of the sclerite, which provide the head-prothorax-articulation with rigidity. These so-called "sclerite-condyle internal muscles" arise from the lip of the sclerite's scoop and taper towards the head, where they are either attached to the overhang of the occipital condyle or to thickened cuticle close to the condyle (Figure 11).

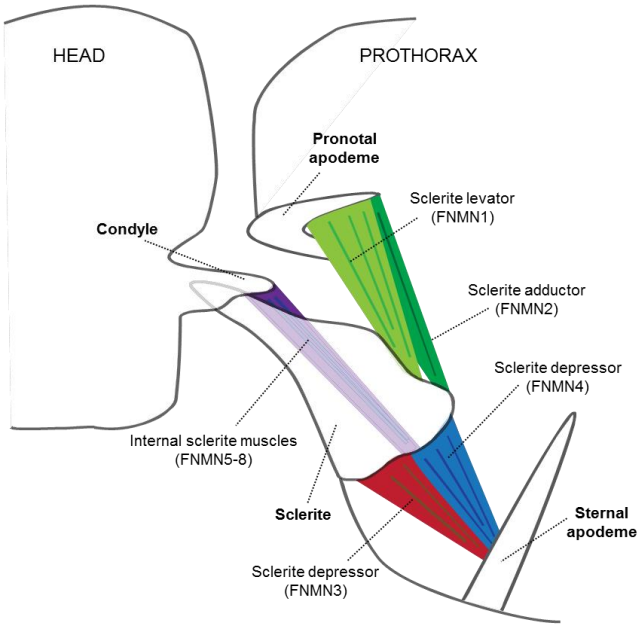

Figure 11: Sagittal scheme of the cuticular structures and neck muscles associated with FNMNs. Names in brackets denote the motor neuron innervating the respective muscle. External sclerite muscles are attached to the pronotal and sternal apodeme and project to the outer margins of the cervical sclerite to pull it either up (sclerite levator and adductor, innervated by FNMN1 and FNMN2) or down (sclerite depressors, innervated by FNMN3 and FNMN4) upon contraction. The sclerite articulates with the occipital condyle of the head, forming a lever that in turn pushes the head up or down. Sclerite and condyle are paired structures: the left sclerite is associated with motor neurons of the left FN, the right sclerite with FNMNs from the right FN. Movement of one sclerite moves only the ipsilateral side of the head up or down. Internal muscles of the sclerite (only one drawn here) provide the structure's rigidity. Redrawn after *Strausfeld et al. (1987).*

1.3.3.2. FNMN anatomy

As observed in cobalt and Lucifer Yellow dye-filling experiments (*Strausfeld and Seyan 1985; Strausfeld et al. 1987*), the eight motor neurons of the frontal nerve, FNM1-8, have strongly arborized dendritic fields that lie in a large bundle in the anterior-lateral part of the thoracic ganglion. All eight are morphologically very similar, making identification based solely on anatomy difficult (Figure 12). Some characteristic features shall be specified here nevertheless: the FNM1 main dendrite is thick and pole-shaped without further large dendritic arborizations, FNM2

extends part of its dendrites contralaterally, FNM3 and FNM4 have the two largest axons (~25µm), and both FNM7 and FNM8 have slender dendrites that extend posteriorly (Figure 12).

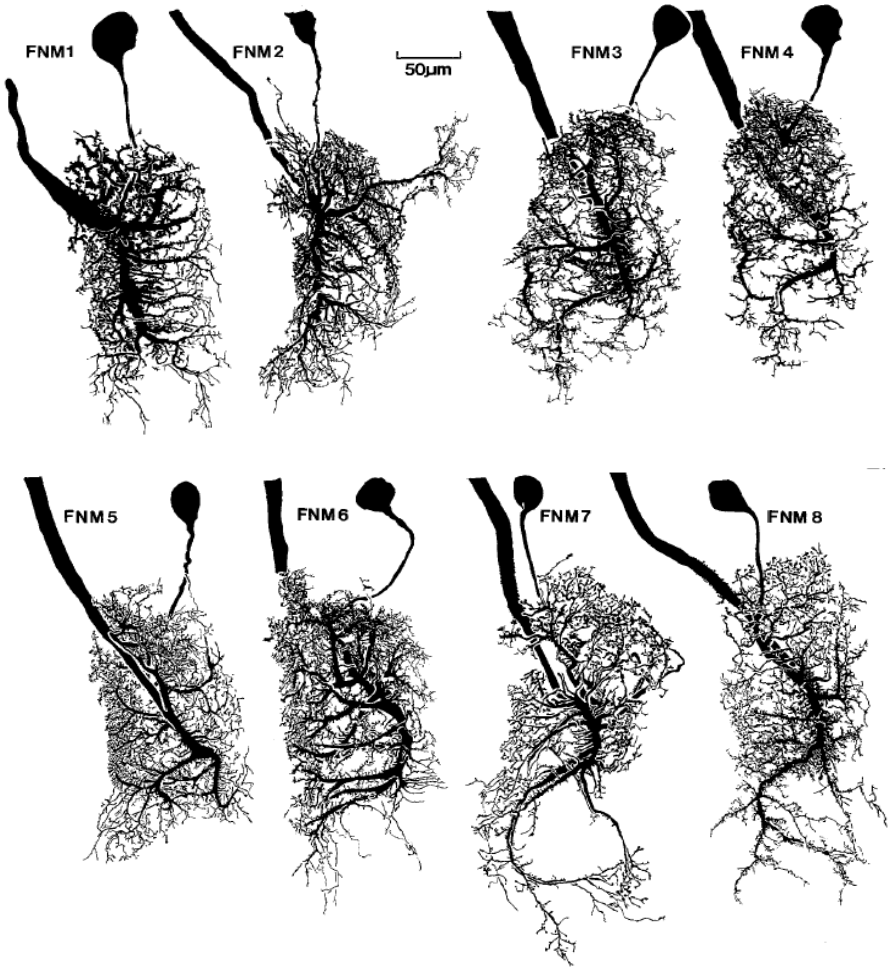

Figure 12: Two-dimensional projections (camera lucida drawings) of the eight cobalt-filled large-diameter motor neurons of the left frontal nerve as illustrated by *Strausfeld et al. (1987).* They all possess extensively arborized dendritic trees and are anatomically similar.

1.3.3.3. FNMN physiology

In a pioneering study *Milde et al. (1987)* recorded extracellularly from the FN and tested for the nerve's preferred direction of a moving grating. They measured a preference for downward motion in the lateral field of view and tuning to a variety of directions in the frontal visual field. They concluded that FN motor neurons are sensitive to roll-like rotations. Moreover, electrical stimulation of the whole nerve rolls the head of the fly from an upright position downwards towards the stimulated side, which supports the prediction that FNMNs are engaged in head rolling (*Gilbert et al. 1995*).

As for the ADNMs, *Huston and Krapp (2008)* mapped the receptive fields of single FN units in greater detail. They recorded from the nerve extracellularly and assigned the action potentials they measured to different motor units, according to their shape and amplitude identifying three

FN units that are tuned to different axes of rotations, very similar to VS-cells of the lobula plate (Figure 13).

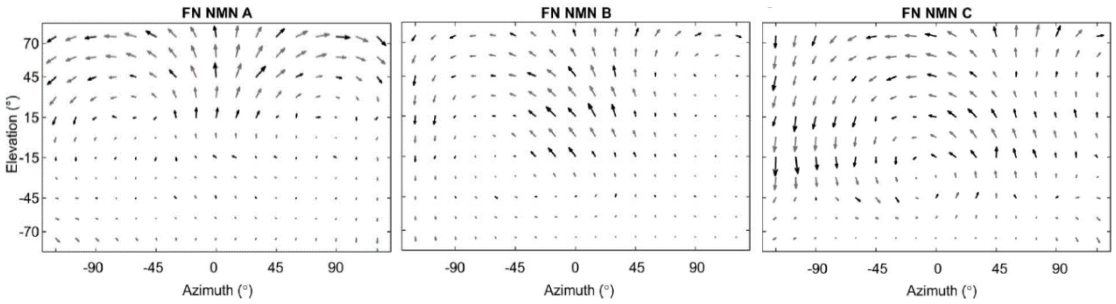

Figure 13: Receptive fields of three motor units of the left FN. A local grating was displayed moving in 16 different directions. Black arrows represent experimental data, grey arrows were calculated by interpolation. While the motor neuron "FN NMN A" is tuned to optic flow reminiscent of upward pitch, the neuron "FN NMN C" prefers counterclockwise roll and "FN NMN B" is tuned to an intermediate pitch-roll-like rotation. From *Huston and Krapp (2008).*

1.3.3.4. Dye coupling

Visual input from the eyes and input from the halteres converge on the FNMNs. The visual input is provided by descending neurons like DNOVS1, which receives input from VS-cells of the ipsilateral lobula plate (*Strausfeld and Seyan 1985; Haag et al. 2007*). Cobalt backfills of the frontal nerve revealed dye-coupling of the motor neurons with afferents from the prosternal organ and the halteres, and with the descending neuron DNOVS1 from the visual system (*Strausfeld and Bassemir 1985; Strausfeld and Seyan 1985; Gronenberg et al. 1995*) (Figure 14, Figure 15). The halteres monitor changes of angular velocity during flight (*Pringle 1948; Sandeman and Markl 1980; Hengstenberg 1993; Nalbach 1993*). The prosternal organs are mechanosensory hair fields in the neck region that monitor head position via proprioception *(Milde et al. 1987; Preuss and Hengstenberg 1992*). The prosternal nerve shares its origin with the FN (*Sandeman and Markl 1980*).

The descending neuron DNOVS1 receives its main input from VS6 and VS7 and additional weaker input from VS4, VS5, VS8 and VS9 via the chain-like electrical connectivity between neighboring VS-cells (*Haag and Borst 2004*) (Figure 15). Cobalt fills into single FNMs revealed the faint outline of the DNOVS1 axon, which led *Strausfeld et al. (1987)* to the conclusion that at least FNM1-4 and FNM7 are coupled to VS4-9 via DNOVS1.

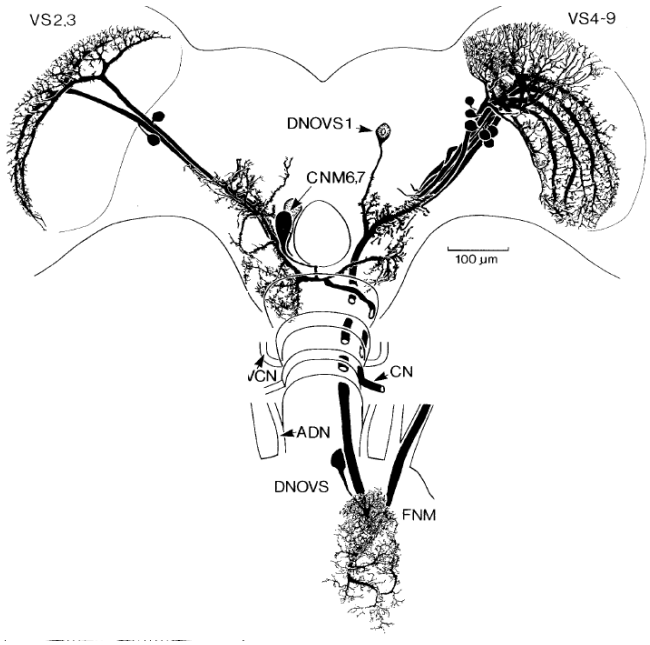

Figure 14: Relationship between VS-cells and neck motor neurons. Camera lucida drawing from *Milde et al. (1986).* VS2 and 3 are cobalt-coupled to the motor neurons CNM6 and 7, which are directly postsynaptic (see also **Figure 6**). VS4-9 provide indirect visual input for FNMs: they are synaptically connected to the thoracic neck motor neurons via a large diameter descending neuron, DNOVS1.

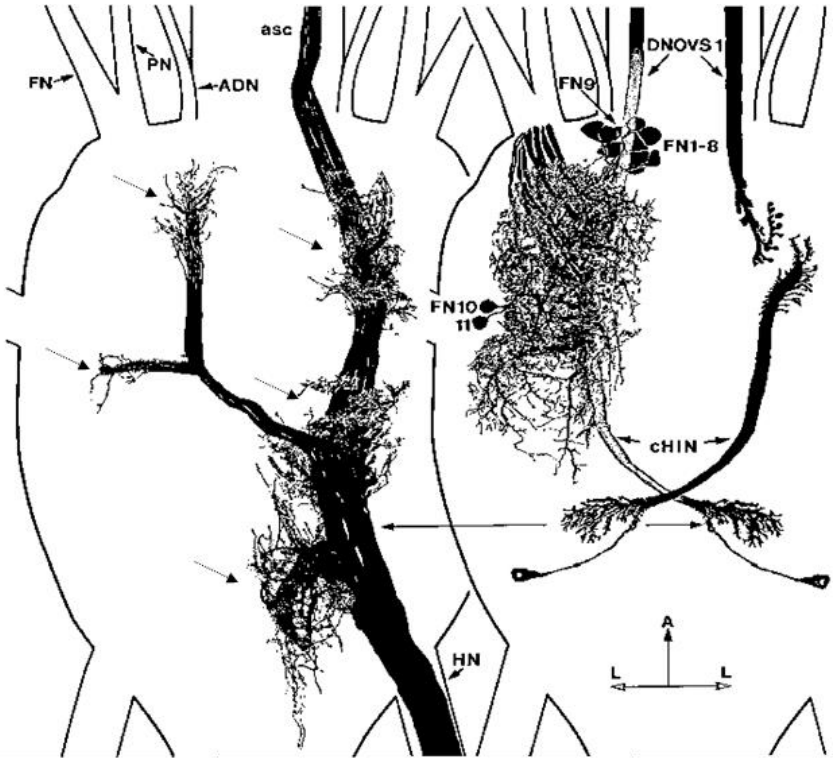

Figure 15: Relationship between halteres and FNMNs. Left: The haltere nerve (HN) has ipsi- and contralateral terminal domains (dashed arrows) and ascends further to the brain (asc) through the cervical connective; PN = prosternal nerve. Right: When the frontal nerve is backfilled with cobalt chloride, at least 11 motor neurons are labeled. Coupling is observed between the FN bundle and the descending neuron DNOVS1 and a contralateral haltere interneuron (cHIN). The dendrites of the cHIN innervate one of the HN trunks (indicated by the long horizontal arrow). The right part of the panel shows the cHIN and the DNOVS1 terminal o the right side of the nervous system without the FNMNs. From Strausfeld and Seyan (1985).

1.4. Aim of the present study

The main aim of the present study is to functionally characterize the prothoracic neck motor neurons of the frontal nerve (FN) and the anterior dorsal nerve (ADN). Linking well-described visually sensitive lobula plate tangential cells to the neck motor neurons that execute movements in response to visual input will enable us to discuss the roll of LPTC motion tuning in visually guided head turning behavior.

It is known so far that the motor neurons of the ADN are both visually sensitive and respond to horizontal motion. Their presynaptic partners have not been identified yet. In this study, the potential synaptic connection between HS-cells and ADNMNs will be investigated, since experimental evidence for a connection via descending neurons is still missing. Moreover, the detailed tuning to full-field rotations around various axes in visual space will be compared in ADNMNs and HS-cells, to test if the HS-cells alone are sufficient to account for the motion-sensitivity of the ADNMNs.

For the FNMNs it is known that some of them are visually sensitive but it is yet unclear if all of them are. They have been shown to respond to roll-like optic flow and to make synaptic contact with the large descending neuron DNOVS1, which receives input from ipsilateral VS-cells. In this study, the detailed tuning to full-field rotations will be measured in single FNMNs. Individual targeting and dye-filling allows for the matching of anatomical and physiological characteristics of these neurons, so that for the first time visual motion tuning can be assigned to particular anatomical cell types and predictions about the acuity of this tuning for the pulling plane of the innervated muscle can be made.

2. Material and methods

2.1. Preparation and setup

For intracellular recordings from FNMNs and from the DNOVS1 descending neuron, four- to eight-day-old female blowflies (*Calliphora vicina*) from the laboratory stock were used. For extracellular whole nerve recordings from the ADN with suction electrodes, up to 12 days old animals were used.

Experimental animals were shortly anesthetized with CO_2 and immobilized as follows: A small rectangular glass holder was glued to the fly's scutum using droplets of heated wax, the bases of the wings were glued to the body and the legs were removed with scissors. The head was bent forward 90° and fixed in this position so that the back side of the head was accessible for recording. The proboscis was removed to prevent peristaltic movements of the esophagus and the abdomen was dorsally fixed to the holder and covered with a thin wax layer to prevent contractions (see Figure 1 and Figure 16 for anatomical orientation).

To record from prothoracic neck motor neurons, the back of the thorax was opened from behind. Muscle blocks and intestinal tracts covering the thoracic ganglion and associated nerves were removed to gain access to the nerves and to keep contractions to a minimum.
The tissue was regularly rinsed with saline solution to prevent desiccation. Although most recordings were performed on the right side of the nervous system, the recorded data was mirror-transformed and plotted with respect to recordings from the left part of the nervous system for reasons of uniformity and comparability with other studies (e.g. *Huston and Krapp 2008; Borst and Weber 2011; Wertz et al. 2012*).

For all experiments the animal was oriented using the alignment of the two deep pseudopupils (*Franceschini 1975*). After alignment, the fly was placed in the center of a semi-cylindrical LED arena so that the pseudopupils faced zero degrees elevation and zero degrees azimuth.

The experimental set-up comprising the LED arena, the fly holder and three micromanipulators controlling the grounding electrode and intra- and extracellular recording electrodes, was arranged on a heavy recording table. A fluorescence stereoscope (MZ FLIII; Leica) was used to visually control the placement of the electrodes in the fly's head and prothorax. Intracellular recording electrodes were filled with 5mM green (Alexa Fluor® 488; Life Technologies) or red (Alexa Fluor® 594; Life Technologies) fluorescent dye to verify that only one axon was filled at a time. Later, blue (for Alexa Fluor® 488) or green (for Alexa Fluor® 594) fluorescent light was used to check if an axon was filled during the recording.

For monocular measurements of visual sensitivity, one eye was occluded by applying multiple layers of black permanent marker (Edding 3000) onto the retina. After mirror transformation the

left eye is referred to as ipsilateral, the right eye as contralateral. As a control, both eyes were occluded in the same procedure. Permanent marker was preferable to viscous ink since in trials with ink the animals were strongly disturbed by the mechanical effect the liquid had onto the sensitive bristles surrounding the fly's eyes. Covering the eye itself was preferable to single eye stimulus presentation because it allowed for the stimulus to be presented in front of the fly, within the region of binocular overlap.

2.1.1. Recording haltere activity

Haltere activity was monitored by filming the left (contralateral) haltere from the side using a highspeed camera (MotionPro Y3; Integrated Design Tools Inc.) with a macro objective (105 mm F2, 8 EX DG, Sigma) at a distance of 14 cm between the camera and the haltere. Three different preparations of the animal were used:

To monitor haltere activity without simultaneous electrophysiological recording, the fly with its legs cut was glued to the glass holder on its scutum but apart from this left free to move its head, wings and abdomen (Figure 16 A). This resulted in high activity of the animal during visual stimulation, including head turns, high frequency haltere beating and large amplitude contractions of the abdomen (see Results). To simultaneously record extracellularly from the ADN and monitor haltere activity, the animal was firmly fixed as described above, with its thorax opened from dorsally (Figure 16 B). This included bending and gluing the head in an upright position and firmly waxing the abdomen onto the glass holder to minimize muscle contractions and allow for stable recordings. This preparation resulted in a complete lack of haltere activity (see Results). As a compromise between the two configurations, the abdomen was left free to move but the rest of the body was waxed, so that recordings from the ADN were still possible and muscle activity in the thorax was prevented, but the animal was allowed to move its abdomen (Figure 16 C).

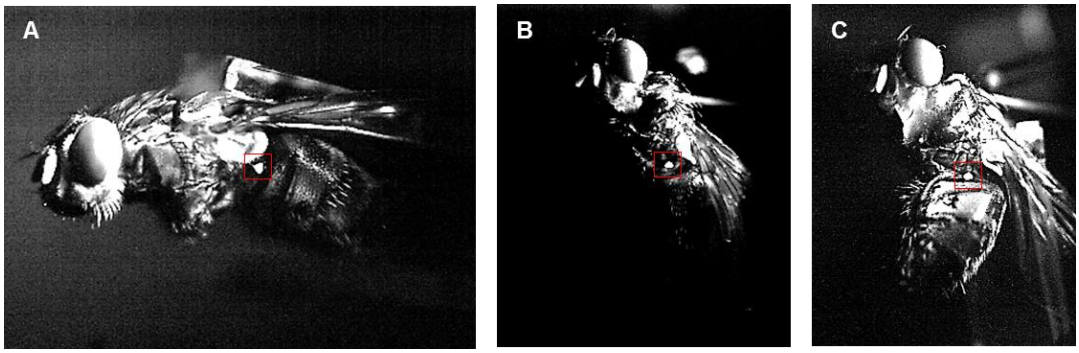

Figure 16: Fixation of the fly on the glass holder for recording haltere activity with a high speed video camera. A: Without electrophysiological recording, the animal was attached to the holder only on its scutum and left free to move its head and contract its body. **B:** Recording extracellularly from the ADN, the animal with its head bent forward in a 90° angle was entirely prevented from moving by fixing it with wax to maximize recording stability. **C:** Monitoring haltere activity and recording from the ADN as in panel B was also possible when only the head was fixed but the abdomen was left free to contract. The red square in all panels indicates the rounded tip of the haltere which was tracked off-line in single frames of the recorded movies.

2.1.2. Extracellular recording from ADNMNs

For extracellular recordings of the ADN the nerve was cut with fine scissors approximately 1 mm from its origin at the prothoracic ganglion. Since the nerve is very thin and slack it could easily be sucked into the open tip of an extracellular nerve suction capillary, while it was not large enough in diameter (~30µm, Figure 22) and therefore not stable enough for penetration with a sharp intracellular pipette.

Electrodes with a resistance of 40-80 MΩ were pulled on a Flaming/Brown type micropipette puller (P-97; Sutter Instruments) out of glass capillaries with an outer diameter of 1 mm (GB100F-10; Science Products). The sharp tip of the pulled capillary was evenly blunted by gently pushing it against a piece of metal, leading to a rounded tip diameter that was slightly larger than the diameter of the nerve, around 40 - 50 µm. The capillary was backfilled with physiological saline solution and the ≈ 1 mm long cut stump of the nerve was pulled into the opening by applying negative pressure through the electrode holder (Figure 17). Recording from the whole nerve yields voltage traces from all neurons that project through the nerve.

2.1.3. Intracellular recording from LPTCs and DNOVS1

For dual recordings of single HS-cells (intracellular) and ADNMNs (extracellular), HS-cell axons in the lobula plate were targeted with a sharp glass electrode (Figure 17). Electrodes had a resistance of 40-80 MΩ and their tip was filled with Alexa Fluor® 488 (green) or Alexa Fluor® 594 (red) fluorescent dye.

The identity of the recorded LPTC (HSN, HSE, or HSS) was determined using its visual response properties (membrane depolarization upon ipsilateral front-to-back movement, Figure 4 B) and its anatomy (Figure 4 A). Current pulses of alternating sign ("buzzing") were used to break through the cell membrane and to release Alexa Fluor® into the axon through the electrode tip. This allowed for the visualization of the neuron's anatomy during recording (fluorescent stereoscope MZ FLIII; Leica). Due to their exceptionally large size (10 - 25 µm diameter, 200 - 300 µm length from dendrites to axon terminal) and well-described position within the lobula plate, HS-cell axons were relatively easy to locate and target (see *Hausen et al. 1980; Hausen 1982a, Strausfeld and Bassemir 1985b*).

When recording intracellularly from DNOVS1 dendrites or from VS-cell axons, the thorax was left intact while the head capsule was opened from behind to gain access to the lobula plate and the deutocerebral brain region around the oesophageal foramen, where DNOVS1 dendrites are located (see Figure 14 and Figure 41). DNOVS1 recordings were obtained from the cell's dendrites close to the oesophageal foramen in the deutocerebrum. To locate the cell's dendritic region in immediate proximity to the VS-cell output region (Figure 14, Figure 41), one or more VS-cells were penetrated with the recording electrode and filled with Alexa Fluor® to serve as a landmark (see also *Haag et al. 2007*). VS-cells are, like HS-cells, large and easy to target and fill fast with fluorescent dye, so that the cell can be rapidly anatomically identified during recording using the fluorescent stereoscope. The tip of the recording electrode was filled with 5 % Neurobiotin™

Tracer (Vector Laboratories) dissolved in 5 mM Alexa Fluor® 488 green fluorescent dye (Life Technologies). The shaft of the electrode was backfilled with 2 M KAc plus 0.5 M KCl solution. The mixture of Alexa Fluor® and Neurobiotin was injected into the descending neuron during the recording to trace its anatomy and visualize its electrically coupled synaptic partners post-hoc.

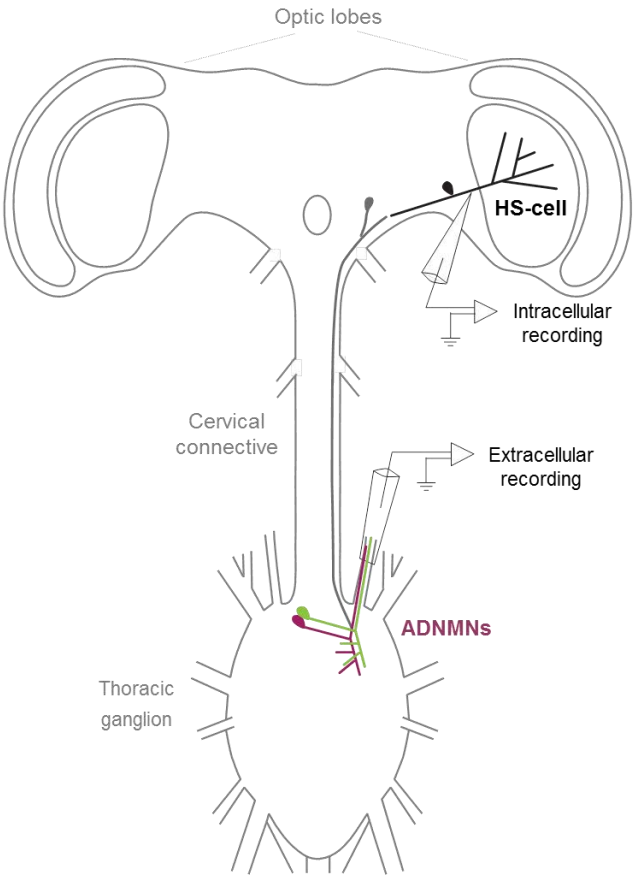

Figure 17: Extracellular nerve suction recording from the ADN and intracellular single cell recording from an HS-cell. The cut ending of the ADN is inserted into the tip of the nerve suction electrode. ADNMNs (green and red) are thought to receive visual input from HS-cells (black) via descending interneurons (gray) that project through the cervical connective. For dual recordings from HS-cells and ADNMNs both preparations were used simultaneously as shown here.

2.1.4. Intracellular recording from FNMNs

To record from single FNMN axons with a sharp intracellular electrode, the back of the thorax was opened from behind to gain access to the FN, while the head was left intact. Due to its large diameter (~80 µm, see **Figure 34, Figure 36**) the FN was stable enough to insert a sharp glass pipette for intracellular recording but too stiff for stable insertion into the large cut tip of a suction pipette for extracellular recording.

Single FNMN axons were recorded intracellularly using sharp glass electrodes with a resistance of 40-80 MΩ. To obtain a post-hoc staining from the recorded cell and its electrically coupled synaptic partners, the electrode tip was filled with 5 % Neurobiotin™ Tracer (Vector Laboratories) dissolved in 5 mM Alexa Fluor® 488 (Life Technologies) and the shaft of the electrode was backfilled with 2 M KAc plus 0.5 M KCl solution. The nerve was penetrated with the tip of the recording electrode close to its origin at the prothoracic ganglion under visual control (**Figure 18**). The axon membrane was broken through and the dye mixture was released into the cell by buzzing the electrode tip.

The measured membrane potential (around -40 mV), the occurrence of spikes and diffusion of the dye into an axon served as indications that cell contact was established. Due to their large diameter FNMN axons filled quickly with dye. No further mechanical support of the nerve was needed to keep the recording stable for up to 30 minutes. After visual stimulation positive and negative current of up to +5 nA and -8 nA was passed through the recording electrode for several minutes to enhance the diffusion of Neurobiotin into the cell.

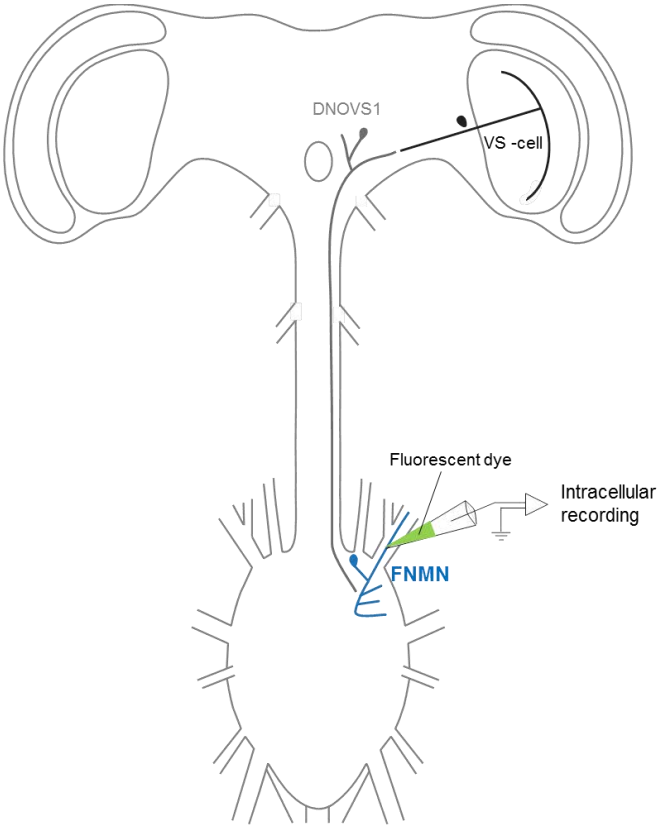

Figure 18: Intracellular recording from a single FNMN axon. The electrode tip is inserted into the FN close to its origin. FNMNs (blue) are thought to receive input from VS-cells (black) via descending interneurons such as DNOVS1 (gray). Recording electrodes were backfilled with Alexa Fluor® as to stain the neuron for post-hoc identification.

2.2. Sensory stimulation

2.2.1. Stimulus device

A custom-built LED arena as introduced in *Wertz et al.* (*2009a, 2009b*) based on open-source information from *Reiser and Dickinson* (*2008*) was used to display visual stimuli in a virtual reality setting (**Figure 19**).

The arena consists of 30 x 16 TA08-81GWA dot matrix displays (Knightsbridge), each containing 8 x 8 single green LEDs with a spectral peak at 568 nm. The LED arena is built as an open cylinder with 240 LEDs arranged along its horizontal and 128 LEDs arranged along its vertical extent. This equals 240° in azimuth and 96° in elevation of the fly's visual field. The angular resolution between adjacent LEDs is between 0.5° (at 45° elevation) and 1° (at 0° elevation). An angular

resolution of 1° is sufficient for *Calliphora*, where the typical spatial resolution between neighboring ommatidia is 2° (*Petrowitz et al. 2000*) and the highest resolution in the frontal visual field was found to be up to 1.2° (*Land and Eckert 1985*).

The arena is capable of running at frame rates above 600 fps and stimuli can be displayed at 16 different light intensity levels, with luminance ranging from 0 to 80 cd/m^2. Stimuli were distorted along the vertical axis to correct for the non-spherical shape of the arena. Stimulus patterns were programmed, generated and controlled with MATLAB (MathWorks).

2.2.2. Visual stimulation: panoramic stimuli

Two sets of stimuli were used for panoramic pattern presentation: For the first set, a three-dimensional rectangular virtual room in which a virtual fly was rotated around and translated along the X-, Y- and Z-axis was programmed ("3 degrees of freedom" stimulus). The images projected onto the virtual fly's eye were used as movies displayed to the real fly during the experiment on the LED arena at maximum contrast (see *Wertz et al. 2009b*).

For the second set, a virtual fly was rotated around a total number of 31 axes in the virtual room. These were spaced 30° apart from each other in azimuth and elevation ("31 axes" stimulus) and covered the full 360° in azimuth and 180° in elevation of visual space. The walls of the rectangular virtual room were tiled with checkerboard wallpaper and measured 1 m in height and width and 2 m in length (**Figure 19 B**).

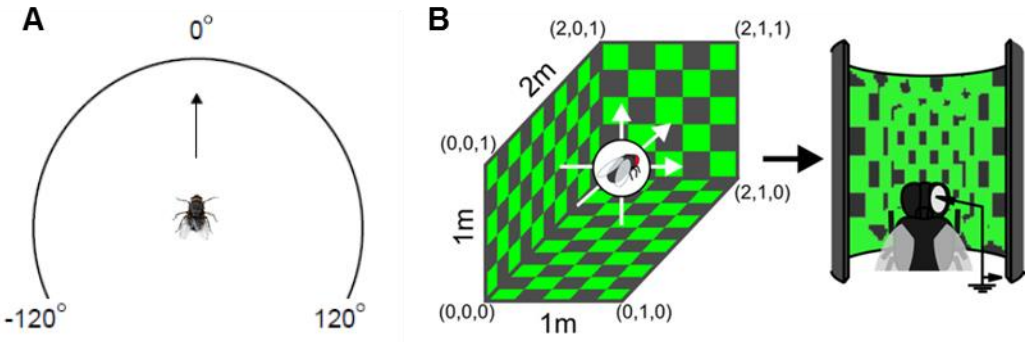

Figure 19: Presentation of panoramic visual stimuli in the LED arena. A: Schematic representation of a fly in the center of the LED arena viewed from above. The arena is cylindrical with a horizontal extent of 240°. The fly faces the arena at 0° azimuth and 0° elevation. **B:** Panoramic stimulus movies for the "3 degrees of freedom" stimulus were generated by moving a virtual fly along or around its three main body axes in a virtual rectangular room that measured 1 m along the X- and Y-axis and 2 m along the Z-axis. The room was lined with equally distributed checkerboard squares. Movies were then presented on the LED arena to a real fly in the experimental set-up during the recording of neuronal activity. For the "31 axes" stimulus the virtual fly was rotated around 31 body axes in the checkerboard-wallpapered virtual room. Pictures in **B** taken from *Wertz et al.* (*2009b*), for more detailed information on movie generation see *Wertz et al.* (*2009b*).

Movies of each set were displayed in random order. The 12 movies for the "3 degrees of freedom" stimulus were the translations "sideslip leftward", "sideslip rightward", "lift up", "lift down", "thrust near" and "thrust away", and the rotations "pitch upward", "pitch downward", "yaw leftward", "yaw rightward", "roll clockwise" and "roll counterclockwise". The 62 movies for the "31 axes" stimulus corresponded to a clockwise and a counterclockwise rotation around each axis.

Movies were presented for either 1 s with a 1 s pause in between stimuli, or for 500 ms with a 1 s pause in between stimuli. The shorter (500 ms) stimulation periods were often used for the "31 axes" stimulus because of its overall duration (125 s per trial for 1 s per stimulus, 94 s per trial for 500 ms per stimulus). During the 1 s pause between stimuli, the pattern stood still and the arena stayed illuminated.

All stimuli were presented at a frame rate of 150 fps, which equals a velocity of 150°/s on the circular arena for rotations, translational speeds of 0.3 m/s for lift and sideslip, and 0.4 m/s for thrust. Panoramic pattern rotations and translations ("3 degrees of freedom" and "31 axes" stimulus) were used to measure the rotational tuning and optic flow preferences of all cells that are described in this account: ADNMNs, FNMNs, HS-cells and DNOVS1.

All previous experiments measuring neck motor neuron motion preferences used locally restricted grating stimuli, which may result in an underestimation of overall response strength. *Huston and Krapp* (*2008*) mapped the receptive fields of ADNMNs and FNMNs using square wave gratings with a side length of 62.6° that moved in 16 different directions on a CRT monitor mounted on a semicircular frame (for further details see *Huston and Krapp 2008, 2009*). This allowed for a spatially structured measurement of the motor neurons' directional preferences. The advantage of this technique is that locally measured motion sensitivities add up to a particular arrangement of motion vectors that represents the cell's preferred global optic flow at high spatial resolution. However, there is a potential underestimation of response strength due to the small size of the local stimuli and a high activation threshold of the neuron. In such case, the neuron would respond to the full optic flow pattern because it is stimulated above its spiking threshold, but it would not respond to single local components of the pattern because they are too weak to depolarize the cell strongly enough. This in turn would lead to a wrong understanding of the neuron's preferred optic flow. The set-up used in the present account is the first measurement of motion-tuning in neck motor neurons that uses panoramic full field stimulation with complex patterns and pseudo self-induced movement.

2.2.3. Visual stimulation: local stimuli

Local square wave gratings were presented to assess the sensitivity of the ADNMNs for local preferred stimuli of the HS-cells. The HS-cells have their peak sensitivity for front-to-back optic flow at different elevations in the visual field (**Figure 4**) and are prime candidates for relaying visual information onto ADNMNs via yet unidentified descending neurons (presumably DNColHS, **Figure 9**). Thus, ADNMNs are expected to respond to the same stimuli as HS-cells.

According to these peak sensitivities, square-wave gratings that would maximally excite HSN, HSE or HSS were programmed. The gratings covered ipsilateral parts of the arena, extending horizontally from 20° to 120° on the right side (0° azimuth is in front of the fly), sparing the region of binocular overlap to make sure that only cells on the ipsilateral side were stimulated and contralateral input onto ADNMNs would be excluded. Vertical extents ranged from -48° to -8° (for HSS), from -20° to 20° (for HSE) and from 8° to 48° (for HSN) in elevation (Figure 20 A-C, see also Figure 4). Additionally, gratings that extended across the full ipsilateral vertical extent of the arena (Figure 20 D) and gratings that covered the full arena were used.

Figure 20: Local stimuli with different vertical extent to maximally stimulate individual ipsilateral HS-cells. A square wave grating of λ = 30° spatial wavelength, 100° width and 40° height was displayed on the right part of the arena, so that it would maximally excite either A HSN, B HSE or C HSS. D To excite all three HS-cells equally, the grating covered the full vertical extent of the arena on the right side (100° width, 96° height). The region of binocular overlap (0°-20° frontally on both sides) was not activated to exclude contralateral ectivation.

All square wave gratings had a spatial wavelength of 30° and were moved front-to-back and back-to-front for 1 s at a temporal frequency of 5 Hz (frame rate 150°/s) at maximum contrast for maximum stimulation of the respective HS-cell. The vertical edge length of 40° (Figure 20 A-C) led to an overlap of neighboring stimuli of 12°, so that one stimulus would always excite two HS-cells (i.e. the stimulus extending from -48° to -8° would excite HSS maximally but HSE would also respond to it). This stimulus design was chosen because smaller sizes (i.e. stimulus extents of -48° to -16° for HSS, -16° to 16° for HSE and 16° to 48° for HSN) failed to elicit responses in the ADN motor neurons in a set of preliminary experiments.

The small field square wave grating stimuli were used exclusively in experiments on the ADN. They served to measure the ADNMNs' sensitivity to local versus global stimuli as well as to activate the HS-cells during dual recordings of HS-cells and ADNMNs.

2.2.4. Visual stimulation: sudden luminance changes

Low frequency flicker was used to test responses to light-on and light-off in FNMNs. For this, the full LED arena was lit up for 2 seconds displaying the virtual checkerboard room at maximum contrast (Figure 19 B), and switched off for 2 seconds displaying darkness ("ON/OFF" stimulus). This was repeated three times. Response frequencies were calculated by measuring the response time and counting single spikes. Responses to the switching on and switching off of the fluorescent lamp were often observed but not quantified.

2.2.5. Tactile stimulation

Tactile stimuli were delivered to the fixed fly in the set-up when the arena was switched off and the animal was in complete darkness (only a computer monitor was illuminated at considerable distance from the electrophysiology setup). A small piece of cleaning tissue was gently streaked across the bristles on the back and the vertex of the animal's head, as well as across the ventral side of its abdomen. Tactile stimulation was only used during recordings from FNMNs, responses were not quantified.

2.3. Data analysis

2.3.1. Signal detection

The output signals of the amplifiers operating in bridge mode (extracellular amplifier: custom built from the MPI of Biological Cybernetics workshop, Tübingen; intracellular amplifier: SEC-10L, npi electronics) were fed to a PC via an A/D converter (PCIDAS6025, Measurement Computing) at a sampling rate of 10 kHz for intracellular recordings and 30 kHz for extracellular and dual (intra- and extracellular) recordings. Stimulus patterns and control, data acquisition, spike sorting and data analysis were programmed in MATLAB (MathWorks).

In extracellular recording traces from the ADN, two motor units were present which were classified according to their spike amplitude. A maximum of two waveforms were present in the recordings (see Figure 23 A). In intracellular recordings from individual FNMNs only one unit was present at a time (see Figure 35, Figure 42 A). Spikes were separated from the baseline using a threshold operation in MATLAB.

Response frequencies of spiking motor neurons were quantified by calculating the spike frequency during stimulation (1 s or 500 ms) and subtracting the mean resting frequency calculated 500 ms before stimulus onset. Trials in which spontaneous bursts occurred during spontaneous muscle contractios were discarded.

For the quantification of graded responses in HS-cells (Figure 4 B), DNOVS1 and in some subthreshold FNMN responses, the average membrane potential for equivalent time windows was compared (i.e. average membrane potential in mV during stimulation time minus average membrane potential during 500 ms before stimulus onset).

2.3.2. Plots

The responses of all types of cells (ADNMNs, FNMNs, HS-cells, DNOVS1) to the set of 62 rotations ("31 axes" stimulus) were plotted in three-dimensional spherical representations of visual space and in two-dimensional Mercator maps (*Borst and Weber 2011*). Both the three-dimensional sphere and the two-dimensional map cover the full extent of visual space (360° in azimuth and

180° in elevation). Gridlines run in 30° intervals along azimuth and elevation, with each gridline crossing defining a particular axis (see **Figure 26**).

A rotation of the virtual fly - used to generate the stimulus movies (**Figure 19**) - around any of these axes produces rotational optic flow in the opposite direction that is then displayed to the real fly in the experiment on the LED arena (i.e. a clockwise rotation of the virtual fly around the [0,0] axis results in counterclockwise optic flow displayed to the real fly, a clockwise rotation of the virtual fly around the [90,0] axis results in downward-pitch optic flow displayed to the real fly, etc.) (**Figure 19, Figure 21**).

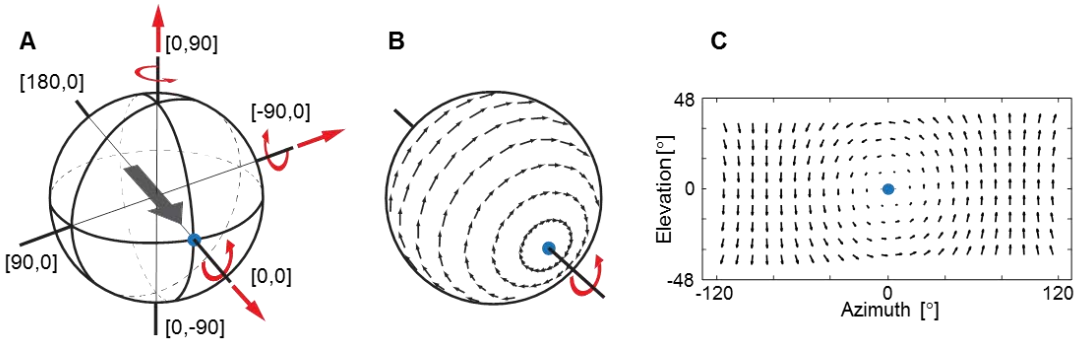

Figure 21: Optic flow field resulting from a clockwise roll rotation of a virtual fly. A: The gray arrow represents a virtual fly which is used for stimulus design, oriented along the Z-axis in the center of a three-dimensional sphere, facing the coordinates [0,0] (marked by the blue dot). For the "3 degrees of freedom" stimulus, the fly can be rotated around and translated along its X-, Y- and Z-axis (red arrows). These movements result in image shifts on the eyes of the fly (optic flow). **B:** The virtual fly is rotated around its Z-axis (longitudinal axis) in a clockwise fashion. The optic flow field resulting from this rotation is plotted on the visual sphere, where the length of the motion vectors represents the speed of the rotation at the respective point. The optic flow field opposes the direction of rotation with the highest speed of optic flow at 90° from the axis of rotation. **C:** The same optic flow field as depicted in **B**, projected onto a 2D coordinate system. The clockwise rotation oft he virtual fly leads to counterclockwise optic flow with the blue dot marking the coordinates of the axis of rotation [0,0]. The orientation and length of each arrow in this representation of optic flow indicate the direction and speed of local image shifts at different positions within the visual field. Only the part of the visual field that is presented on the LED arena is shown in **C**.

The arrows indicating the direction of rotations and translations (**Figure 21 A**) refer to the movement of the virtual fly, which opposes the direction of optic flow displayed on the arena. In the graphical representations of the receptive fields as in **Figure 21 C**, the left border of the arena corresponds to an azimuth of -120° and the lower border corresponds to an elevation of -48°. In this configuration, the point [0,0], towards which the fly's pseudopupils are oriented lies in the center of the arena surface.

Although most recordings derive from the right side of the nervous system, the data were mirror-transformed in order to allow for better comparability with previous accounts, where data was plotted with respect to recordings or simulations from the left part of the nervous system (*Huston and Krapp 2008; Borst and Weber 2011; Wertz et al. 2012; Kauer et al. 2015*).

For the calculation of the average preferred optic flow vectors in the FNMNs from the responses to the “31 axes” stimulus, the motion vector distribution from each of the 62 presented rotations was multiplied with the relative response strength of the FNMN for that particular stimulus (see Figure 39 C).

2.3.3. Measurement of haltere movements

During the recording of haltere activity with a highspeed camera (MotionPro Y3; Integrated Design Tools Inc.), the “3 degrees of freedom” stimulus was displayed for its whole duration of 12 s in non-randomized order.

Video data was acquired with the Motion Studio software package at a rate of 100 frames per second. A custom-written MATLAB script that tracks the position of the haltere in each frame from a 288 x 312 pixel ROI (full resolution of the image was 1280 x 1024 pixel) as described in *Haag et al. 2010* was used to analyze the movies. The knob of the haltere measured around 6 x 6 pixels within the ROI and was clearly visible (Figure 16).

A frame rate of 100 fps was not high enough to reliably track the natural haltere beating frequency of 110-180 Hz in flying blowflies (*Nalbach 1993*), but it allowed the storage of longer movies. A frame rate of 100 fps was sufficient for the present set of experiments because only the presence of haltere activity per se and its total duration were of interest, not its exact frequency. To quantify the relative duration of haltere activity, the number of frames in which the haltere oscillated during the movie was counted and divided by the full duration of the movie (2500 frames).

Movies in which the animal was free to move its head and abdomen were filmed without simultaneous electrophysiological recording, movies from fully fixed flies and flies that were able to move their abdomen were filmed during simultaneous whole-nerve recording from the ADN with a suction electrode.

2.4. Histology

2.4.1. Nerve cross sections

For nerve cross sections as shown in Figure 22 and Figure 34, a fly was fixated in glutaraldehyde (Science Services). The nervous system was dissected out, washed in 0.1 M phosphate buffer and embedded in 4 % low melting agarose (Serva). A small block comprising the thoracic ganglion and the thoracic nerves was cut out and washed in 0.1 M sodium cacodylate (Sigma-Aldrich). It was incubated in 1 % osmium tetroxide (Science Services) for 15 minutes and dehydrated in a series of 30, 50, 70, 90, 96, and 2 x 100 % ethanol. The tissue was embedded in Epon (Serva) and polymerized at 60° C for 2 days.

For electron microscopy, ultrathin sections of 60 nm were cut with an ultramicrotome (EM UC6i; Leica), collected on grids coated with formvar (Science Services) and counterstained in 1 % uranylacetat. Sections were observed with a transmission electron microscope (JEM-1230, Jeol) at an accelerating voltage of 80 kV and 4000-fold magnification. Images were acquired with a CCD camera (SC1000 Orius; Gatan) and processed with the related software (DigitalMicrograph, Gatan). For light microscopy, semithin sections of 1 µm were cut with an ultramicrotome (Leica Ultracut E; Reichert-Jung) and stained with Toluidine blue O (Sigma-Aldrich). The cross-sections were observed with a light microscope (Axiophot; Zeiss) and photos were taken with a CCD camera (DFC 490; Leica).

2.4.2. Single cell staining

For single cell stainings as shown in Figure 36 and Figure 41, cells were injected with a mixture of Alexa Fluor® 488 (Life Technologies) and Neurobiotin (Vector Laboratories) through the tip of the intracellular recording electrode. The fluorescent dye Alexa 488 made it possible to identify the cell type during the intracellular recording. Neurobiotin was essential to reveal the cell's anatomy in greater detail post-hoc and visualize electrical coupling with other neurons using a confocal microscope (TCS SP5; Leica).

The fly was kept intact after injection and rinsed with saline solution for at least 60 minutes at room temperature in the dark to allow for diffusion of the Neurobiotin into the entire recorded cell and into neighboring cells sharing gap junctions. The whole animal was fixed in 4 % paraformaldehyde (PFA) and 0.2 % glutaraldehyde at 4°C overnight. The next day, the nervous system was dissected out, washed for 2 x 45 minutes in phosphate-buffered saline (PBS) containing 2.5 % Triton X-100 (Sigma-Aldrich) and for 10 minutes in PBS containing 1 % Triton X-100 (PBT). Streptavidin-Alexa 568 Conjugate (Life Technologies) was added at a ratio of 1:50 to the PBT to visualize the Neurobiotin by coupling it to Streptavidin carrying Alexa 568 as a fluorophore. The tissue was incubated overnight at room temperature in darkness. The next day, the tissue was rinsed in PBS for 4 x 20 minutes and mounted (ibidi Mounting Medium; ibidi) for confocal microscopy to check for red fluorescent Alexa 568 staining, which represents effective binding of Streptavidin to Neurobiotin. If strong red fluorescence was present under the confocal microscope, the tissue was further processed to become translucent and permit better optical resolution in the Z-plane.

The Sca*l*e method developed by *Hama et al.* (*2011*) for optical clearing of mouse brain was employed and proved suitable to clear samples as small as a fly nervous system. The method cleared the surrounding tissue while the brightness of the conjugated Alexa 568 was not affected.

To apply Sca*l*e, samples were incubated in PBS containing 20 % sucrose for one day and shortly frozen with liquid nitrogen afterwards to make them porous. They were thawed and rinsed with PBS and re-fixed in 4 % PFA for 30 minutes. Then they were incubated in Sca*l*e A2 solution (4M urea + 0.1 % Triton X-100 + 10 % glycerol) until they became transparent, which took 5-10 days. All Sca*l*e-steps were carried out at room temperature to speed up the clearing process.

Transparent tissue was then washed in PBS and mounted again for confocal microscopy. Three-dimensional reconstructions of dye-filled cells were produced with the AMIRA software package (version 5.3.1) (see **Figure 36**).

3. Results

The aim of this study is the characterization of prothoracic neck motor neurons of the anterior dorsal nerve (ADN) and the frontal nerve (FN) to gain insight into their visual sensitivity for panoramic optic flow and into their presynaptic visual input.

In extracellular recordings, the tuning of ADNMNs to panoramic visual stimuli was measured and compared to the tuning of the three HS-cells, which are prime candidates for relaying visual signals onto the ADN motor neurons via yet unidentified descending neurons. Furthermore, dual recordings from ADNMNs and HS-cells were carried out to test for the suggested neuronal pathway from HS-cells via descending neurons onto the ADNMNs.

In intracellular recordings, the tuning of individual FNMNs to panoramic visual stimuli was measured. Injecting Neurobiotin tracer into the recorded cells at the same time allowed for post-hoc anatomical reconstruction of the recorded motor neuron and assignment of the measured visual motion tuning to a specific anatomical cell type.

3.1. The anterior dorsal nerve (ADN)

In order to characterize the response properties and the sensitivity for panoramic visual stimuli in ADNMNs as well as to identify their presynaptic visual input from LPTCs, extracellular nerve suction recordings from the ADN and intracellular recordings from HS-cells in the lobula plate were carried out. In addition, the membrane potential of either HSN or HSE was manipulated during simultaneous recording from ADNMNs to test proposed synaptic connections (*Strausfeld and Bassemir 1985b; Strausfeld et al. 1987; Huston and Krapp 2008*).

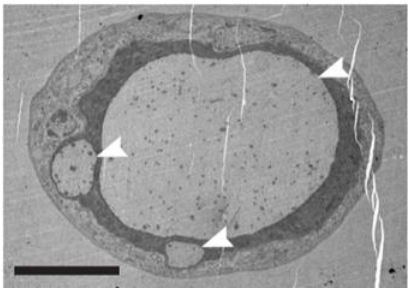

Figure 22: Transmission electron microscope image of an ultrathin (60 nm) ADN cross section. White arrowheads mark the profiles of three axons that differ strongly in their diameter. The large profile belongs to ADNM1, the two smaller profiles belong to ADNM2 and the VUM neuron. The cross-section was taken approximately 200 µm away from the prothoracic ganglion. Scale bar: 10 µm.

Nerve cross-sections confirmed the existence of three axons projecting through the nerve, as reported from earlier studies: They belong to the two ADNMNs and the ventral unpaired medial neuron (VUM), which is not visually sensitive (*Strausfeld and Seyan 1985; Milde et al. 1992*). The profiles of the three axons in the cross-section differ considerably in size, the large one measuring

around 20 µm in diameter, and the two small ones only around 4 µm (Figure 22). This difference in cell size has been reported in earlier studies (*Strausfeld and Seyan 1985; Strausfeld et al. 1987,* see Figure 8 A), where the larger cell was termed ADNM1 and the smaller cell ADNM2. *Strausfeld and Seyan* (*1985*) report an axon diameter of 5-8 µm for ADNM1 and 1-1.5 µm for ADNM2, which reflects a similar size ratio as measured in the present study.

3.1.1. Recording from ADNMNs

Two units that both fire action potentials in response to visual motion in a direction selective manner were present in extracellular whole-nerve recordings from the ADN. In earlier studies it has been reported that the preferred direction of optic flow for both motor units is horizontal front-to-back motion (*Milde et al. 1987; Gilbert et al. 1995; Huston and Krapp 2008*).

Here, a checkerboard-wallpapered virtual room (see Figure 19) was rotated around the Y-axis in both directions (yaw rotation) at a velocity of 150°/s to activate the motor neurons. The two ADNMN units differ in their spike amplitude and response characteristics.

One unit was usually spontaneously active and exhibited tonic excitation upon stimulation in the preferred direction, while being inhibited by the stimulus moving in the anti-preferred direction (null direction) (Figure 23 A). It fired action potentials with smaller amplitudes than the other unit in all experiments, thus it was termed “small ADNMN”. The second motor unit was not spontaneously active and responded to a smaller set of stimuli than the small ADNMN. Due to its larger spike amplitudes it was termed “large ADNMN” (Figure 23 A). The response behavior of the two ADNMNs has also been described in earlier studies, where local square wave gratings were used as visual stimuli (*Milde et al. 1987; Huston and Krapp 2008*).

On average, the small unit responded with a lower spike frequency than the large unit. The frequency was calculated from n = 28 trials in N = 7 animals. The mean response frequency per cell type (small ADNMN, large ADNMN) was calculated for each animal first and then the mean ± SEM over all animals was calculated for the two cell types.

The mean response frequency had its maximum at 45.1 ± 5.4 Hz for the small ADNMN and at 77.8 ± 5.9 Hz for the large ADNMN (Figure 23 B). In many recordings only one unit was present while the second unit was absent even with full field visual stimulation in the preferred direction (front-to-back yaw). Based on its amplitude and response behavior, this active unit was always the small ADNMN. In many recordings, two units were active initially, but after a short time (2-3 sets of visual stimuli) the large ADNMN became silent and responded no longer.

Since a definite assignment of the neuronal signals to the anatomical profiles of the ADNMNs (Figure 22) is not possible in the present account, the features “small” and “large” refer to the spike amplitude, not to the axon diameter of the motor neurons. However, it is likely that the large spikes derive from the large diameter unit ADNM1 and the small spikes from the small diameter unit ADNM2.

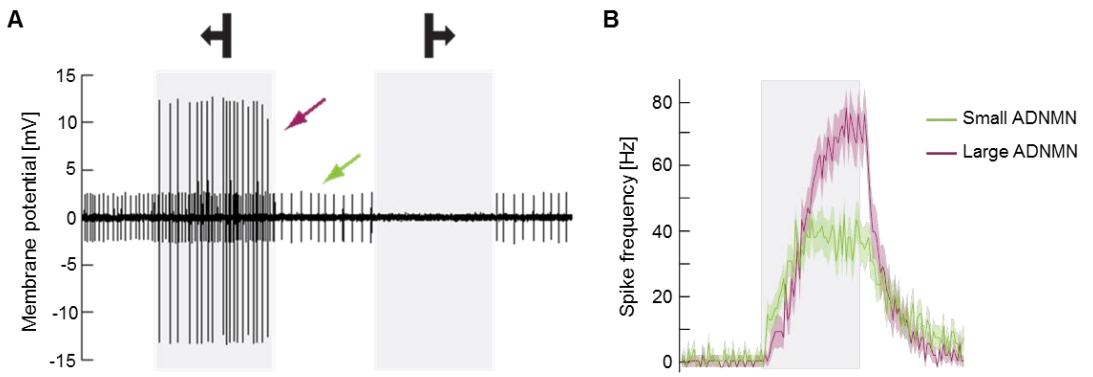

Figure 23: Extracellular recording from the ADN as measured from the left part of the nervous system. A: Two visually sensitive units are present in the nerve suction recording. They differ strongly in spike amplitude and respond to motion in their preferred direction with an increase in firing rate, while they are not responsive to or inhibited by motion in their null direction. The two units were classified as "large ADNMN" (red arrow) and "small ADNMN" (green arrow) according to their action potential amplitude. Gray bars mark 1 s of visual stimulation with a panoramic yaw stimulus at 150°/s; black arrows indicate the direction of horizontal rotation. **B**: Mean response rate ± SEM of the two cell types to a panoramic pattern moving in the preferred direction. The gray bar marks 1 s of visual stimulation. Bin size = 20 ms, n = 28 trials in N = 7 cells of each type.

3.1.2. Local versus global sensitivity

To compare the visual sensitivity of the ADNMNs for spatially restricted stimuli with the sensitivity for panoramic wide-field-motion, the responses to local and global square wave gratings with λ = 30° spatial frequency and maximum contrast were measured in N = 4 flies. The gratings rotated horizontally (yaw movement) in both directions at 3.3 Hz temporal frequency and covered either the whole LED-arena or only ipsilateral parts of it that spared the region of binocular overlap and corresponded to the peak sensitivities of HSS, HSE and HSN (**Figure 24**).

The small ADNMN was weakly spontaneously active and exhibited excitation and inhibition upon both binocular and monocular visual stimulation. Among the small field stimuli it was most sensitive for the grating displayed most dorsally, which corresponds to the maximum sensitivity of HSN (**Figure 24**). Overall, the small unit preferred global over local optic flow. Irregular bursting activity was observed occasionally and always occurred together with bursts in the large ADNMN (see white arrowheads in **Figure 24**). The bursts do not seem to be triggered by the visual stimuli.

The large ADNMN exhibited irregular bursting activity that was not consistent across trials neither in its strength nor in its timing and thus seems uncorrelated with the visual stimulus (**Figure 24**). In trial 1-5 of **Figure 24** (lower panel) the large ADNMN apparently responds to the full field grating as the only stimulus that is able to elicit a visual response. In trials 6-16 irregular bursting dominates. It can be concluded from this experiment that the large motor unit of the ADN is not sensitive to small field motion, while global stimulation as shown in figure **Figure 23** does trigger responses. The 16 trials depicted in **Figure 24** are identical for both cells, i.e. the small and the large unit are firing together in the 16 original recordings (see **Figure 23 A**) but are plotted separately.

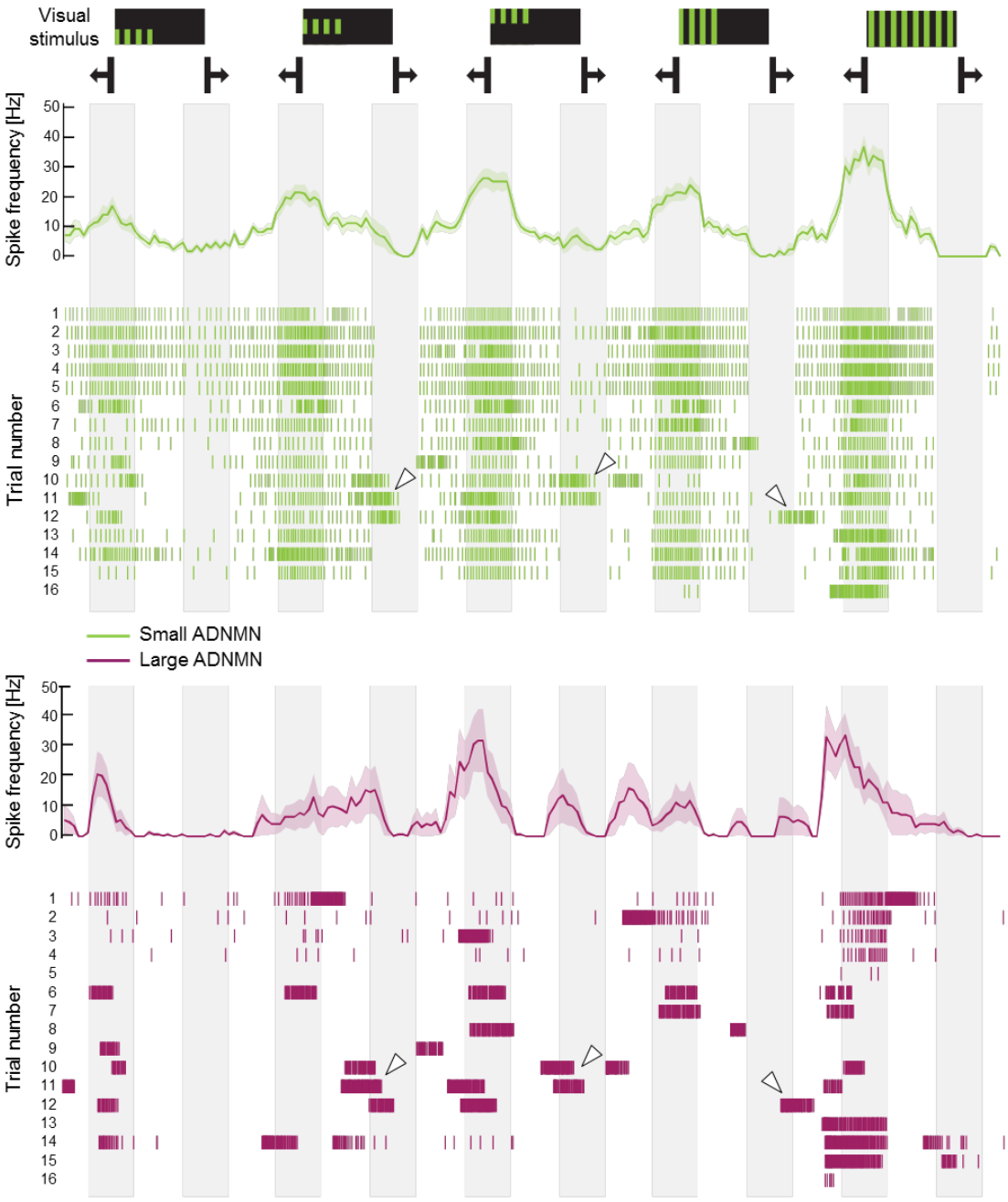

Figure 24: Activity of the two ADNMNs during presentation of a grating moving horizontally at different sizes and positions. The local stimulus is presented on the ipsilateral side of the LED arena, sparing the region of binocular overlap and covering either the lower, central or upper 40° of the 96° vertical extent. Larger stimuli cover the left monocular visual field or the full binocular extent of the arena. Stimuli were presented in the order depicted here from left to right. The mean ± SEM spike frequency was calculated from the same n = 16 trials in N = 4 animals for both ADNMNs (bin size = 100 ms). Individual trials are numbered in the raster plot below each other, where each bar represents an action potential. Gray bars mark 1 second of stimulus presentation, white arrowheads indicate exemplary bursts that seem uncorrelated with the visual stimulus. Black arrows indicate the direction of motion of the grating on the arena. All data are mirror-transformed: originally, stimuli were presented on the right side of the arena while recording from the right ADN.

3.1.3. Preferred optic flow of the ADNMNs

As shown in the previous chapter, ADNMNs prefer global over local stimuli and are thus expected to respond more vigorously to a visual scene that is displayed simultaneously to both eyes. The weak responses to local stimuli in the small unit and the absence of responses in the large one indicate that responses to panoramic stimulation would yield a more reliable representation of the ADNMNs' motion tuning.

To investigate the response characteristics of the ADNMNs for panoramic translations and rotations as they would occur when the fly was moving through its environment, high-contrast checkerboard patterns covering the full LED arena were used as visual stimuli (**Figure 19**). Three translations (sideslip, lift and thrust) and three rotations (pitch, yaw and roll) were displayed ("3 degrees of freedom" stimulus). The tuning was measured in N = 30 small ADNMNs and in N = 14 large ADNMNs.

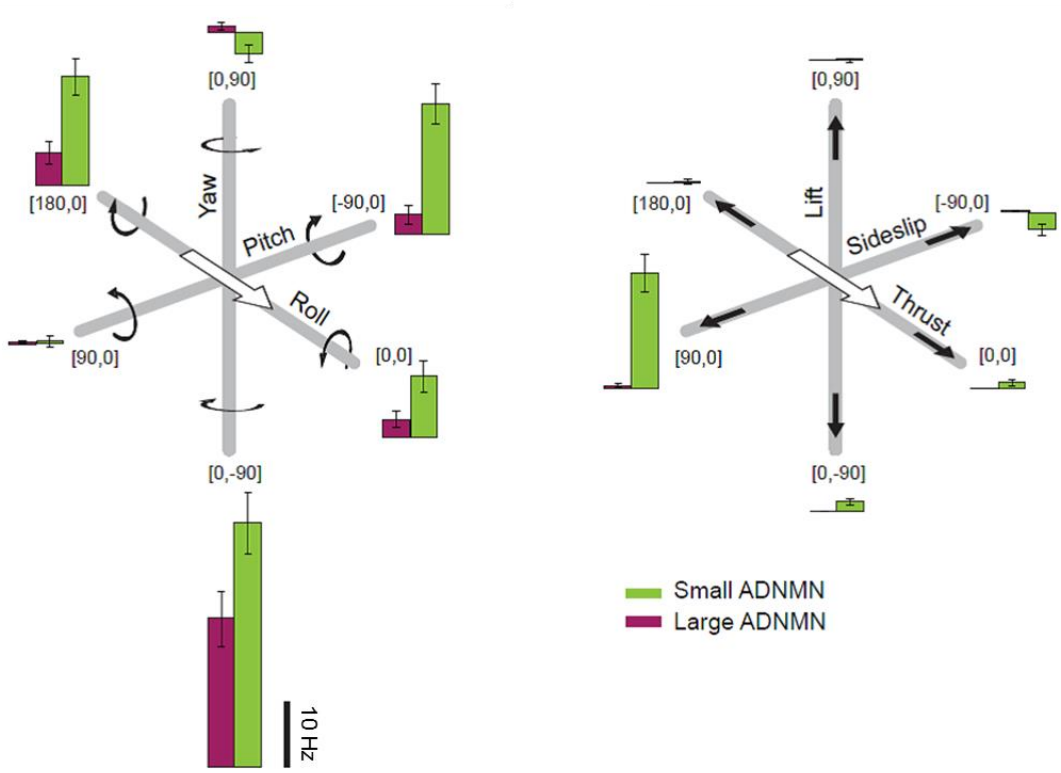

Figure 25: Visual sensitivity of the two ADNMNs for panoramic rotations and translations using the "3 degrees of freedom" stimulus. The white arrow marks the orientation of a virtual fly with its eyes pointing at [0,0]. Black arrows indicate its direction of rotation around the three main body axes (left panel) and translations along them (right panel). Movement of the virtual fly indicated by the black arrows results in optic flow in the opposite direction of motion displayed to the experimental fly. Both ADNMN units prefer yaw optic flow towards the recorded side (leftward yaw optic flow), as generated by a rightward rotation of the virtual fly. While the large ADNMN is not strongly tuned to any rotations other than yaw, the small ADNMN responds to clockwise and counterclockwise roll and upward pitch optic flow as well. Translations do not elicit responses in the large ADNMN at all. The small ADNMN responds exclusively to a sideward slip. Mean ± SEM response frequency from 30 small ADNMNs and 14 large ADNMNs.

In both the small and the large motor unit, rotations led to stronger responses than translations did (Figure 25). As expected from previous studies (*Milde et al. 1987; Huston and Krapp 2008*), both cells were most sensitive for a horizontal yaw rotation towards the recorded side. However, especially in the small ADNMN, pitch and roll rotations also elicited strong responses. Although the receptive fields published by *Huston and Krapp* (*2008*) contain weak vertical components, the responses to pitch and roll rotations recorded here are much stronger than expected from these receptive fields (see Figure 9).

3.1.4. Rotational motion tuning of the ADNMNs

Having observed a distinct preference of rotational over translational global optic flow (Figure 25), I continued with a more detailed characterization of the two motor neurons' sensitivity for rotations. From the tuning to the six rotational optic flow patterns of the "3 degrees of freedom" stimulus it is not yet possible to draw a detailed picture of the neurons' panoramic motion tuning. A larger set of rotational test stimuli is necessary.

Therefore, rotations around 31 axes in three-dimensional space were displayed on the LED arena ("31 axes" stimulus) in the next set of experiments. Rotations around each axis were displayed in clockwise and counterclockwise direction, resulting in 62 stimuli per trial.

The response strength of the two ADNMNs for each of the 62 stimuli was plotted in two-dimensional Mercator maps and three-dimensional spherical plots (see Material and Methods) that represent the same set of data in two different ways. The coordinates [0,0] represent the longitudinal axis of the fly, along which it is positioned to look at the stimulus on the LED arena. A rotation around this axis would result in "roll" optic flow. In all plots presented here, the black arrows indicating rotations mark the movement of the virtual fly that was used to design the visual stimulus (see Figure 21). A clockwise rotation of the virtual fly around the [0,0] axis results in counterclockwise roll optic flow presented to the experimental fly on the arena. Optic flow as generated by rotations around the three main axes is depicted in the 2D- and 3D-plots (Figure 26) as follows: counterclockwise roll optic flow at [0,0], clockwise roll optic flow at [180,0], downward pitch optic flow at [90,0], upward pitch optic flow at [-90,0], rightward yaw optic flow at [0,90] and leftward yaw optic flow at [0,-90].

Rotational motion-tuning of the small ADNMN was measured in N = 26 flies (n = 77 trials), tuning of the large ADNMN was measured in N = 14 out of these (n = 35 trials). In the other 12 recordings the large unit was either inactive or very weakly active (i.e. firing single spikes). These trials were discarded.

The mean response frequency for each of the 62 stimuli was calculated from all trials for one cell, then the mean ± SEM was calculated over all animals. The color coding in both plot types of Figure 26 represents the response strength for each axis, with red indicating an increase in spike frequency upon visual stimulation, blue indicating a decrease and green indicating no change in spike frequency upon visual stimulation. To smooth the intervals between neighboring axes, the values of the response frequencies were interpolated, rendering the color changes in the plots

smooth instead of patchy (**Figure 26**). Each crossing of gridlines in the Mercator maps and spherical plots represents one of the 62 tested axes. In the sphere plots it becomes obvious that 1) the axes at [-180,0] and [180,0] are identical and 2) both yaw axes run through just one pole that is the same for all azimuthal positions (**Figure 26**).

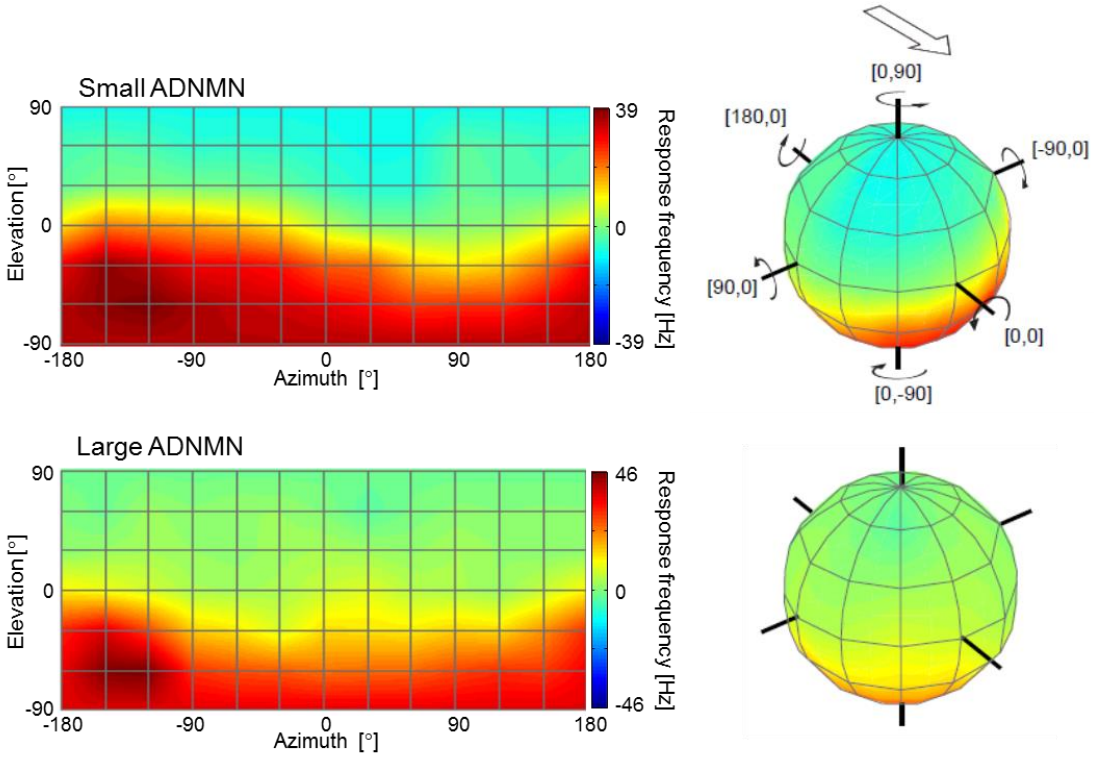

Figure 26: Rotational motion tuning of the two ADNMNs as measured with the "31 axes" stimulus. Two-dimensional Mercator maps (left) and three-dimensional spherical plots (right) reflect the motor neurons' sensitivity for panoramic rotations as they would occur during self-motion of the animal. Each crossing of gridlines represents an axis of rotation in both plot types, around which a virtual fly rotates, resulting in optic flow of the opposite sign being presented to the experimental fly on the LED arena. Response strength is color-coded: red represents an increase in spike rate, blue a decrease, green no response to a rotation arolund the respective axis. The white arrow in the upper right panel depicts the orientation of the virtual fly along the longitudinal axis (roll axis) with its eyes pointing at [0,0]. The rotations of the virtual fly around the three cardinal axes are depicted by the black arrows in the upper right panel.

The small and large ADNMN are tuned to similar panoramic optic flow, as expected from their receptive fields published by *Huston and Krapp* (*2008*) (**Figure 9**). They mainly respond to rotations with a front-to-back yaw component, represented by elevation positions between 0° and -90° in the 2D- and 3D-plots (**Figure 26**).

Averaged over all animals, in both motor units the strongest responses were measured for a clockwise rotation around the [-120,-60] axis: 38.68 ± 3.33 Hz (N = 26) in the small ADNMN and 46.09 ± 10.64 Hz (N = 14) in the large ADNMN (**Figure 26**). This rotation corresponds to leftward yaw optic flow with an upward pitch component (**Figure 27**). Again, no negative responses were observed in the large ADNMN due to its lack of spontaneous activity.

The tuning was broader in the small ADNMN, which responded not only to mainly horizontal optic flow but also to optic flow containing stronger upward pitch components (e.g. at [-60,-30], Figure 26). Figure 27 illustrates the vector distribution of two example optic flow fields on the LED arena, as generated by a clockwise rotation around the [-120,-60] and [-60,-30] axis.

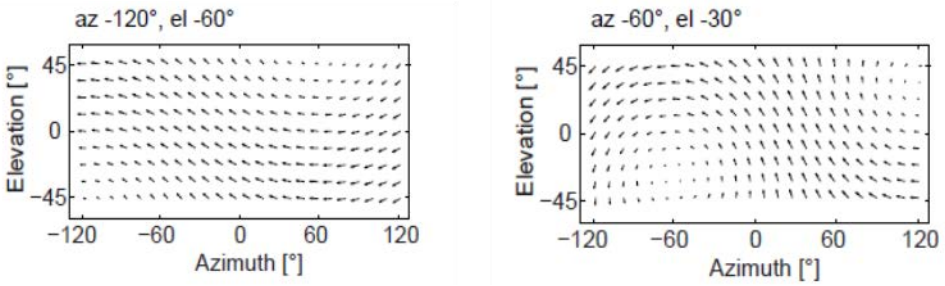

Figure 27: Example optic flow fields illustrating the distribution of motion vectors in the stimulus pattern. The optic flow fields correspond to rotations around the axes [-120, -60] (left) and [-60,-30] (right). Only the part of the visual field that is displayed on the LED arena is shown. The length of the vectors represents the motion speed, their orientation represents the direction of motion of the pattern. Both ADNMNs respond strongly to a rotation around the [-120,-60] axis, which is dominated by horizontal vectors (left), while only the small ADNMN responds to a rotation around the [-60,-30] axis, which is characterized by stronger vertical components reminiscent of a mixture between leftward yaw, upward pitch and counterclockwise roll (right).

3.1.5. Variability of responses

The strength of the ADNMN responses varied strongly across animals: Spontaneous firing rates varied between 0 and 99 Hz in single trials, the maximum response strength (regardless of the stimulus-axis) varied between 16.67 and 101.11 Hz in individual trials in small ADNMNs. The mean ± SEM over all maximum responses was 48.34 ± 2.61 Hz (n = 77 trials). In 11 out of 77 trials a rotation around the [-120,-60] axis was the preferred stimulus, in the other 66 trials other axes elicited stronger responses. Averaged over all animals the greatest mean response to the stimulus occurred at [-120,-60] (Figure 26).

In the large ADNMN, maximum responses in single trials ranged from 4.44 to 191.11 Hz. The mean ± SEM over all maximum responses was 59.68 ± 10.09 Hz (n = 35 trials). In 8 out of 35 trials a rotation around the [-120,-60] axis was the preferred stimulus, in the other 27 trials other axes led to stronger responses. Averaged over all animals (N=14) the mean response was greatest at [-120,-60] in the large ADNMN too (Figure 26).

3.1.6. The role of ipsi- and contralateral visual input

Neck motor neurons are expected to integrate signals from both visual hemispheres to selectively extract rotation information needed for gaze stabilization: with a higher degree of binocularity, the neurons can differentiate between rotations and translations (*Huston and Krapp 2008*). Since no direct anatomical evidence for visual input to ADNMNs exists, it is currently unknown if they receive signals from just the ipsilateral or both the ipsi- and contralateral lobula plate.

To elucidate the role of binocularity for the signal processing in ADNMNs, the effect of monocular occlusion on the rotational tuning and on response strength of the two motor neurons was tested. In this set of experiments only the small ADNMN was considered because monocular visual input did not elicit any responses in the large ADNMN (see Figure 24).

The ADNMN tuning was measured using the "31 axes" stimulus as described in the previous chapter, but in this set of experiments only one eye was open. In one group of flies the contralateral eye (i.e. on the opposite side to the recorded side) was occluded with black paint (N = 7 flies), in a second group the ipsilateral eye was occluded (N = 7 flies), and controls were performed on a third group of flies (N = 3) with both eyes painted black to verify the effectiveness of the eye cover. Responses were then compared with the binocular condition as depicted in Figure 26.

The strongest mean response calculated over all intact animals (N = 26) was 38.68 ± 3.33 Hz for a clockwise rotation around the [-120, -60] axis (Figure 26). When the contralateral eye was covered and the ADN received visual input only from the ipsilateral eye, the mean response rate of the small ADNMN was still highest for a clockwise rotation around the [-120,-60] axis, with 30.54 Hz ± 6.47 Hz mean response rate for this stimulus (n = 29 trials in N = 7 flies) (Figure 28 A). When the ipsilateral eye was covered and the ADN received visual input only from the contralateral eye, the strongest response frequency with a mean of 25.54 ± 7.35 Hz (n = 28 trials in N = 7 animals) was measured for the pure yaw stimulus at [0,-90] (Figure 28 C).

Vision was only weakly affected by the monocular covers: Maximum response rates of the small ADNMN varied between 15 and 85.56 Hz in single trials for the ipsilateral eye (39.03 ± 8.64 Hz across all maximum responses). For the contralateral eye, maximum responses ranged from 15 to 89.44 Hz in single trials (32.57 ± 4.25 Hz across all maximum responses).

All responses were normalized to the maximum response rate (38.68 Hz) in intact flies. Subtracting the relative response strength for all 62 axes in intact flies (Figure 26) from the relative response strength in flies with only ipsilateral visual input (Figure 28 A) revealed a significant difference for only one axis at [-150, 0] (paired t-test, $p < 0.05$ marked with an asterisk in Figure 28 B). Similarly, comparing the tuning of the small ADNMN with only contralateral visual input (Figure 28 C) with the rotational action field of intact conspecifics, differences were significant only for rotations around the [±180,-30] and the [-30, 0] axis (asterisks in Figure 28 D). Both the directional tuning and the response strength are very similar to the binocular condition.

Responses of both ADNMNs to yaw, pitch and roll optic flow are presented in Figure 29 to illustrate the effects of a one-sided eye cover. In the small ADNMN, response frequencies are lower when visual input reaches it only from the ipsilateral eye than when both eyes are open. However, this effect is not significant. The same is true for visual input reaching the small ADNMN only from the contralateral eye. Only when the animal is fully blind, effects are significant (paired T-test, $p < 0.05$) (Figure 29 A).

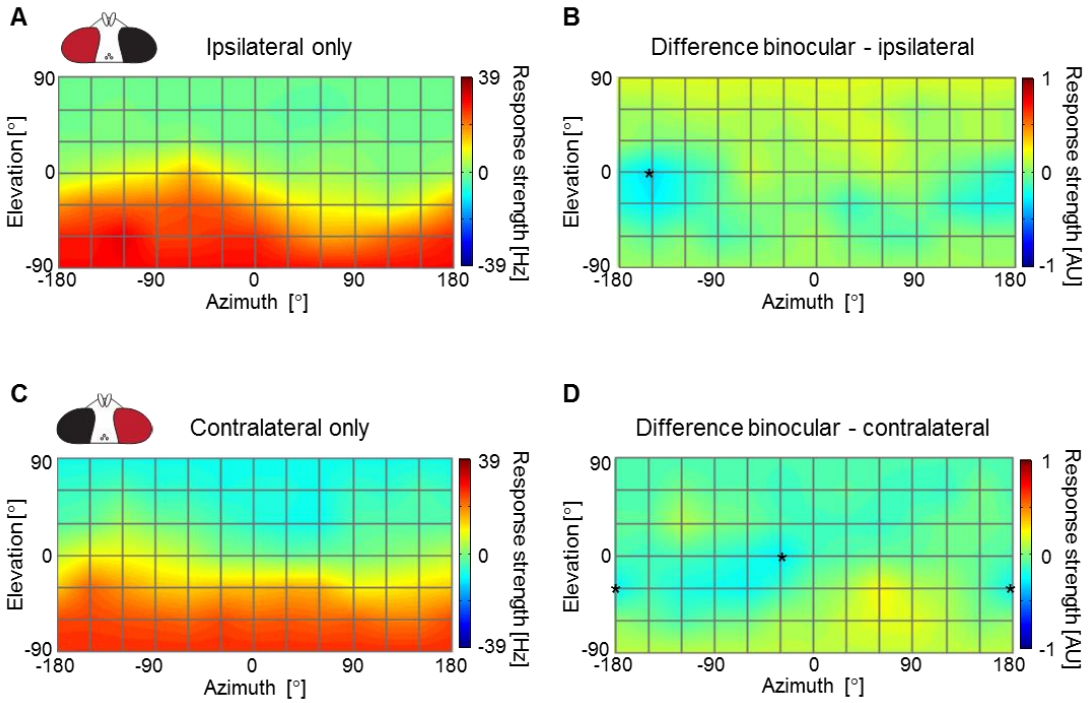

Figure 28: Monocular components of the rotational tuning in the small ADN motor unit. A: Rotational motion tuning with only the ipsilateral (left) eye open. The measured response strength is normalized to the maximum response strength from the binocular condition (**see Figure 26**). **B:** Subtracting the relative response strength for each stimulus in the binocular condition from the relative response strength with only ipsilateral visual input (N = 7) reveals only small differences. The asterisk marks the only stimulus where response reduction was significant ($p < 0.05$), a rotation around the [-150,0] axis. **C:** Tuning of the small ADNMN with only the contralateral (right) eye open (N = 7). Comparing it to the binocular condition, the sensitivity appears somewhat flattened. **D:** Significantly weaker responses were measured for clockwise rotations around the axes [-30,0] and [±180,-30] (marked by asterisks).

An interpretation for the weak impairment of function by monocular eyecover in the small ADNMN is that it receives about equally strong visual input from both eyes and that in the binocular condition the responses from the left and right eye are summed up in a highly sublinear manner, so that the response reaches its saturation level far below a linear addition of left and right input. Responses in the large ADNMN in contrast are abolished when visual input originates only from one eye (**Figure 29 B**). Roll and pitch rotations are non-preferred stimuli of the large motor unit and thus lead to only weak responses in the binocular condition already, so that the eye cover has no more effect. The fact that the large ADNMN responds to its preferred stimulus only when input arrives from both eyes leads to the conclusion that input from one eye alone is not strong enough to drive the neuron across its spike generation threshold.

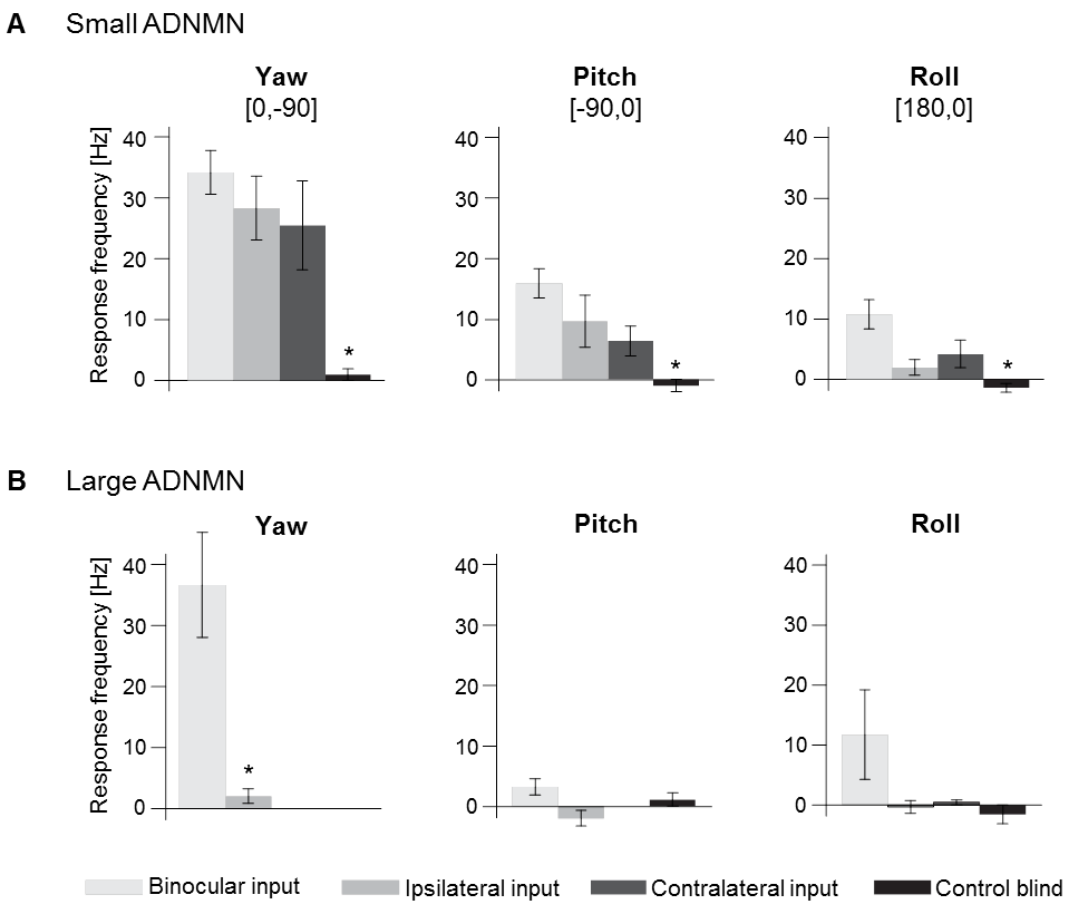

Figure 29: Responses to yaw, pitch and roll optic flow when vision is impaired. Leftward yaw, upward pitch and clockwise roll optic flow was presented to intact flies (data included in Figure 26) and flies with only their ipsilateral or contralateral eye intact (data included in Figure 28). Controls were carried out on flies with both eyes covered black (n = 12 trials in N = 3 flies). **A:** In the small ADNMN, the response frequencies upon monocular stimulation were not significantly different from responses to binocular stimulation. **B:** In the large ADNMN, responses were almost fully abolished for the yaw stimulus, when visual input was reduced to one eye. The roll and pitch stimulus did not elicit reliable responses in the binocular condition or with reduced vision. The mean ± SEM over all tested flies was calculated after averaging across trials in each fly.

3.1.7. Rotational motion tuning of the HS-cells

With their selectivity for horizontal motion, the HS-cells of the lobula plate are prime candidates to relay visual information onto the neck motor neurons of the ADN, which steer muscles governing head yaw movements. The tuning of the three HS-cells to panoramic rotating patterns ("31 axes" stimulus) was measured and compared to the tuning of the small ADNMN in the following set of experiments (**Figure 30**).

The motor neuron generates spikes while the HS-cells respond to visual stimuli with graded membrane potential changes. To enable comparison of tuning data from the motor neuron and from the three HS-cells, it was normalized to the respective maximum response after the mean over all animals was calculated for each of the 62 stimuli to allow for comparison. The normalized mean response of the motor neuron was then subtracted from the normalized mean response of

HSN, HSE and HSS respectively. Differences in their motion tuning are color coded in the right panels of **Figure 30**: green represents equal response strength, red a stronger response in the HS-cell and blue a weaker response in the HS-cell compared to the small ADNMN.

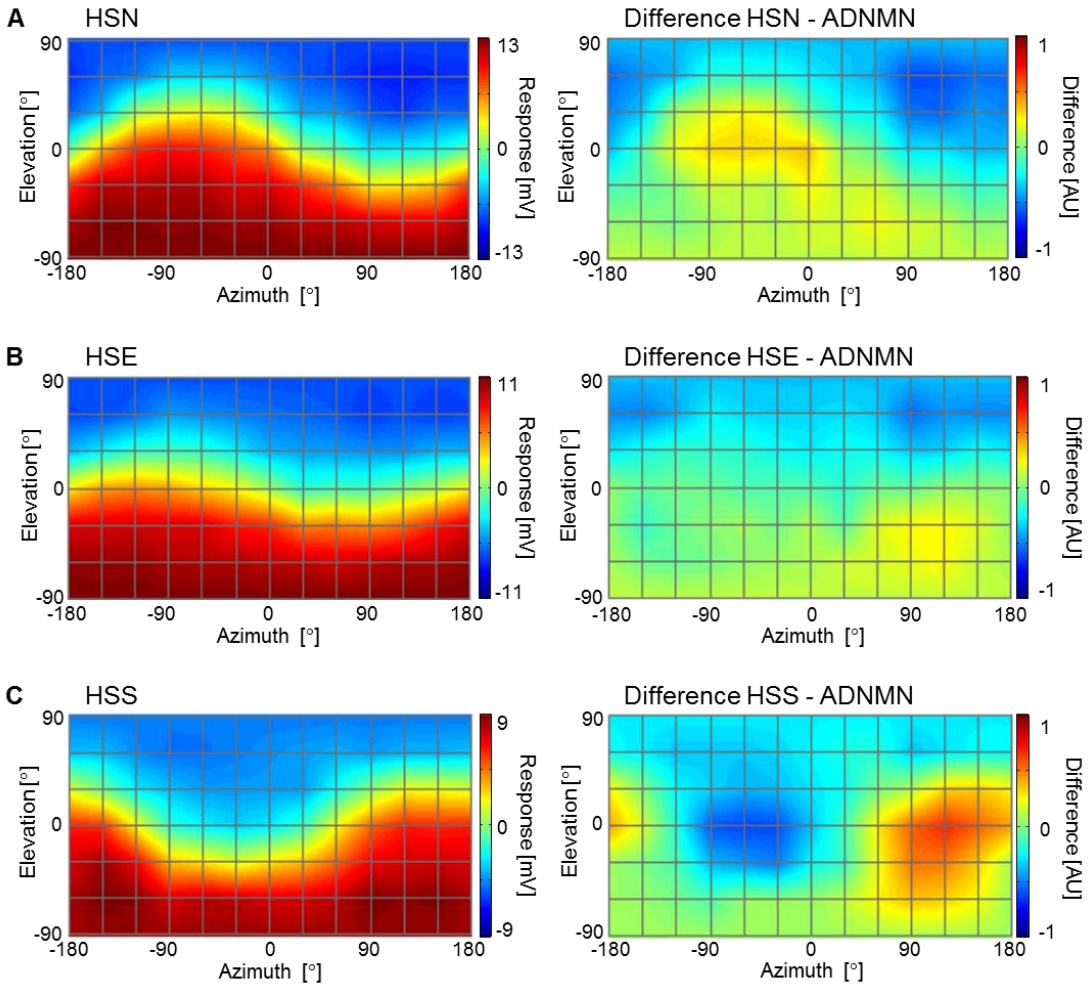

Figure 30: Rotational motion tuning of the three HS-cells in comparison to the small ADNMN. A: HSN responds to a very similar set of rotations as the ADNMN, it prefers leftward yaw and responds to even stronger upward pitch components (around [-90,0]) than the ADNMN. Mean of n = 11 trials in N = 5 cells, maximum response = 13.07 ± 2.72 mV (SEM) at [0,-90]. Note that the negative differences in the right panel mainly derive from the HS-cell's graded hyperpolarization compared to zero activity in the ADNMN. **B:** The tuning of HSE is also strongly reminiscent of the ADNMN tuning. Mean of n = 15 trials in N = 7 cells, maximum response = 11.69 ± 1.29 mV (SEM) at [0,-90]. **C:** Unlike HSN and HSE, the rotational tuning of HSS diverges from the ADNMN. HSS prefers downward oriented optic flow, while the motor neuron is more sensitive to upward rotations. This is reflected in the strong differences around 120° azimuth (right panel). Mean of n = 10 trials in N = 5 cells, maximum response = 9.28 ± 1.37 mV (SEM) at [90,-60].

The tuning of HSN and HSE to panoramic rotations is highly similar to the tuning of the small ADNMN. HSN and HSE both prefer horizontal rotations towards the ipsilateral side (leftward) that contain an upward pitch component. HSS in contrast, responds more strongly to leftward yaw with a downward pitch component. This is in line with results from earlier studies, where small field stimuli have been used to map the receptive fields of the three HS-cells (**Figure 4**).

Not only the preferred direction of motion but also the spatial structure of the receptive field is very similar in HSN/HSE compared to the small ADNMN: the motor neuron is sensitive for spatially restricted horizontal motion in the upper and equatorial ipsilateral visual field, while a horizontal grating in the lower ipsilateral visual field that excites HSS is not able to trigger responses in the motor neuron (Figure 24). Hence, HSS is unlikely to play a role in shaping ADN motion tuning.

Thus far, the experiments of this study point strongly towards HSN and HSE playing a major role in the shaping of the ADNMN response, possibly they are even sufficient to provide exclusive ipsilateral input. However, the physiological proof of signal transmission from HSN and HSE onto one or more descending neurons that innervate one or both ADNMNs is still missing. The attempt to bridge this knowledge gap is subject of the next chapter.

3.1.8. Dual recording and current injection

To unambiguously prove a physiological connection between two neurons, activation or inactivation of one cell must have an effect on the other one. If they are connected by electrical synapses, this effect has the same sign: depolarization of neuron 1 leads to depolarization of neuron 2, hyperpolarization of neuron 1 leads to hyperpolarization of neuron 2. If the synapse is chemical, the sign can also be inverted.

To test for connectivity between HSN/HSE and the motor neurons, ADN activity was recorded with an extracellular suction electrode while the membrane potential of either HSN or HSE was manipulated by passing positive or negative current through the tip of a sharp intracellular recording electrode into the HS-cell axon (Figure 17).

Surprisingly, depolarization or hyperpolarization of HSN or HSE affected the activity of the small ADN motor neuron only weakly (Figure 31 A) and had no effect at all on the large unit. However, the effect on the small ADNMN was significant for HSN in both polarities ($n = 10$ trials in $N = 4$ flies, t-test comparing the net change in spike frequency during current injection with the change in spike frequency without the current injection: $p < 0.05$) and for HSE only upon depolarization ($n = 6$ trials in $N = 4$ flies, $p < 0.05$). Only trials in which the HS-cell responded to visual stimulation and had a resting potential below -35 mV were included in the analysis to make sure that the cell was physiologically functional and the contact of the intracellular electrode was stable. In most trials both ADNMNs were not spontaneously active, a circumstance that could not be changed by depolarizing either HS-cell. This led to the assumption that the resting potential of the motor neurons is too negative for the current injection alone to elicit spikes if the neuron is not spontaneously active. The results plotted in Figure 31 A derive from a small number of recordings in which the small ADNMN was spontaneously active.

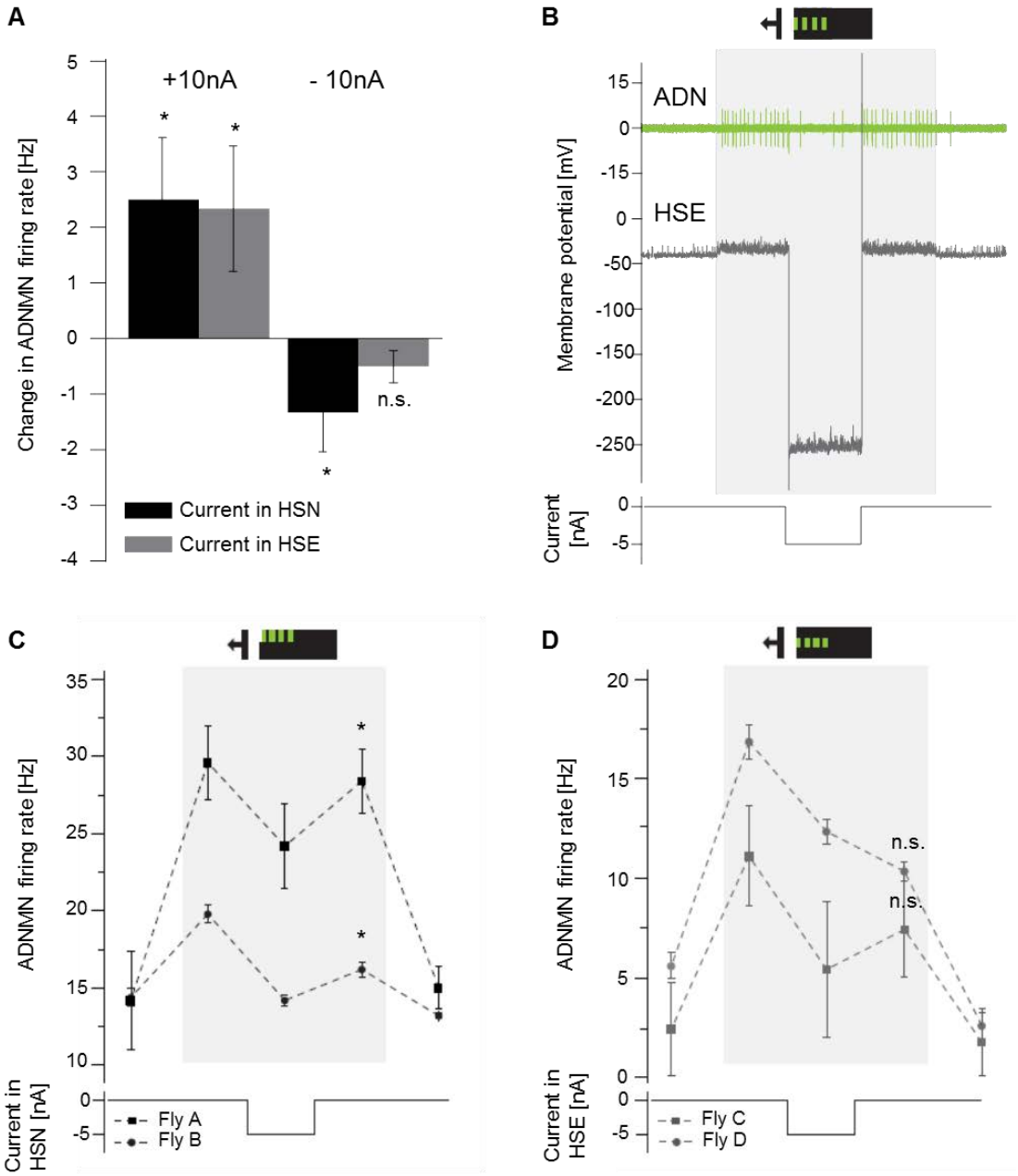

Figure 31: Paired recordings from the ADN and HS-cells. A: De- and hyperpolarization of HSN or HSE by passing +10 nA or -10 nA current through the tip of the intracellular recording electrode without simultaneous visual stimulationhad only weak effects on the spontaneous firing rate of the small ADNMN. Mean ± SEM of N = 4 flies for both HSN and HSE. **B:** Paired recording from the ADN and the HSE cell including hyperpolarization during visual stimulation. Both the small ADNMN and the HS-cell respond to a grating moving in the preferred direction of the two cells (horizontal front-to-back motion) for 6 seconds as indicated by the gray bar. Hyperpolarizing HSE for 2 seconds by passing -5 nA current through the tip of the intracellular electrode leads to a decrease of the ADNMN firing rate that recovers when HSE is back at its normal membrane potential and the grating is still moving. Before and after the visual stimulation the ADN is silent. **C:** Hyperpolarization of HSN during presentation of a grating in the upper part of the ipsilateral LED arena leads to a significant and reversible decrease of the small ADNMN's firing rate. Mean ± SEM of n = 4 trials in each of the two flies. **D:** Hyperpolarization of HSE during visual stimulation with a grating in the equatorial part of the ipsilateral arena also led to a reduction of the ADNMN firing rate but recovery was not significant. Mean ± SEM of n = 3 trials in Fly C, n = 4 trials in Fly D. One example trial of Fly D is shown in panel B.

To make a measurement of spike frequency changes possible, another set of experiments was carried out: visual stimulation was used to generate baseline spiking in the motor neurons before the membrane potential of an HS-cell was manipulated. A horizontal small-field grating as shown in Figure 20 A and B was displayed on the ipsilateral side of the arena to activate either HSN or HSE as well as the small unit of the ADN. The grating was moved front-to-back at a temporal frequency of 3.3 Hz for 6 seconds. This triggered spiking activity in the small ADNMN. The large ADNMN was silent throughout all experiments, which can be explained by its lack of sensitivity for monocular small field stimuli (see Figure 24). The HS-cell was hyperpolarized for 2 seconds during the movement of the grating to silence its activity and monitor the effect of its shutdown on the visually evoked spiking response of the ADNMN (Figure 31 B). Due to technical limitations it was not possible to shut down both HSN and HSE at the same time by passing hyperpolarizing current through their axons.

Shutting down either HSN or HSE during visual stimulation by injecting -5nA negative current into its axon led to a weak suppression of the small ADNMN's visually evoked response (Figure 31 C and D). Recovery of the ADNMN response after the HS-suppression indicated that the effect was indeed a result of the HS-cell hyperpolarization and not a consequence of adaptation. Weak but significant recovery was found only in trials with HSN stimulation and shutdown ($n = 3$ trials per fly, t-test comparing the ADNMN spike frequency during the first second of HS-hyperpolarization with the ADNMN spike frequency in the first second after the hyperpolarization, $p < 0.05$) (Figure 31 C).

Since both HSN and HSE are supposed to be indirectly presynaptic to the ADN motor neurons it was surprising to observe such a small effect of their respective shutdown onto the visual ADNMN response. Possible reasons for this will be discussed later.

3.1.9. Responses to nonvisual input

In extracellular recordings from the ADN, the large unit often fired bursts that were not clearly correlated with the visual stimulus (see Figure 24). These high frequency discharges occurred randomly, rarely between trials but often during panoramic visual stimulation without an obvious correlation to the stimulus itself. They could possibly derive from sensory input other than vision or alternatively be triggered internally.

Non-visual sensory input was reduced to a minimum in the experimental setup: Air stream or mechanical stimulation can be excluded as sources of sensory stimulation. However, although the animal is firmly attached to the glass holder with wax and cannot move its head or body, its halteres are free to oscillate and their feedback might trigger bursts. Even though they are not wax embedded during electrical recordings, the halteres were shown to move only when the fly is moving (*Sandeman and Markl 1980*), so they are expected to be inactive also during the recordings in this study.

To definitely exclude movement of the halteres as a source of the bursts, the fly on the holder was filmed from the side to track its left (contralateral) haltere with a high-speed video camera while panoramic rotations and translations ("3 degrees of freedom" stimulus) were presented on the LED arena. The animal was either fully fixed (**Figure 16 B**), or its abdomen was left free to move (**Figure 16 C**) or both its head and abdomen were left free to move (**Figure 16 A**).

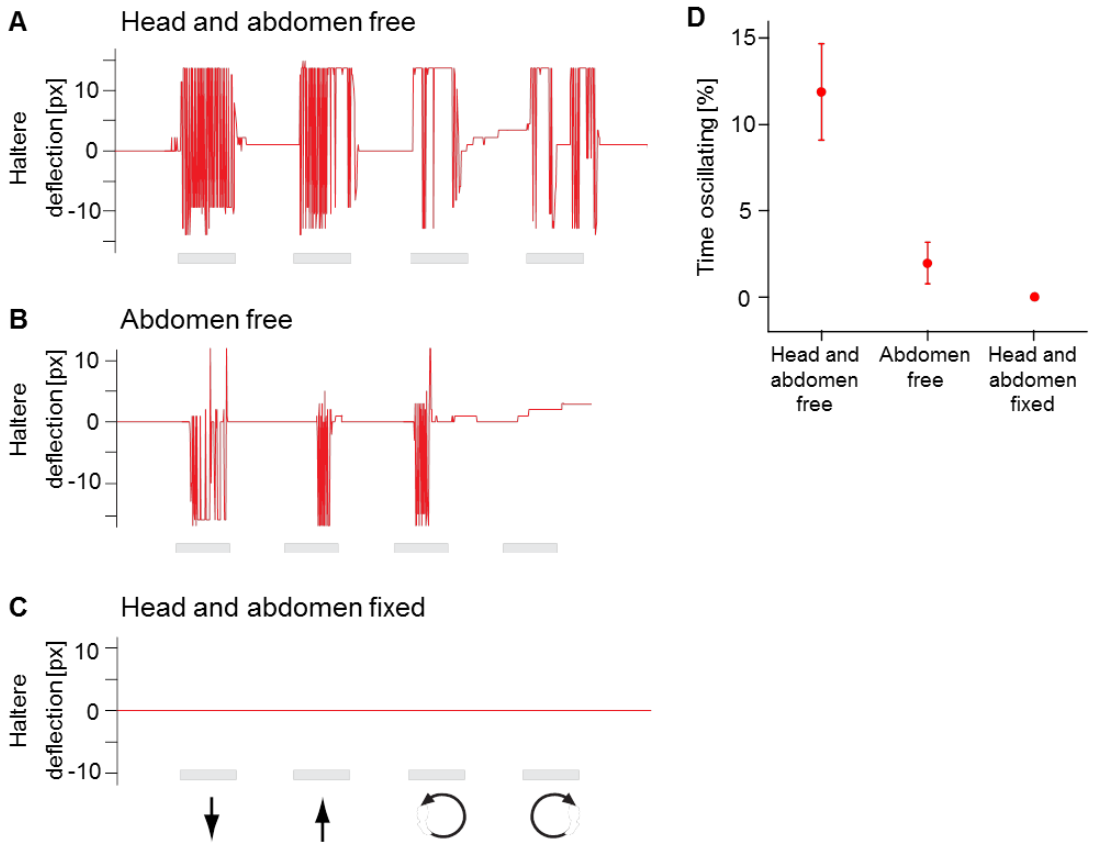

Figure 32: Activity of the contralateral haltere during panoramic visual stimulation. A: Haltere deflection (measured in pixels in the movie) during visual stimulation with pitch and roll rotations in a fly that is free to move its head and abdomen. The example trace shows one trial, gray bars each indicate 1 second of visual stimulation. The haltere oscillates for long periods and beats when the visual stimuli are presented. **B:** A fly with its head fixed in place beats its haltere for shorter periods but still in correlation with the visual stimuli. **C:** When both the head and abdomen are fixed and unable to move, the halteres do not move at all. This is the configuration used during all extracellular recordings from the ADN. **D:** Relative total duration of haltere beating in each trial for the three situations presented in A, B and C (mean percentage ± SEM of n = 4 trials in N = 2 flies for each situation).

Flies that were allowed to move their head and abdomen (without simultaneous nerve recording) strongly beat their halteres in response to rotational optic flow, especially to pitch and roll rotations (**Figure 32 A** and **D**). Haltere activity was correlated with the visual stimuli. In flies where the head was fixed but the abdomen was left free to move, haltere oscillations were still present but shorter (**Figure 32 B** and **D**). Statements about the absolute frequency of oscillation cannot be made because of the too low frame rate of the video recording (100 fps). However, observations during the recording indicate that the frequency was higher in trials with a free head and free

abdomen than in trials with a fixed head and a free abdomen. In fully fixed flies, no haltere activity was observed at any time (**Figure 32 C** and **D**). This corroborates the prediction that during recordings - where the animal is firmly waxed - the halteres are still and motor neuron bursts are thus highly unlikely to derive from haltere feedback.

To test a possible correlation between haltere movement and motor neuron bursts, extracellular recordings from the ADN were established while the contralateral haltere was filmed during visual stimulation. Unlike in the usual recording situation, the abdomen was left free to move so that the halteres would oscillate while recording was still possible (**Figure 16 C, Figure 32 B**).

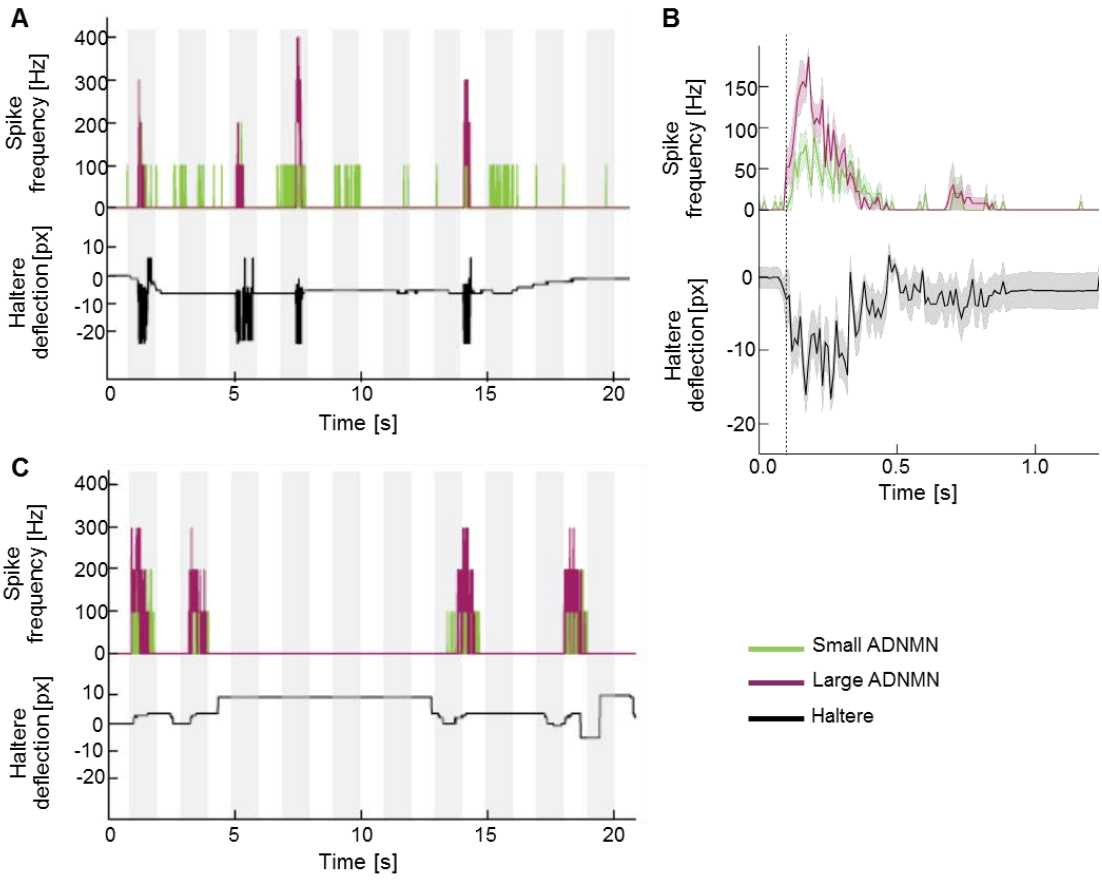

Figure 33: Bursting activity of the ADNMNs with and without haltere oscillation. A: Fast haltere oscillations during visual stimulation with the "3 degrees of freedom" stimulus coincide with burst-like discharges of the two ADNMNs (example trace from a single trial). The large unit is only active when the haltere beats at the same time. Gray bars indicate 1 second of visual stimulation. Binsize = 10 ms, haltere activity was filmed with 100 fps. **B:** Haltere triggered average of the spike frequencies of the two ADNMNs, aligned at the first down stroke of the haltere, indicated by the dashed line at 0.1 s. Haltere activity always coincided with an increase of the ADNMN spike rate in the sampled recordings. Mean frequency ± SEM for n = 10 haltere bursts in N = 3 flies. **C:** High frequency bursts during visual stimulation that are not correlated with the visual stimulus occur in the ADNMNs also without simultaneous haltere oscillation. In the depicted example trace, the halteres follow slow contractions of the abdomen but do not actively beat.

Tracking the position of the haltere in each frame of the movie revealed a clear relationship between high frequency haltere oscillations and motor neuron bursts, especially in the large ADNMN, which was not active otherwise (Figure 33 A). Alignment of the recorded traces at the first downstroke of the haltere for each haltere burst demonstrates that haltere bursts always coincided with a rise of spike frequency in both ADNMNs (Figure 33 B).

Conversely however, bursts in the motor neurons were also present when the halteres did not beat (Figure 33 C). Hence, haltere activity was always accompanied by ADNMN bursts, but ADNMN bursts also occurred without haltere activity.

This demonstrates that the bursts of the large ADNMN observed in many trials (see Figure 24) are unlikely to derive from haltere-feedback, since they were also present when the halteres did not oscillate. A central command that elicits at the same time bending of the abdomen, oscillation of the halteres and movement of the head (by activating the ADNMNs) is an alternative explanation for this observation and will be discussed later.

3.1.10. Summary of anterior dorsal nerve results

Two spiking motor neurons were active in extracellular nerve suction recordings from the anterior dorsal nerve. They were termed “small ADNMN” and “large ADNMN” (Figure 23). They differed in their response behavior but both showed a clear preference for global versus local optic flow and both responded maximally to a yaw rotation with an upward pitch component (Figure 26). The preferred rotations contain stronger pitch and roll components than estimated from the receptive fields mapped in an earlier study using local gratings. A possible explanation for this is a previous underestimation of vertical sensitivity components due to the size of the stimulus, which are now revealed by the stronger panoramic stimulus. This is the first time that full field rotations were used to stimulate ADN motor neurons.

Experiments using monocular visual input indicate that the small ADNMN receives about equally strong input from both eyes. The large ADNMN must also receive input from both eyes, because it stops responding when visual stimulation becomes monocular (Figure 28, Figure 29). The identification of this visual input was subject of the paired recordings with HS-cells. HSN and HSE and the small ADNMN have strikingly similar tunings to a set of 62 panoramic rotations (Figure 30). Surprisingly, paired recordings did not reveal a clear connectivity: the effects of current injections into HSN or HSE on the activity of the ADN were present, yet very weak (Figure 31).

In many recordings, spontaneous bursting discharges were observed, that derived mainly from the large ADNMN (Figure 24). Recording from the nerve while filming the movement of one haltere showed that these bursts do not derive from haltere feedback (Figure 33).

3.2. The frontal nerve (FN)

The second neck nerve that originates in the prothoracic ganglion, next to the anterior dorsal nerve, is the frontal nerve (see Figure 5). It houses a larger number of motor neuron axons and is therefore larger in diameter than the ADN.

To characterize the response properties and the sensitivity for panoramic visual stimuli of individual FN motor neurons, intracellular recordings from FNMN axons were carried out. Intracellular contact allowed for the injection of the tracer Neurobiotin into each recorded cell to characterize its anatomy post hoc. To assign anatomy and physiology unambiguously, only a single FNMN axon was recorded from and stained in each animal. The sensitivity for panoramic rotations was measured in the putative presynaptic partner neuron DNOVS1 as well.

Nerve cross sections confirmed the existence of eight large diameter axons projecting through the nerve, as reported in earlier studies (*Sandeman and Markl 1980; Strausfeld and Seyan 1985*) (Figure 34). They are accompanied by a large number of small diameter axons. Like the ADNMNs, all recorded FNMNs were able to generate spikes, either spontaneously or in response to visual or tactile stimulation (Figure 35).

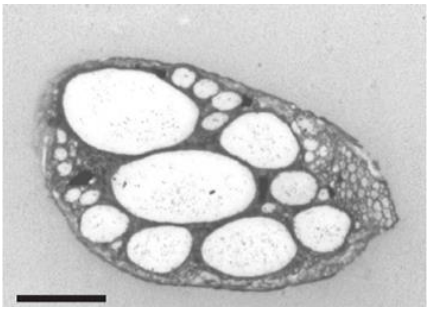

Figure 34: Light microscopic image of a semithin (1 µm) FN cross-section. The profiles of eight large diameter axons are visible along with an unidentified number of small diameter axons. The cross-section was taken approximately 100 µm away from the prothoracic ganglion, where the frontal nerve still consists of a single bundle of axons. The structure on the upper right side of the cross section is the prosternal nerve, which is fused to the frontal nerve at this stage. Scale bar: 25 µm.

3.2.1. Recording from FNMNs

Presented with panoramic visual stimuli, FNMNs mainly fired action potentials. Subthreshold potential changes as well as a mixture of graded and spiking responses were observed as well (Figure 35 A). Often, action potentials and subthreshold potential changes were observed within sequential recordings from the same motor neuron. However, none of the recorded cells responded to visual stimulation with graded potentials exclusively, all of them fired spikes at some point.

To check for mechanosensitivity in FNMNs, the animal was placed in the dark (i.e. the LED arena was switched off) and its fixed head and abdomen was gently touched with a small piece of tissue paper while recording from a single FNMN axon. All tested cells (N = 15) responded to the tactile stimulation by firing bursts of spikes (Figure 35 B), the responses were strongest when the bristles on the vertex and back of the head were touched.

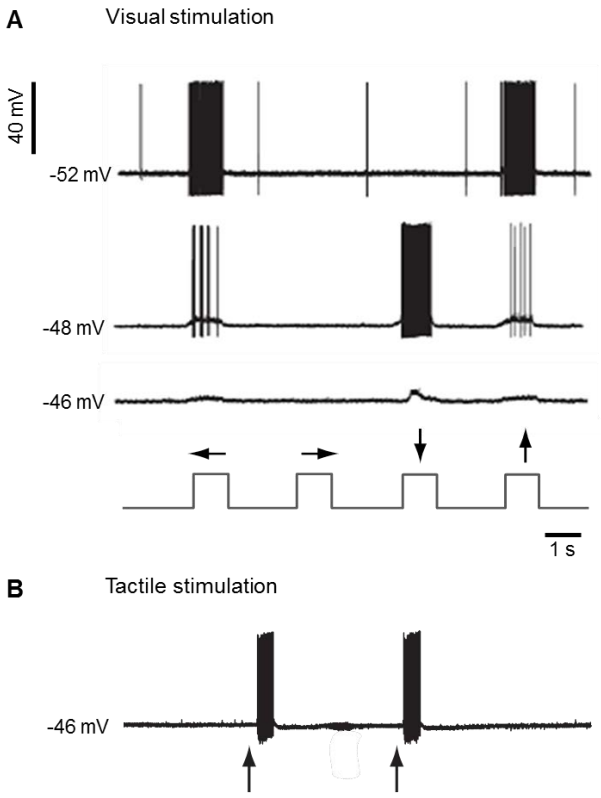

Figure 35: FNMN responses to visual and tactile stimulation.
A: Intracellular recordings from three individual FNMNs responding to yaw and pitch optic flow of 1 s duration. The stimulus is plotted as a step function below the recordings, representing leftward yaw, rightward yaw, downward pitch and upward pitch panoramic optic flow as included in the "3 degrees of freedom" stimulus. The cell in the uppermost row responds exclusively with spikes, the response type which was observed in most cells. The cell in the second row responds with spikes sitting on graded potentials, while the cell in the lower row responds to the visual stimuli with weak subthreshold membrane potential changes alone. The resting membrane potential of each recording is indicated on the left side. **B:** Responses to tactile stimulation of the bristles on the fly's head. Touch often led to bursts of spikes in the motor neurons. The black arrows in the example recording indicate the time points where the bristles were touched with a piece of paper.

Since all FNMNs described in this account were able to generate spikes, a 'spiking' or 'graded' response type does not seem to be characteristic for specific cell types or individual neurons but presumably rather depend on the overall activation of the neuronal circuit which in turn affects the resting potential of the neuron.

3.2.2. Anatomical classification

Among all Neurobiotin-filled cells (N = 33), five distinct morphological types were found (**Figure 36**). Classification was done by taking the dendritic branching pattern of each stained FNMN into account as well as by analyzing the pattern of Neurobiotin-coupling with other cells. The pioneering anatomical study from *Strausfeld et al.* (*1987*) in which the anatomy of eight large diameter FNMNs is presented served as reference (see **Figure 12**).

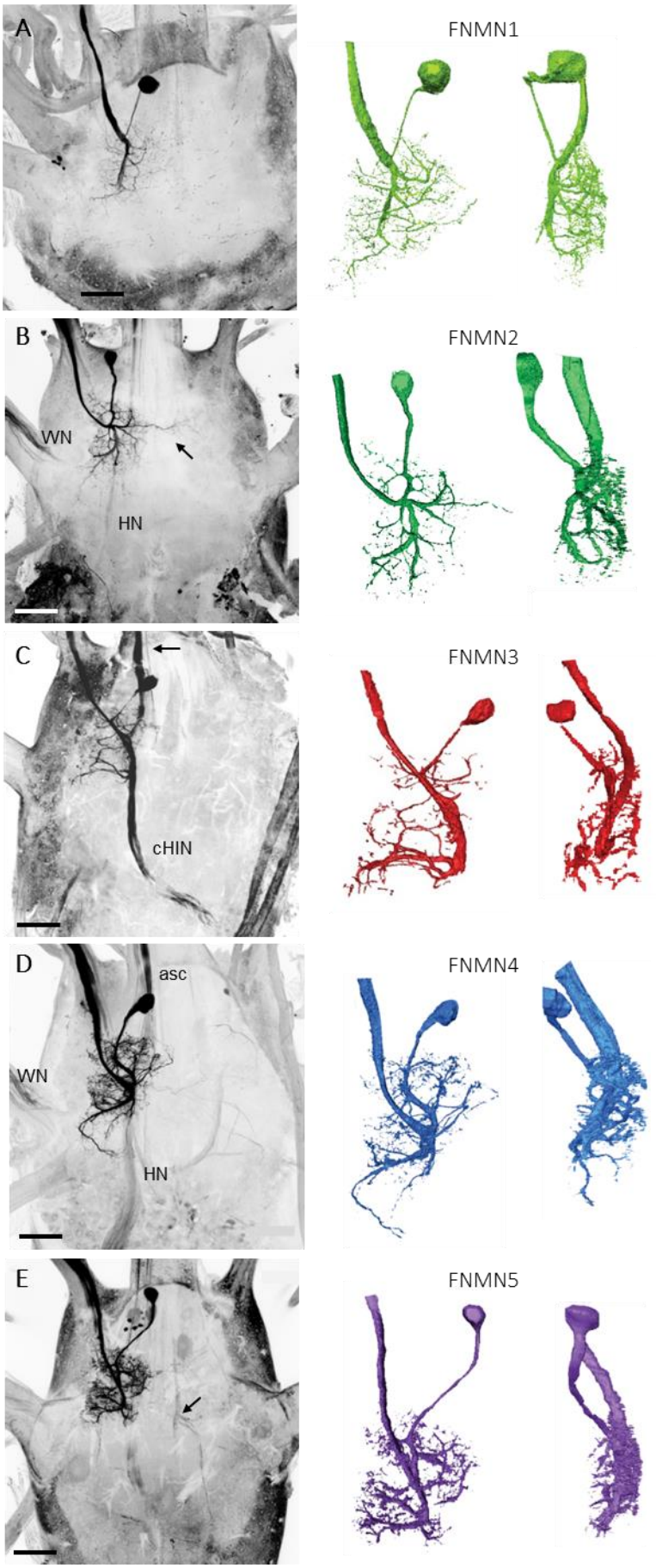

Figure 36: Anatomical classification of the five FNMN types found in this study. A: Left: Z-projection of an FNMN1 profile in the anterior part of the thoracic ganglion, taken from a confocal image stack. No dye-coupling with other neurons is visible in any of the staining of this cell type (N = 4). The cell belongs to the left FN, its cell body is located close to the prothoracic origin of the cervical connective. Right: 3D - reconstruction of one dye-filled neuron of type FNMN1 seen from a frontal (center) and lateral (right) perspective. **B:** FNMN2 (N = 8) is the only unit with its dendritic branch extending to the contralateral side (black arrow). The ipsilateral wing nerve (WN), the very faint profile of the haltere nerve (HN) and fibers of the cervical connective are co-stained. **C:** Injection of Neurobiotin into FNMN3 (N = 13) led to strong dye-coupling with a large diameter descending neuron (black arrow) and a bundle of contralateral haltere interneurons (cHINs). **D:** FNMN4 (N = 2) is dye-coupled to the ipsilateral haltere nerve (HN) that sends ascending fibres (asc) to the brain, and to the wing nerve (WN). It strongly resembles FNMN3 in its shape but differs in its lack of coupling to a large diameter descending neuron. **E:** In FNMN5 (N = 6), Neurobiotin reveals coupling of the motor neuron with a bundle of cHINs and a thin bow-shaped strand of contralateral fibres (black arrow) as well as with several small-diameter axons of the cervical connective. Scale bar: 100 µm.

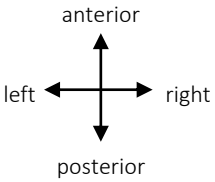

The five cell types found in the present study can be related to FNM1, FNM2, FNM3, FNM4 and FNM5 described by *Strausfeld et al.* (*1987*) (Figure 12). Neurons with anatomy resembling to Strausfeld's FNM6, FNM7 or FNM8 (Figure 12) were not found in the present account. Possible reasons for this will be discussed later.

A motor neuron type that looks strikingly similar to Strausfeld's FNM1 (Figure 12) was found and termed FNMN1. It is characterized by a prominent pole-shaped main dendrite and relatively short arborizations. Dye-coupling with presynaptic afferents was not observed in any of the specimens, indicating that synaptic input reaches this cell chemically (Figure 36 A).

Strausfeld et al. (*1987*) described the FNM2 motor neuron (Figure 12) to be the only motor unit of the frontal nerve that extends its dendrite into the contralateral part of the thoracic ganglion. Here, FNMNs that showed this characteristic feature together with a characteristic bending of the main dendrite were classified as FNMN2 (Figure 36 B). The haltere nerve is weakly dye-coupled to FNMN2, as are the ipsilateral wing sensory nerve and a bundle of small-diameter axons that project through the cervical connective. Regarding the direction of synaptic transmission it is not possible to deduce from the dye-coupling pattern if these small-diameter axons are ascending projections of the haltere nerve that terminate in the subesophageal ganglion (see *Strausfeld and Seyan 1985*), or descending neurons from the brain that project onto FNMN dendrites (see *Gronenberg et al. 1995*).

The third FNMN type, associated with FNM3 (Figure 12) in Strausfeld et al. (*1987*), is S-shaped and shows intense co-staining with a large diameter descending neuron and a bundle of contralateral haltere interneurons (cHINs) (Figure 36 C, see also Figure 14).The descending neuron has a stubby ending that strongly resembles the ending of the well described DNOVS1 descending neuron (*Strausfeld and Bassemir 1985a; Strausfeld and Seyan 1985*), which is the only large diameter descending neuron that is known to terminate in the prothoracic ganglion on FNMN dendrites (*Milde et al. 1986*, see Figure 14).

Strausfeld's FNM4 (Figure 12) resembles FNM3 in its S-shaped appearance, as is the case for the cell type termed FNMN4 here. In contrast to FNMN3, FNMN4 is not dye-coupled to a large diameter descending neuron in any of the specimens (Figure 36 D). It is dye-coupled with the haltere nerve as well as with small diameter axons of the cervical connective and afferents from the wing sensory nerve.

The fifth anatomical cell type found in this study is termed FNMN5, and anatomically resembles FNM5 in *Strausfeld et al.* (*1987*) (Figure 12). It is weakly dye-coupled to a bundle of cHINs and several thin axons that project through the cervical connective (Figure 36 E).

Evidence for electrical synaptic connections from transsynaptic dye-diffusion was found in four out of five cell types: Apart from FNMN1, dye-diffusion into haltere afferents or descending/ascending neurons of the cervical connective was observed in all FNMN types. Since the descending/ascending neurons possess long axons and many of them have a small diameter (for cross sections of the cervical connective see *Coggshall et al. 1983*), it was not possible to follow any of them to their cell bodies or dendritic trees because the Neurobiotin did not travel

this far. Based on its morphologically characteristic axon terminal and the fact that this connection has already been postulated before (*Strausfeld and Seyan 1985*), the co-stained descending input synapsing onto FNMN3 is likely to be DNOVS1 (**Figure 36 C, see also Figure 15**).

3.2.3. Visual sensitivity of the five cell types

Visual motion sensitivity could be measured in 20 out of 33 dye-filled cells that were reconstructed anatomically. In the other 13, intracellular contact could not be kept long enough to measure multiple sets of visual stimuli. Individual FNMNs showed pronounced preferences for certain panoramic rotations in their motion tuning, reflected in a selective increase in their firing rate to specific stimuli (**Figure 37**). As expected from previous studies, pitch and roll rotations triggered responses in FNMNs (Milde et al. 1987; Huston and Krapp 2008; **see Figure 13**).

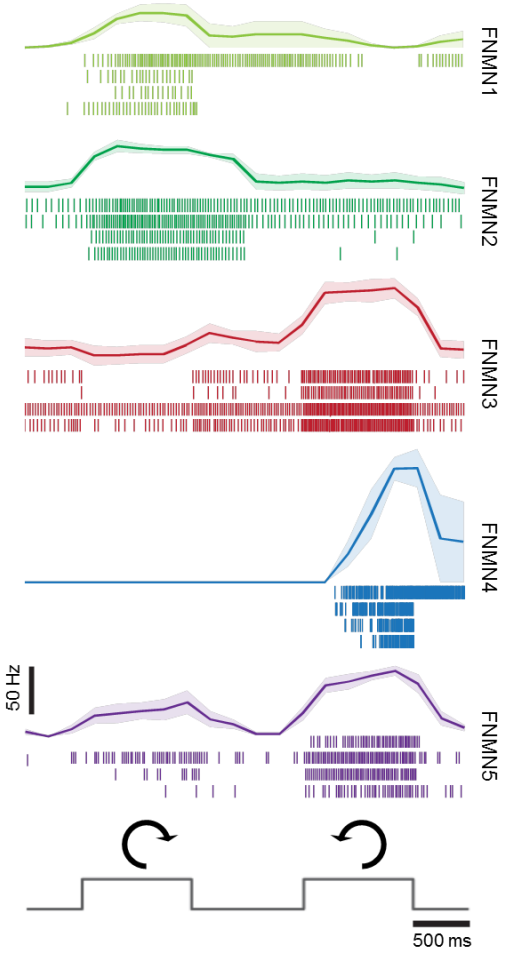

Figure 37: Rasterplots and peristimulus time histograms of the five anatomical cell types in response to roll optic flow.
All five FNMN types fire action potentials and are visually responsive. They all respond to optic flow reminiscent of a roll rotation. While FNMN1 and FNMN2 respond more strongly to a clockwise roll rotation, FNMN3, FNMN4 and FNMN5 prefer counterclockwise roll optic flow (n = 4 trials for each cell class, bin size = 200 ms). Duration of stimulation in both directions is 1 second as marked by the steps at the bottom of the figure, with a 1 second pause in between. The black arrows indicate the direction of the roll optic flow presented on the LED arena using the checker-board wallpapered panoramic room as in the "3 degrees of freedom" stimulus.

In **Figure 37** the spiking responses for a full field clockwise and counterclockwise roll-rotation as displayed in the "3 degrees of freedom" stimulus are plotted for the five different anatomical FNMN types. They all modify their firing rate upon visual stimulation but differ in the directional preference. Regarding the roll-stimulus, a subset of motor neurons (FNMN1 and FNMN2) prefers

rotational optic flow in the clockwise direction, while the other subset (FNMN3, FNMN4 and FNMN5) prefers optivc flow in the counterclockwise direction.

To assess if the five cell types differ in the time-course of their responses, the latency to first spike (measured from stimulus onset) was calculated in trials with very low (< 10 Hz) spontaneous activity and in trials without spontaneous activity for the "3 degrees of freedom" stimulus.
The response latencies varied between 21.2 ms in a spontaneously spiking cell and 605.1 ms in a cell without spontaneous activity and visible subthreshold deflections. Variations were strong across all five anatomical types as well as across the 12 different stimuli: there was no cell-type specific time-course of the visual response. Response onset does not seem to depend on the cell type but rather on the resting potential and activation threshold of the individual neuron.

3.2.4. Preferred optic flow of the FNMNs

FNMNs are predicted to prefer rotational over translational panoramic optic flow, based on earlier studies of their receptive fields and innervated muscles (*Strausfeld et al. 1987; Gilbert et al. 1995; Huston and Krapp 2008*). Also, they have been shown to be tuned to roll- and pitch- like optic flow, using local gratings to map their receptive fields (*Huston and Krapp 2008*).
To investigate the response characteristics of the FNMNs for panoramic translations and rotations as measured in the ADNMNs, the "3 degrees of freedom" stimulus was displayed on the LED arena while individual FNMNs were recorded intracellularly.

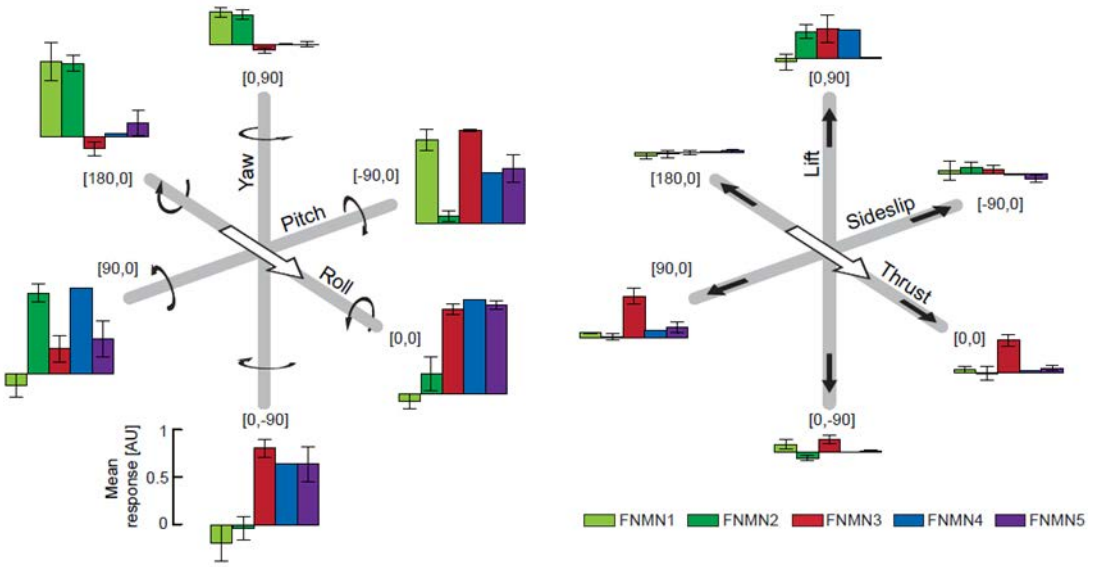

Figure 38: Visual sensitivity of five anatomical FNMN types for panoramic rotations and translations using the "3 degrees of freedom" stimulus. The white arrow marks the orientation of a virtual fly with its eyes pointing at [0,0]. Black arrows indicate its direction of rotation around the three main body axes (left panel) and translations along them (right panel). All five FNMN classes respond more strongly to rotations than to translations. While FNMN1 and FNMN2 prefer clockwise roll optic flow, FNMN3, FNMN4 and FNMN5 are tuned to counterclockwise roll optic flow. The mean over all trials was normalized to its maximum for each neuron, then the mean ± SEM over all cells was calculated for each FNMN type (FNMN1: N = 2 cells; FNMN2: N = 4 cells; FNMN3: N = 3 cells, FNMN4: N = 1 cell; FNMN5: N = 4 cells).

All five FNMN types responded more strongly to rotations than to translations (Figure 38). While panoramic translations only led to minimal activity in all recorded motor neurons, rotations strongly excited them.

The five anatomical motor neuron types are tuned to opposing rotations, which was especially obvious for roll optic flow as presented also in Figure 37: Cells of the FNMN1 and FNMN2 type were strongly excited by clockwise roll optic flow and did not respond to counterclockwise roll, while the opposite was true for the FNMN3, FNMN4 and FNMN5 types. Pitch and yaw rotations also triggered strong responses

3.2.5. Rotational motion tuning of the FNMNs

To measure the tuning to pseudo self-induced rotations in all five FNMN types in more detail, flies were presented the panoramic "31 axes" stimulus as in ADNMN experiments.

Tuning was measured in 17 neurons. Graded membrane potential changes were used to calculate the tuning in 5 out of 17 cells that did not fire action potentials upon stimulation with the "31 axes" stimulus. The characteristic preferences for certain rotations were not affected by calculating graded responses instead of action potentials, as already demonstrated for FN and CN motor neurons by *Huston and Krapp* (*2009*) and *Wertz et al.* (*2012*).

Maximum responses (mean ± SEM) were between 27.97 ± 6.15 Hz measured in an FNMN2 cell and 138.5 ± 18.5 Hz measured in FNMN1. In FNMN3 and FNMN5, both graded potentials and spikes were taken into account as responses: maximum spiking responses were 55.42 ± 13.72 Hz (FNMN3) and 49 ± 9.85 Hz (FNMN5). In FNMN4, only graded potentials were taken into account because action potentials occurred very rarely.

Because of the different response types (spikes measured in Hz and graded potential changes measured in mV), data was normalized to the maximum response for each cell after calculating the mean across trials. The mean ± SEM was built across cells of each type and plotted on 3D spheres and 2D Mercator maps as shown in Figure 39.

Vector distributions of the preferred optic flow fields of the five cell types were calculated by multiplying the mean response strength for each rotation with the vector distribution of that particular rotation and summing the values across all 62 rotations (Figure 39, right panels). While FNMN1 and FNMN2 prefer rotations close to clockwise roll, with motion vectors pointing back-to-front in the frontal and upwards in the lateral field of view of the left eye, FNMN3, FNMN4 and FNMN5 are tuned to rotations close to counterclockwise roll optic flow, with motion vectors pointing front-to-back in the frontal and downwards in the lateral field of view of the left eye (Figure 39).

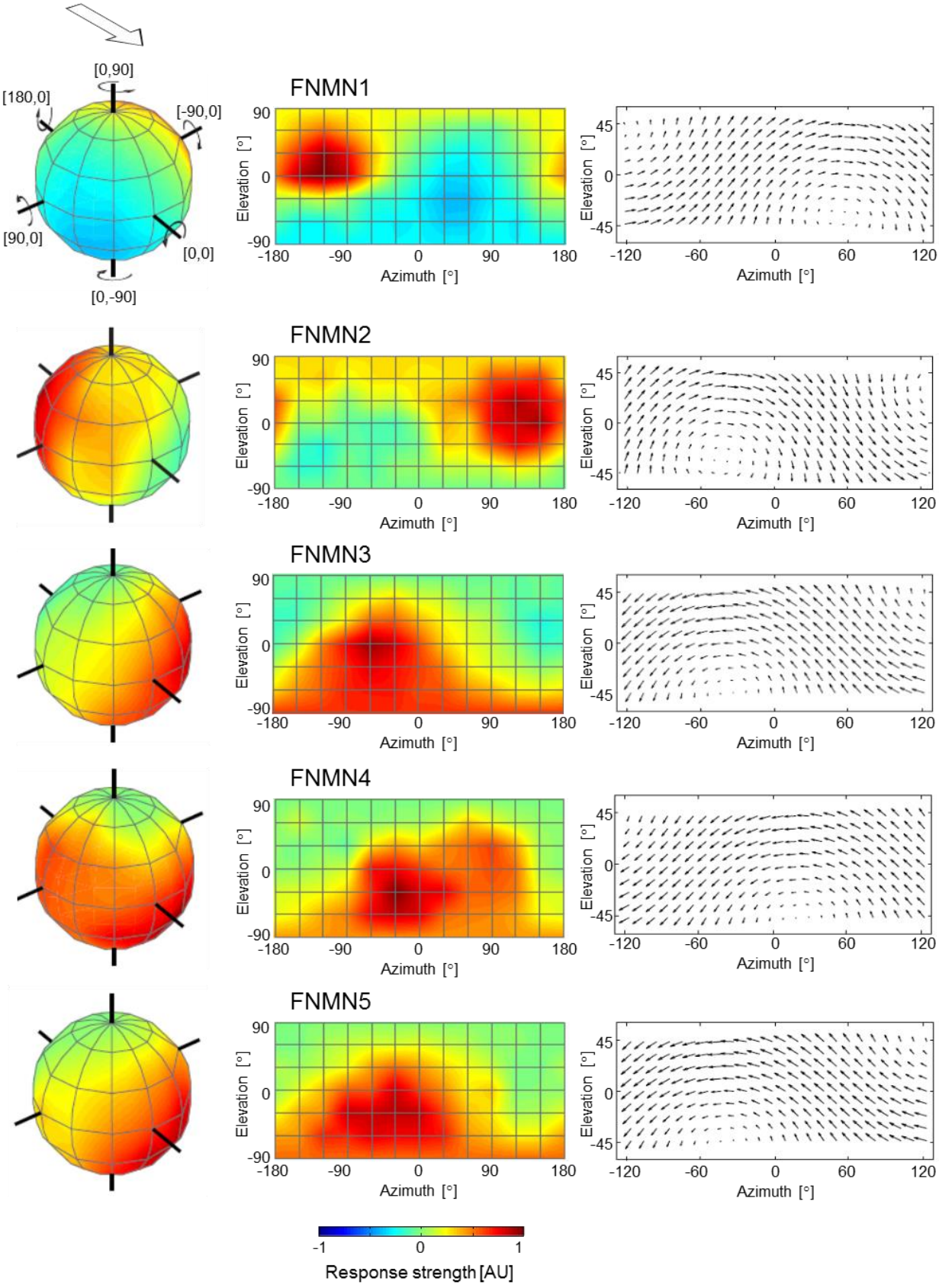
[0,90]
[180,0]
[-90,0]
[90,0]
[0,0]
[0,-90]
FNMN1
FNMN2
FNMN3
FNMN4
FNMN5
Elevation [°]
Azimuth [°]
90
0
-90
-180
180
45
-45
-120
-60
60
120
-1
1
Response strength [AU]

Figure 39 (left page): Rotational action fields of the five FNMNs. Three-dimensional sphere plots (left) and two-dimensional Mercator maps (center) reflect the tuning to panoramic rotations as they would be observed during self-motion of the animal for five different FNMN cell types. Each crossing of gridlines represents an axis of rotation in both plot types, around which a virtual fly rotates, resulting in optic flow of the opposite sign being presented to the real fly in the LED arena. Response strength is color-coded: red represents an increase in spike rate or graded potential, blue a decrease, green no response. The responses are normalized to the maximum of the mean over all animals for each cell type. While FNMN1 and FNMN2 maximally respond to counterclockwise rotations of the fly around axes close to [±180,0], FNMN3, FNMN4 and FNMN5 prefer clockwise rotations around axes close to [0,0]. The mean preferred optic flow fields for each FNMN type were calculated from the relative response strength (right). Only the dimension of the LED arena (azimuth: -120° to +120°, elevation: -45° to +45°) is shown here. All data is plotted as if recorded from the left part of the nervous system. FNMN1: n = 2 trials in N = 1 cell; FNMN2: n = 11, N = 4; FNMN3: n = 13, N = 6; FNMN4: n = 3, N = 1; FNMN5: n = 15, N = 5.

Interestingly, FNMN1 and FNMN2 are most strongly excited by rotations around a subset of axes that exactly complement the set of axes FNMN3, FNMN4 and FNMN5 are tuned to. This is illustrated in **Figure 40**. Plotting the positive responses of all five cell types into a single coordinate system illustrates that together they cover all tested axes in visual space. This means, that every rotation would be represented by at least one FNMN. Moreover, it seems that FNMN2 and FNMN3 alone would be sufficient to react to any rotation in space (**Figure 39, Figure 40**). This potential redundancy will be discussed later with regard to the pattern of muscle innervation.

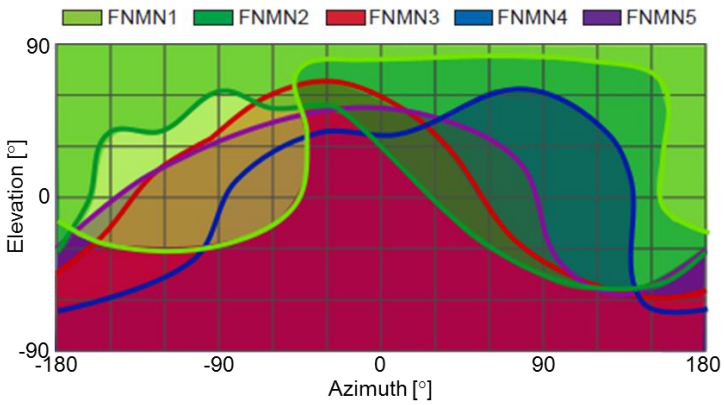

Figure 40: Complementarity of motion tuning in the five FNMN types. The positive responses from Figure 39 are outlined and filled in the colors associated with the respective FNMN type. Together they cover the full extent of visual space with their rotational sensitiviti-es. FNMN2 (dark green) and FNMN3 (red) alone would be even sufficient to cover it.

3.2.6. Visual input via a descending neuron

In the 1980s, pioneering anatomical studies revealed transsynaptic dye-diffusion between FNMNs and DNOVS1, a large diameter descending neuron (*Strausfeld and Bassemir 1985a; Strausfeld and Seyan 1985; Milde et al. 1987,* **see also Figure 14**). This anatomical evidence for a connection between DNOVS1 and FNMNs in the prothoracic ganglion strongly suggested a relay of visual input from a VS-cell subset onto the motor neurons. Indeed, DNOVS1 was later demonstrated to receive synaptic input from rotation-selective VS6 and VS7 (*Haag et al. 2007*).

In the present account, the stubby axonal ending of a large diameter descending neuron was found dye-coupled each time a motor neuron of the FNMN3 type (N = 13) was injected with Neurobiotin (**Figure 36 C**). The transsynaptic tracer did not diffuse far up enough along the axon to reveal the descending neuron's characteristic dendritic morphology and position within the deutocerebrum. Therefore it is not certain that the axonal ending belongs to the DNOVS1 large diameter descending neuron.

To address this issue, experiments were carried out on DNOVS1 itself: its rotational motion tuning was measured employing the "31 axes" stimulus while Neurobiotin was injected into its dendrites in the deutocerebrum during the intracellular recording (**Figure 41**). The graded membrane potential changes of DNOVS1 were very weak: maximum depolarization measured 3.46 ± 0.23 mV (mean of n = 4 trials ± SEM in N = 2 cells). Data was first normalized to the maximum per cell and then the mean ± SEM over the two DNOVS1 cells was calculated.

The preferred stimuli of the two tested cells were rotations around [-30, -30] and [-30,-60] (**Figure 41 A**). Despite their low response strength, DNOVS1 neurons were clearly tuned to rotational axes similar to FNMN3, FNMN4 and FNMN5 (see **Figure 39 C, D and E**).

In an earlier study, the receptive field of the left DNOVS1 was mapped with local small-field stimuli. Its selectivity for optic flow was found to match counterclockwise roll-like rotations (*Wertz et al. 2009*). This is in line with the present results, where the DNOVS1 maximum sensitivity was also measured at rotations resulting in counterclockwise roll-like optic flow (**Figure 41 A**).

When Neurobiotin was injected into DNOVS1 dendrites during intracellular recording, retrograde coupling with a set of VS-cells (VS4-9) was observed (**Figure 41 B**) as expected from the literature (see *Haag et al 2007; Strausfeld and Bassemir 1985a*). Anterograde coupling with the main dendrite of a single FNMN was also observed (**Figure 41 B**). The FNMN type cannot further be identified from the staining because the dye stained only the axon and did not diffuse into the dendritic tree. However, it is likely to be an FNMN3, since this neuron type was the only one dye-coupled to the axon terminal of a large descending neuron (see **Figure 36 C**).

The connection between DNOVS1 and the single FNMN was the only synaptic connection found between a descending neuron and a neck motor neuron of the frontal nerve in the present study. Considering that all FNMN classes that were characterized here are highly responsive to panoramic visual stimuli as well as the observation that FNMN1 and FNMN2 are tuned to clockwise rotations, DNOVS1 with its preference for counterclockwise rotations cannot be the only relay of descending visual information onto FNMNs. Signal transmission by chemical synapses, which cannot be revealed by dye coupling, is one possible explanation for this result.

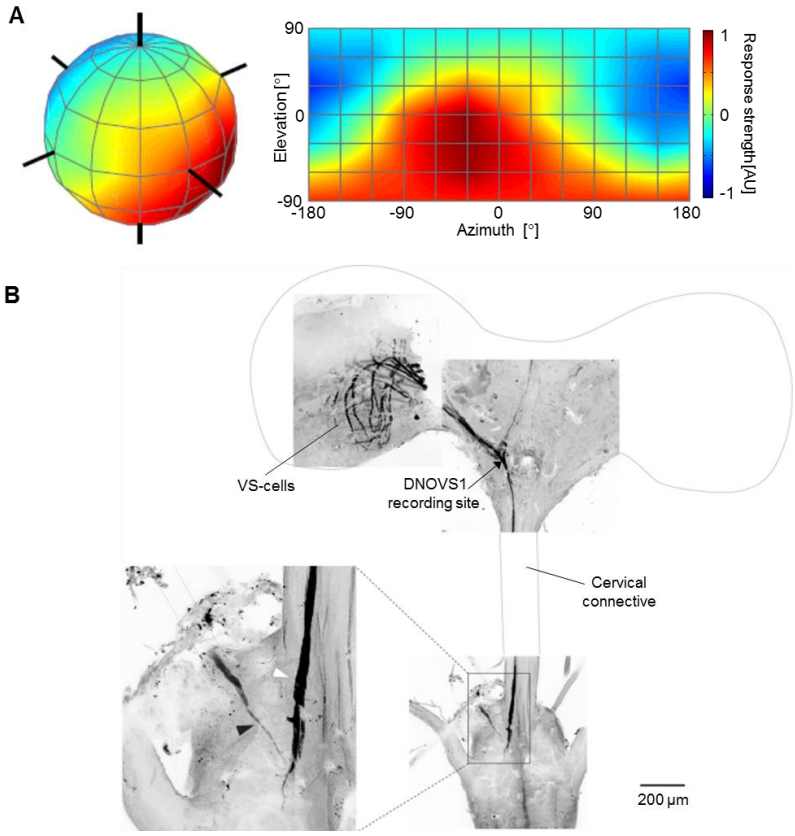

Figure 41: Rotational tuning and dye coupling pattern of the descending neuron DNOVS1. A: With its preferred axis around [-30,-30], the rotational tuning of DNOVS1 strongly resembles the tuning of FNMN3 and FNMN5 (**see Figure 39**). In contrast to the spiking nature of the motor neurons, responses in DNOVS1 are represented by graded membrane potential changes (n = 4 trials in N = 2 flies). **B:** Neurobiotin injection into a DNOVS1 dendrite reveals presynaptic dye-coupling with VS-cells and postsynaptic dye coupling with a single FNMN. Only the axon of the motor neuron is filled, making a classification according to its dendritic branching pattern impossible. The brain, cervical connective and frontal nerve profile are outlined for better orientation. The enlarged image on the left shows the coupling site of DNOVS1 (white arrowhead) and the principal FNMN dendrite (black arrowhead).

3.2.7. Responses to sudden luminance changes

During intracellular recording from single FNMNs, responses to the flashing of LED panels at the start as well as to their cessation at the end of single trials using the panoramic checkerboard stimulus (see **Figure 19 B**) were observed in all five cell types but were not quantified. Switching a blue fluorescent light on and off to check for Alexa Fluor® 488 staining of the FNMN during recording also led to responses. Response strength varied from single spikes to high frequency bursts.

Similar findings of ON/OFF responses in FNMNs and spike-generating descending neurons have been reported before by *Milde et al.* (*1987*), *Gronenberg and Strausfeld* (*1991*) and *Gronenberg et al.* (*1995*). In DNOVS1, responses to light on and light off were shown to derive from the ocelli, three dorsal light-sensitive organs on the fly's head (*Haag et al. 2007*).

To quantify this phenomenon in FNMNs, a stationary full field checkerboard pattern as used for the “3 degrees of freedom” and “31 axes” stimulus was employed. It flickered at a frequency of 0.5 Hz, so that the visual stimulus alternated between the pattern being displayed for 2 seconds and the LED panels being switched off for 2 seconds (**Figure 42 A** and **B**). The “ON/OFF” stimulus was tested in the two cell types FNMN3 (n = 3 trials in N = 1 cell) and FNMN5 (n = 9, N = 2). Both responded to the stimulus either with spikes or with subthreshold membrane potential changes. Spiking responses were quantified and found to be stronger for a light-off than for light-on switch (**Figure 42**). Graded potential changes without spikes were often observed in response to the “Light on” stimulus.

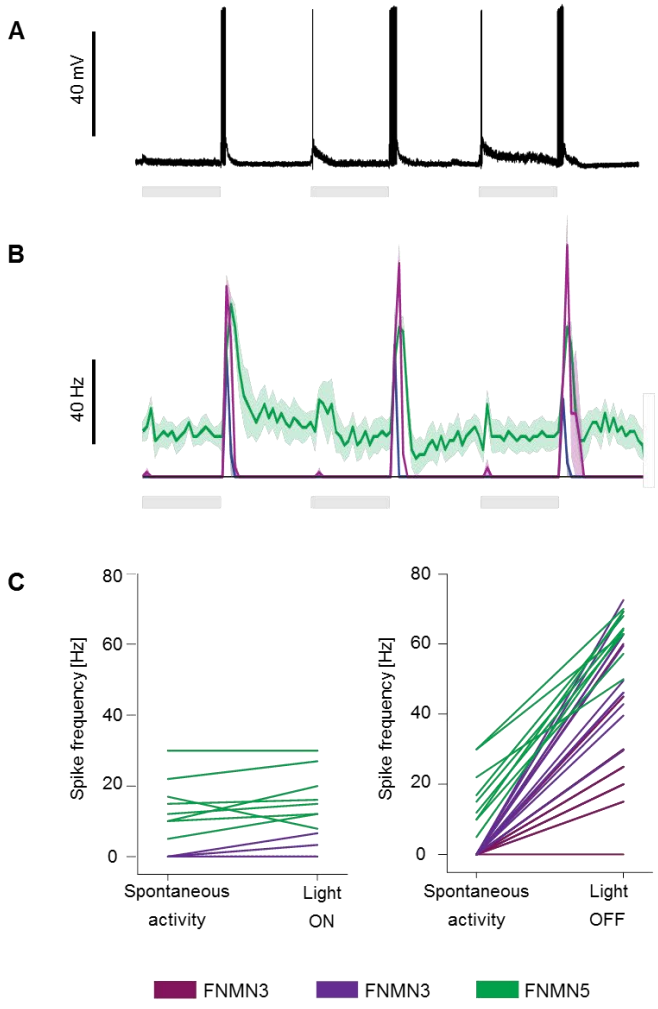

Figure 42: FNMN responses to light-on and light-off stimuli.
A: Single cell recording from FNMN3. The cell lacks spontaneous activity but fires short bursts of action potentials in response to the full LED arena being switched on and off, displaying the checkerboard wallpapered virtual room or darkness. „Light on“ episodes are represented by the gray bars.
B: Spike frequency of three individual neurons of the FNMN3 and FNMN5 cell type monitored during the “ON/OFF” stimulus. Mean ± SEM for n = 3 trials in each. Bin size = 100 ms. C Single trials of the three neurons depicted in B. Responses are stronger upon light-off (right panel) than upon light-on (left panel). One trial consists of 3 on and 3 off switches: n = 9 (FNMN5), 12 and 15 (FNMN3) on/off switches per cell.

Thus, sudden light changes do not specifically excite particular motor neurons but rather seem to serve a general system, possibly collision warning. The behavioral relevance of these motor neuron bursts will be discussed later.

3.2.8. Summary of frontal nerve results

The activity of single motor neurons of the frontal nerve was recorded with sharp intracellular electrodes. By means of dye-injection through the recording electrode, different anatomical profiles of FNMNs were found that could be grouped into five anatomical classes and associated with five of the anatomical FNMN types described by *Strausfeld et al*. (*1987*) (see Figure 12).

FNMN receptive fields have been mapped using local gratings before and found to work like matched filters for roll- and pitch-like rotations (*Huston and Krapp 2008*). Here, for the first time, the tuning of FNMNs was measured using pseudo self-induced full field rotations presented on an LED arena. Using single cell recordings paired with intracellular Neurobiotin injection, it was possible for the first time to assign to each cell's motion tuning its distinct anatomy and thus characterize the tuning properties of each of the anatomical cell types FNMN1-5. Based on this information, the accordance of a cell type's optic flow selectivity with the pulling plane of the muscle it innervates can be discussed.

Like the ADNMNs, FNMNs responded more strongly to rotations than to translations. They preferred mixtures of roll, pitch and yaw optic flow. The tuning to rotational optic flow was different in the five cell types: while FNMN1 and FNMN2 of the left side mainly responded to optic flow in the clockwise direction, FNMN3, FNMN4 and FNMN5 responded to optic flow in the counterclockwise direction. Their sensitivities seem to complement each other so that together their tuning covers all 62 tested rotations in space.

4. Discussion

In this thesis I individually characterized motor neurons of the two prothoracic neck nerves of the *Calliphora vicina* nervous system, the anterior dorsal nerve (ADN) and the frontal nerve (FN). The selectivity of each motor neuron for specific optic flow fields was measured, using an LED arena covering large parts of the *Calliphora* visual field.
ADNMNs and FNMNs both displayed a distinct preference for rotational over translational optic flow when presented with full-field stimuli. In addition to earlier studies that had revealed this specificity for rotational flow fields (*Milde et al. 1987; Huston and Krapp 2008*), the present account enables us for the first time to characterize FNMNs individually and bring their anatomy and physiology together. Moreover, ADNMNs were shown to receive visual input from both eyes with HSN and HSE playing a role in the shaping of the motor neuron response.

4.1. The anterior dorsal nerve (ADN)

An extracellular nerve suction electrode was used to record from the two visually sensitive ADNMNs. Panoramic full field rotations and translations were used to characterize their preferred optic flow. They were presented with stimuli of different sizes. In addition, vision was impaired by covering one eye to test if they receive input from both eyes or from one eye only. The identity of presynaptic neurons relaying input onto the ADNMNs has not yet been discovered by dye coupling experiments. *Strausfeld et al. (1987)* suggested a connection between HS-cells and the ADNMNs via DNColHS based on the proximity of DNColHS axon terminals and ADNMN dendritic branching areas (Figure 9). Thus it is still unknown which LPTCs provide ADNMNs with visual sensitivity and which descending pathways connect them.

A technique to test connectivity between cells is to directly record from two neurons simultaneously. This was done for the small ADNMN and two HS-cells of the lobula plate, HSN and HSE. Although it is – deducing from their motion preferences - highly probable that HSN and HSE shape the motion tuning of the ADNMNs via descending neurons, altering the membrane potential of either HS-cell had very small effects on the ADNMN (Figure 31).

4.1.1. Visual response characteristics and motion tuning

The results obtained from extracellular recording demonstrate both ADNMN units to be most sensitive for horizontal optic flow containing an upward pitch component as generated by a rotation around the [-120,-60] axis (Figure 26, Figure 27). While translations do not lead to

responses in the large ADNMN at all, the small unit responds to a horizontal translation (Figure 25).

In contrast to the small ADNMN, which generates visual responses also when it receives information from only one eye, the large ADNMN responds to full field motion only when both eyes are intact (Figure 29). This was also reflected by the vector distribution in the receptive field of one ADNMN measured by *Huston and Krapp* (*2008*), which contains motion vectors only in the frontal part of the visual surround, where the local stimulus they used was visible binocularly (Figure 10). Ipsilaterally displayed small-field stimuli did not elicit spiking responses in the large ADNMN but led to moderate responses in the small ADNMN, depending on the vertical stimulus location (Figure 24). Occlusion of one eye had almost no effect on the response strength of the small ADNMN to panoramic rotations, regardless of whether the ipsilateral or the contralateral eye was occluded (Figure 28).

This indicates that the small motor neuron receives visual input from both eyes that is added up in a highly sublinear fashion, so that monocular vision is as effective as binocular vision. Thus, monocular vision is still sufficient to drive the small ADNMN but impairs responses in the large ADNMN (Figure 29).

4.1.2. ADNMN features in a behavioral context

The small ADNMN is often spontaneously active while the large ADNMN never is, horizontal small field stimuli elicit responses in the small ADNMN but not in the large one (Figure 24), and reducing the visual input to monocular vision has almost no effect on the small ADNMN while it abolishes all responses in the large one (Figure 29).

These observations altogether suggest that the two motor neurons differ in their activation threshold: The large ADNMN presumably has a lower resting membrane potential than the small ADNMN, which in consequence requires neuronal input to be more depolarizing to elicit responses. This assumption could explain why the visual stimuli used in this study elicited responses in the small ADNMN with a higher probability than in the large ADNMN.

Although head turning behavior upon unilateral eye occlusion was not monitored in the present study, the generation of an optomotor response is uncertain when the two motor neurons are not active at the same time: the two ADNMNs innervate neighboring muscles TH1 and TH2 (Figure 8) that both steer the same movement by collectively pulling the same skeletal structures. It is unlikely that activation of only one of the muscles is sufficient to make a head turn.

In a similar study by *Wertz et al.* (*2012*), unilateral eye occlusion significantly reduced the response strength of a cervical nerve motor neuron and fully abolished the head optomotor response of a tethered fly to a pitch rotation. In behaving flies however, monocular blinding had surprisingly little effect on the directed flight and walking behavior of blowflies *(Kern et al. 2000a)*. Furthermore, HSE responses were unaltered after monocular blinding *(Kern et al. 2000b*). The results of these two related studies indicate that monocular vision does neither impair the responsiveness of the HSE-cell in the lobula plate nor the fly's flight and walking behavior.

A possible explanation for these contradictory observations can be found in gain modulation by behavior as demonstrated for LPTCs: during locomotor activity like walking or flying, the VS- and HS-cells respond in a larger range than they do when the fly is standing still. The peak-to-peak responses are larger and the range of stimuli that elicit responses is broadened during locomotion (*Jung et al. 2011; Chiappe et al. 2010; Maimon et al. 2010*). It is highly likely that motor neurons alter their resting potential during behavior in a similar way. In an active behavioral state, the neurons would be less hyperpolarized than in an inactive state occurring when the animal is constrained for electrophysiological recording. It is most likely that during flight or walking the activation threshold of the large ADNMN for visual input is lower, both ADNMNs would be activated by a yaw visual stimulus, both muscles would contract and a yaw optomotor response would be generated.

4.1.3. Sufficiency of ipsilateral HSN and HSE as visual inputs

The two ADNMNs innervate muscles that control a horizontal yaw rotation of the head (*Strausfeld et al. 1987; Gilbert et al. 1995*). Their visual sensitivity is appropriate for this movement: they are tuned to horizontal front-to-back rotational optic flow. But which type of neuronal input shapes their visual sensitivity?

The rotational tuning of the ADNMNs, especially the small unit, is strikingly similar to the tuning of the ipsilateral HSN and HSE cells (Figure 26, Figure 30). The HS-cells have been suggested to synapse onto descending neurons that provide synaptic input to the ADNMNs (*Gronenberg and Strausfeld 1990; Strausfeld and Bassemir 1985b; Strausfeld and Seyan 1985*). HSN and HSE also synapse directly onto motor neurons of the VCN that emerge from the brain (*Haag et al. 2010*). VCN motor neurons possess receptive fields reminiscent of the ADN motor neuron receptive fields (*Haag et al. 2010; Huston and Krapp 2008*) and likewise control head yaw by controlling the oblique horizontal muscles that directly link the head to the thorax (*Strausfeld et al. 1987*).

The tuning of the small ADNMN could be provided by the ipsilateral HSN and HSE alone (Figure 30). Both HS-cells receive excitatory input from the spiking H1 and H2 neurons of the contralateral lobula plate and therefore have large binocular receptive fields that are matched filters for a yaw rotation (*Farrow et al. 2006; Haag and Borst 2001; Horstmann et al 2000*). The descending neuron might in this context function as a simple cable for transmission of the pre-processed visual signal from HSN and HSE onto the motor neurons, rather than pooling and comuputing signals from different cells from both hemispheres. Extraction of visual information that already fulfills the requirements of the motor system by LPTCs is an efficient strategy in the transformation of the sensory signal into a motor command. Exclusive input from ipsilateral HSN and HSE is also sufficient to shape the VCNMN receptive field as shown by *Haag et al. (2010)*.

Two important questions that remain in this context are 1) why simple current injections did not work as they did for VCN and CN (*Haag et al. 2010, Wertz et al. 2012*), and 2) why the silencing of a single HS-cell by hyperpolarization did not have a stronger effect on the ipsilateral small-field response of the small ADNMN (see Figure 31).

An explanation for why a pure depolarization or hyperpolarization, without a visual stimulus (Figure 31 A), yielded such weak effects, could simply be the nature of the electric circuit: while previous studies focused on dual recordings between neighboring cells and found direct synaptic connectivity between LPTCs and neck motor neurons (*Haag et al. 2010; Wertz et al. 2012*), an additional resistance needs to be overcome in the present set of experiments, which is originating in the descending neurons whose identity is unknown.

The weak effect of HS-cell hyperpolarization on the ADNMN response (Figure 31 B) could be due to an insufficient input shutdown, with HSE still active while HSN is hyperpolarized and vice versa: By sparing the region of binocular overlap in the stimulus design (Figure 20), the influence of the contralateral H1 and H2 cell onto HSN and HSE could be excluded. The response from the ipsilateral HS-cells could be therefore isolated. However, the vertical side length of the square-wave-grating used to stimulate either HSN or HSE measured 40°, which overlaps with the receptive fields of both cells (see Figure 4, Figure 20). The HSE stimulus overlaps with the HSN receptive field by approximately 10° and the HSN stimulus overlaps with the HSE receptive field by about 20°. A preliminary set of experiments had been conducted with a grating of only 20° vertical extent that would not excite neighboring HS-cells but only the targeted one. This smaller stimulus had not been able to evoke responses in the motor neuron (data not shown), therefore the stimulus size had to be adjusted to an extent that would stimulate the neighboring HS-cell as little as possible while at the same time be strong enough to drive the small ADNMN above threshold. This results in the excitation of two HS-cells while controlling the membrane potential of only one of them.

The HS-cells have been proposed as prime candidates for controlling the yaw optomotor response in flies for decades (*Blondeau 1981; Geiger and Nässel 1981; Hausen and Wehrhahn 1983; Heisenberg et al. 1978*) and a recent study could prove that exclusive input from the ipsilateral HS-cells is sufficient to generate a yaw head optomotor response as well as a flight-turning response in *Drosophila* (*Haikala et al. 2013*).

Thus, corroborated by the present findings I propose that HSN as well as HSE play a key role in the visuo-motor circuit extracting horizontal rotatory information from the environment to generate an appropriate yaw response of the head that is mediated not only by the motor neurons of the VCN but also by those of the ADN. However, more dual recordings would be necessary to definitely prove this. Also, further connectivity of the motor neurons with visually sensitive neurons other than the HS-cells, that respond to the same stimuli and could not be targeted in the present set of experiments, cannot be excluded. Taken together, double recordings are not easily feasible, especially when the duration of the stimulus (“31 axes”) requires them to be stable for a long time on both ends. Also, only positive results can be analysed in this context since negative results (i.e. the absence of a transmitted response) can have two reasons: either the cell contact is not good enough or there is no physiological connection between the two cells.

4.2. The frontal nerve (FN)

Five visually sensitive FNMN types were recorded intracellularly with a sharp electrode. This allowed for injection of the tracer Neurobiotin into single FNMNs during and after the recording and thus made an association of anatomy and physiology possible. Neurobiotin also visualizes neighboring cells due to its small molecular size, which enables it to diffuse across gap junctions. Dye-coupling of stained motor neurons with neighboring cells indicates functional connections via electrical synapses.

4.2.1. Anatomical assignment of cell classes

The FN was demonstrated to contain at least eight large diameter motor neuron axons that innervate eight ipsilateral muscles one-on-one by *Strausfeld et al.* (*1987*). In this pioneering study, single motor neurons were filled with 5 % cobalt chloride retrogradely from their innervated muscle. The eight motor neurons were camera lucida reconstructed in great detail (Figure 12).

Relying on these histological data, I was able to compare individual dye-filled FNMNs to the eight anatomical cell types introduced by *Strausfeld et al.* (*1987*) and shown in Figure 12. Recording from single motor neurons and testing their visual properties made an attribution of a motor neuron's motion tuning to its respective anatomical type possible.

This is the first time that physiology and anatomy are being linked together in FMNMNs: Before, the motion tuning of three anatomically unclassified FNMNs had been measured (*Huston and Krapp 2008*) and the anatomical properties of eight physiologically uncharacterized FNMNs were known (*Strausfeld et al. 1987*).

In the present study, 33 stained FNMNs could be grouped into five different anatomical classes and associated with FNMN1-5 as described by *Strausfeld et al.* (*1987*) based on morphological similarities (Figure 36). Stainings were first compared among each other and taken together in groups depending on their dendritic branching pattern in the X-, Y-, and Z-planes of the confocal image as well as on the presence of co-staining of particular structures like the haltere nerve, cHINs or large descending neurons. Then, the groups themselves were compared to the eight described cell types (compare Figure 36 and Figure 12). No Neurobiotin-filled cell found in this study was morphologically similar to FNMN6, FNMN7 or FNMN8 as depicted in Figure 12. One possible reason for this is, that FNMN5-8 innervate the most dorsally situated muscle block comprising the internal muscles of the sclerite (*Strausfeld et al. 1987,* Figure 11). Given that their axons are running through the FN most dorsally (*Strausfeld et al. 1987)*, the initial penetration might have pushed the recording electrode too far ventral already. This is likely because the electrode tip was pushed into the nerve by buzzing and softly tapping onto the micromanipulator leading it, which may have caused it to enter the tissue abruptly, missing the parts of the nerve close to its dorsal surface. Another possible reason for the lack of FNMN6-8 stainings is that they might not generate spikes upon intracellular penetration with the electrode tip, even with buzzing or visual stimulation, and may have been missed because of this.

4.2.2. Muscle pulling planes

With the present findings both the visual response properties of the FNMNs and the pulling planes of the muscles they innervate (*Strausfeld et al. 1987*) - assuming the present anatomical assignment of the five cell types is correct - are known now. Consequently, the precision of visual motion tuning for controlling head movement can now be investigated for each of the five FNMN types.

FNMNs innervate a set of muscles that indirectly pull the side of the head downwards (depressors) or push it upwards and inwards (levator and adductor) by either pushing the cervical sclerite down or pulling it up. A third set of muscles provides internal rigidity to the sclerite (Figure 11, *Strausfeld et al. 1987; Gilbert et al. 1995*). The cervical sclerite is a paired structure: the left sclerite is associated with muscles innervated by the left FN, the right sclerite is associated with muscles innervated by the right FN (*Strausfeld et al. 1987*). A contraction of both depressors would lead to a downward pitch movement of the head, contraction of both levators to an upward pitch movement. Contraction of the levator on one side and the depressors on the other side results in a roll movement of the head around the Z-axis.

The levator muscle pulls the head up on the ipsilateral side and is innervated by FNMN1. This is reflected by the preferred optic flow measured in FNMN1 (representing the left part of the nervous system): the motor neuron is maximally tuned to a mixture of clockwise roll and upward pitch (Figure 38, Figure 39). Strong neuronal activity in the left FNMN1 would lead to a contraction of the left levator that indirectly pulls the left side of the head upwards, reminiscent of a clockwise roll rotation of the head. Also for FNMN2 the preferred axes of panoramic rotations measured in this account match the pulling plane of its innervated muscle: it is maximally tuned to clockwise-roll-like optic flow (Figure 38, Figure 39) and it innervates the adductor muscle that pulls the ipsilateral side of the head upwards and inwards upon activation (Figure 11). The other three FNMN types I recorded from are tuned to optic flow with vectors pointing in the opposite direction: a counterclockwise roll rotation. FNMN3 and FNMN4 innervate two depressor muscles that pull the ipsilateral side of the head downwards (Figure 11), reminiscent of a counterclockwise rotation of the head (for the left side). This head movement is antagonistic to the clockwise rotation mediated by FNMN1 and FNMN2, as is the motor neurons' rotational selectivity: FNMN3 and FNMN4 are most sensitive to counterclockwise roll like optic flow with motion vectors pointing upwards in the contralateral and downwards in the ipsilateral field of view (Figure 38, Figure 39), matching the pulling plane of the depressor muscles.

Interestingly, FNMN5 is also visually sensitive and exhibits a rotational tuning that makes it a prime candidate to innervate a muscle that pulls down the ipsilateral side of the head (counterclockwise roll). This is an unexpected finding because FNMN5-8 innervate internal muscles of the sclerite that provide rigidity of the head-prothorax-articulation and do not control a particular movement of the head. From the five anatomical cell types found in this study, the FNMN5 group was the hardest to assign to one of Strausfeld's (*1987*) established anatomical cell classes (compare Figure 12 and Figure 36). It is possible that the FNMN3 and FNMN4 cells are so heterogeneous that the neurons classified as FNMN5 are actually part of the two other types. This

could explain their tuning and would support the previous hypothesis that FNMN5-8 were not targeted with the electrode because of their superficial location. However, assuming that the FNMN5 group (N = 6 dye filled cells) does represent a discrete cell type other than FNMN1-4, it is surprising that they respond to optic flow when their sole assumed function is the suspension of the head on the thorax (*Strausfeld et al. 1987*).

4.2.3. Complementary tuning of FNMNs

The results of the panoramic vision experiments demonstrate that the rotational tuning of FNMNs which innervate muscles that pull the ipsilateral side of the head downwards (FNMN3 and FNMN4) is complementary to the rotational tuning of FNMNs which innervate muscles that pull the ipsilateral side of the head upwards (FNMN1 and FNMN2) (Figure 39, Figure 40). In other words: the preferred axes of one group of motor neurons are congruent with the non-preferred axes of the other group, so that all axes of rotations in three-dimensional space are covered by a combination of the two FNMN groups (FNMN1-2 / FNMN3-5). The combination of only two motor neurons, FNMN2 and FNMN3, would even be sufficient to respond to all 62 tested rotatory optic flow fields (Figure 40).

To roll the head in a clockwise or counterclockwise manner, one depressor muscle on each side would be sufficient: unilateral muscle activity would pull one side of the head down by contracting the muscle, while the muscle on the other side would stay inactive. In a study by *Gilbert et al.* (*1995*) the frontal nerve on one side was stimulated electrically, which primarily led to a roll down movement of the head to the ipsilateral side. This supported the conclusions drawn from anatomy, that the FN mediates roll movements, but poses the question what the role of the other motor neurons is, when contraction of the ipsilateral depressor muscles alone seems to be sufficient for head roll. A corresponding finding was obtained by *Gilbert and Bauer* (*1998*) in a behavioral assay: to correct for imposed perturbations around the roll axis (i.e. to regain an upright head position after the head had been passively rolled down to one side), the contraction of the contralateral depressor muscles alone was shown to be both necessary and sufficient. When the innervation of the contralateral depressor was cut, however, the ipsilateral adductor and levator were not able to pull up the side of the head and correct the error when activated. Thus, when investigated individually, the depressor muscles of one side can sufficiently turn the head around the roll axis, while the levator and adductor muscle of the other side cannot.

Why are there at least five visually sensitive motor neuron types when only FNMN3 and 4, which innervate the depressor muscles, would be sufficient to rotate the head around the roll axis?
If only the two depressor muscles would control roll rotations of the head, the movement of the head would be more instable than it would be if it was controlled by muscles from both sides that ensure it to follow a directed trajectory by actively pushing one side of the head up while actively pulling the other side down. Also, the activation of antagonistic muscles on either side of the nervous system, pulling down one and pushing up the other side of the head in parallel, could lead to head rotations with higher amplitudes compared to rotations caused by unilateral depressor contraction alone.

Another aspect of the FNMNs' rotation tuning is that on each side of the nervous system only part of the muscles is activated by a certain optic flow while the other part is actively silenced: a movement that excites FNMN1 and FNMN2 will at the same time inhibit FNMN3, FNMN4 and FNMN5 on the same side so that one muscle group is not only silent but contraction is actively inhibited while the other muscle group contracts (Figure 39). This could serve as a simple mechanism to reduce noise and maximize the efficacy of the movement generated by the active muscle group. For example, counterclockwise roll optic flow will excite FNMN3 on the left side of the nervous system, while inhibiting it on the right side as well as it inhibits antagonistic muscles on the left side. This results in a downward pull of the head to the left that is not held against by muscles from either side of the head. Moreover it is even supported by the antagonistic muscles of the right side of the head, whicht react to counterclockwise roll optic flow with a contraction and push the right side of the head up. Although in the present set of experiments inhibition was weak due to weak or absent spontaneous firing activity, stronger spontaneous firing is very likely to occur in actively behaving animals (*Jung et al. 2011*) and inhibition can be expected to be more pronounced then.

4.2.4. Similarities with LPTC motion tuning

Comparing the receptive fields and rotational action fields of *Calliphora* VS-cells measured by *Krapp et al.* (*1998*) and *Wertz et al.* (*2012*) with the motion tuning of FNMNs found in this study, similarities with ipsilateral VS4-VS9 in FNMN3, FNMN4 and FNMN5 become evident. FNMN1 and FNMN2 bear resemblance to contralateral VS8-VS10 and contralateral VS3-VS4 in their tuning profiles.

Well-characterized large descending neurons integrate output signals from ipsilateral VS6/VS7 (DNOVS1, *Haag et al. 2007*) and VS5/VS6 respectively (DNOVS2, *Wertz et al. 2008*). So far it is not known if the other VS-cells (VS1-VS4 and VS8-VS10) themselves synapse onto similar descending neurons. Descending neurons that integrate signals from VS3-4 and VS8-10 and synapse onto FNMN1 and 2 on the contralateral side have not been found. If these two motor neuron types would be electrically coupled to presynaptic descending neurons, this would be visible in Neurobiotin-filled cells. Indeed, dye-coupling was present in FNMN2, but the co-stained fibers are thinner than DNOVS1 or 2 and do not have a distinct synaptic site as seen in the descending neuron contacting FNMN3 (Figure 35). Thus, FNMN1 and FNMN2 could obtain signals from small diameter descending neurons that did not stain well in the present study due to their small size, or they could receive visual input via chemical synapses.

FNMN3 was the only motor neuron co-stained with a large descending neuron (Figure 36). It is dye-coupled to a descending neuron that is very likely to be DNOVS1 for several reasons: the similarity of the tuning (compare Figure 39 and Figure 41), the distinct morphology of the axonal ending, reminiscent of DNOVS1 as reported in earlier studies (compare Figure 13 and Figure 36) and anterograde coupling with an FNMN (Figure 41). Unambiguous evidence for a functional connection between DNOVS1 and FNMN3, however, could only be provided by simultaneous

recording and current injection as obtained for the VCN (*Haag et al. 2010*) and CN (*Wertz et al. 2012*). Dual recordings between FNMNs and LPTCs or DNOVS1 were not carried out in this study.

Although the tuning to panoramic rotations is strikingly similar in DNOVS1 and FNMN3 (Figure 39, Figure 41), an important difference between the descending neuron and the motor neurons is their sensitivity for small-field stimuli: While the receptive field of DNOVS1 was mapped using a small bright moving dot on a black LED arena in *Wertz et al.* (*2008*), none of the FNMNs could be triggered to fire action potentials upon stimulation with an equivalent small-field stimulus. This could be due to the response types of the two cell classes: while DNOVS1 responds exclusively with graded membrane potential changes, the five tested FNMNs all fire action potentials. Thus, whereas the strength of neuronal input must cross a certain threshold to trigger spikes in the motor neurons, there is no such threshold in DNOVS1. Weaker input therefore can lead to membrane potential changes in the descending neuron, while the depolarization is not strong enough to elicit spikes in FNMNs.

In the past it was proposed that all FNMNs are coupled to DNOVS1 (*Strausfeld and Seyan 1985*). By injecting Neurobiotin into single FNMNs and into DNOVS1, it was now possible to trace the pre- and postsynaptic partners of individual neurons if they share gap junctions. Although it was not possible to prove functional connectivity, it could be shown that DNOVS1 is dye-coupled to only one FNMN and not to all of them. The other FNMNs presumably receive visual input via chemical synapses from descending neurons.

4.2.5. Physiological assignment of cell classes

All five anatomically classified FNMN types responded to panoramic visual motion. This is surprising because until now it has been assumed that only a small number of neck motor neurons are visually sensitive (*Milde et al. 1987; Gilbert et al. 1995; Gronenberg et al. 1995*). At a behavioral level however it makes sense that all FNMNs are visually sensitive: they innervate different muscles, so they are all required to generate movements of the head along different axes. If only a subset was visually sensitive, the fly's head would be less moveable.

The stimuli that were used in this study did not allow for a clear physiological classification of the cell types. Although a rough partition into cells that respond to clockwise rotations and cells that respond to counterclockwise rotations is observed, the response characteristics are not distinct enough to assign them to more than two physiological groups. FNMN classification is thus based on anatomical stainings only.

4.2.6. Multisensory integration

Neck motor neurons must be able to integrate multiple streams of sensory input to generate an appropriate response to environmental influences. Non-visual tactile input is able to trigger responses in FNMNs (Figure 35 B). Airstream (*Gronenberg et al. 1995*) and haltere movement (*Huston and Krapp 2009*) were demonstrated to elicit responses in FNMNs in previous accounts.

This underlines the broad receptivity for different sensory modalities at the level of prothoracic neck motor neurons. Visual signals might shape the responses of neck motor neurons to proprioceptive or other non-visual input just as much as non-visual input shapes the context specificity of visual signals. Sensory afferents from various organs as well as a central input (*Rosner et al. 2009; Haag et al. 2010*) are suggested to act together on the motor neurons' activity by modulating its spike threshold. The nature of this central command will be discussed later.

As depicted in Figure 36, most FNMN types (FNMN2, FNMN3, FNMN4 and FNMN5) are dye-coupled to haltere afferents. They are either directly coupled to the haltere nerve or receive indirect haltere input via interneurons on the contralateral side. This anatomical evidence of electrical synaptic connections between the halteres and FNMNs has been shown as early as in the 1980s, where cobalt was used to backfill the whole frontal nerve (*Strausfeld and Seyan 1985*). Now, using intracellular injection of Neurobiotin it was possible for the first time to trace the synaptic partners of single individual motor neurons of the frontal nerve.
It has been suggested previously that two types of FNMNs exist: a visual and a non-visual type. This assumption is based on the finding that some neck motor neurons responded to visual motion and others did not (*Milde et al. 1987; Gronenberg et al. 1995*). Later it was shown that 'non-visual' FNMNs do respond to visual motion by firing action potentials, but only when the halteres are oscillating at the same time, indicating nonlinear integration of multiple sensory modalities (*Huston and Krapp 2009*). *Huston and Krapp* (*2009*) also postulated that two types of neck motor neurons exist, that differ by their activation threshold. In their series of experiments on FNMNs, "Type I" neck motor neurons respond to visual motion alone, while "Type II" neurons respond to the same visual stimuli only when the halteres were beating concurrently. Their explanation for this observation is a gating effect generated by the halteres: the descending visual inputs that supply "Type II" motor neurons are thought to be too weak to generate action potentials on their own but can affect the probability that haltere-induced postsynaptic potentials in the motor neurons become suprathreshold.

In the present study however it could be shown that all five described FNMN cell types can be triggered to fire action potentials by visual input alone. Two different theories can be deduced from this observation: 1) all FNMNs can be triggered to spike with visual input alone, as long as the input is strong enough (i.e. panoramic rotations). It can be assumed that FNMN6-8 show the same behavior but were not recorded from because of their position, or 2) FNMN1-5 can be triggered to spike with visual input alone, while FNMN6-8 are either non-visual or need to be driven by multiple sensory systems or a stronger visual signal, like the large ADNMN. Their non-responsiveness might explain why FNMN6-8 were not recorded.

4.3. General discussion

4.3.1. Increasing variability along the neuronal pathway

The visual response strength of ADN and FN motor neurons varied strongly, compared to the stereotypic behavior of LPTCs. *Rosner and Warzecha* (*2011*) report that the variability of behaviorally observed optomotor responses in *Calliphora* must arise downstream of the lobula plate - at the level of the descending or motor neurons - because it cannot be explained by the extremely stereotyped responses of LPTCs, which are unaffected by the fly's motor activity. This was observed in the present account as well. It underlines the complexity underlying the sensory-motor pathway: While the nature of a signal at the level of the LPTCs in the optic lobe is purely visual, it is combined with inputs from various other external and internal sources on its downstream path to the neck motor neurons, in order to generate a response that is most appropriate for the animal's multisensory interaction with its environment. This circumstance also explains why it is especially difficult to measure stable results at the output stage of the nervous system: strong inter-individual as well as inter-trial fluctuations were observed in all types of neck motor neurons tested, which are probably due to the large amount of diverse sensory input that combines at this level.

All neck motor neurons that were tested in the present study (ADNMN1 and ADNMN2, FNMN1-5) were sensitive to visual motion. When using strong visual stimuli (maximum contrast panoramic rotations), all recorded cell classes responded to visual input alone. Thus, visual input is sufficient to elicit neuronal responses. In contrast to smaller moving gratings that have been used to characterize the motion sensitivity of FNMNs (*Milde et al. 1987; Huston and Krapp 2008; Huston and Krapp 2009*), binocular full-field rotations of the fly's visual surround were displayed here, which are thought to be most suitable to activate neck motor neurons because of their large receptive fields (*Huston and Krapp 2008; Wertz et al. 2012*). As mentioned in the previous section of the discussion, a model by *Huston and Krapp* (*2009*) suggests two types of neck motor neurons that can be driven by visual input alone or combined visual and haltere input respectively. The results of the present account indicate that all motor neurons can be driven by visual input alone: it is likely that not the sensory modality of the input but its pure strength at the level of dendritic summation in the motor neuron matters most for response generation.

4.3.2. The role of bursts

High frequency bursts were observed in both ADNMNs and FNMNs and quantified in a small number of FNMNs (Figure 35 B, Figure 42). What could be the behavioral relevance of these bursts? A sudden stimulus like touch or abrupt luminance change is likely to elicit an escape or startle response in a behaving fly that is characterized by simultaneous contraction of several muscles (*Holmqvist and Srinivasan 1991; Fotowat and Gabbiani 2007; Card and Dickinson 2008*). An example behavior which could involve simultaneous action of several neck muscles was observed in the fly *Neobellieria bullata* (Sarcophagidae) by *Gilbert and Bauer* (*1998*): When the fly

is stationary, its head is clutched to the thorax by a neuromuscular mechanism that is unknown but does not involve the FN. In this state, the animal corrects for imposed perturbations of its head position with large latencies and insufficient accuracy. When it is moving however, corrections are carried out immediately and with high precision. Interestingly, the authors further report that the correction of imposed perturbations could be triggered by unspecific tactile stimulation, so that touching the animal led to reflexive correction of head posture. The existence of an analogous mechanism in *Calliphora* is very likely because the taxonomic families Calliphoridae and Sarcophagidae belong to the same superfamily, Oestroidea (*Yeates and Wiegmann 2005*).

The vigorous responses to tactile stimulation of the head and abdomen (Figure 35 B) as well as the responses to sudden light flashes (Figure 42) could possibly trigger this head unlocking, moving the animal from a stationary position into an activated state, in which it is ready to react quickly. Locking of the head in a stationary state could be a way to save energy. When animals were filmed for haltere tracking (Figure 16), their whole body was observed to contract from time to time in response to the visual stimulus, even when the haltere was not beating simultaneously.
This can be interpreted as a flight or escape impulse that underlines the theory of a central command that uses information from the eyes to steer both the head and flight motor system and elicits bending of the abdomen, oscillation of the halteres and movement of the head in parallel.

4.3.3. A central command?

The activity of the characterized ADNMNs and FNMNs sometimes reflects a response behavior that is not directly caused by the visual stimuli and characterized by seemingly spontaneous bursts. When no visual stimulus was present, however, both units were usually silent. These bursts hence are very likely to derive from an overall excitation of the animal and reflect muscle contractions in its attempt to either escape or move in response to the visual surround or tactile stimulation of the head and body.

Animals that were only suspended on the back moved their head, abdomen, thorax and antennae when presented with rotating patterns (Figure 32). The attempt to move presumably correlates with motor neuron bursts in the recorded fixed flies. Although neck motor neurons do receive feedback from the halteres (*Huston and Krapp 2009; Haag et al. 2010*), in a large part of the present experiments this can be ruled out as a cause of bursts, since the halteres were not always oscillating when the motor neurons bursted in the haltere movies (Figure 33) and generally never oscillated in the electrophysiological recordings, when the abdomen was immobilized (Figure 32).

Haag et al. (*2010*) and *Rosner et al.* (*2009*) postulated a central command that initiates voluntary movement and overrides optomotor and flight stabilizing pathways. In their model, a central command consisting of one or several neurons, synapse onto both the prothoracic neck motor neurons and the halteres and push the low resting potential of the prothoracic neck motor neurons above threshold while at the same time activating the halteres. The present results also speak in favor of such a central command, since 1) spontaneous bursts were also observed when

the animal was receiving no sensory input, and 2) the bursts in the ADNMNs that were recorded together with haltere activity (Figure 33) had a delayed onset in the halteres compared to the motor neurons.

4.3.4. Comparison of FN and ADN

FNMNs and ADNMNs are similar in their preference for rotations over translations. Although they are tuned to different axes, they clearly respond more strongly to rotational optic flow than to translational optic flow. The behavioral relevance of this could be that the head itself cannot be translated along the x- or y-axis, only rotated, which results in a pitch or yaw movement. From a behavioral point of view it would not make sense for the neck muscles to react to thrust optic flow either because it signalizes a forward translation of the animal on a straight path, which does not need to be corrected.

Both FN and ADN house motor neurons that originate in the thoracic ganglion and are connected to the brain by descending neurons of the cervical connective. In contrast to the CN and VCN they do not receive direct synaptic input from VS- and HS-cells of the lobula plate (*Wertz et al. 2012; Haag et al. 2010*).

As a consequence, the path a neuronal signal must travel to reach the muscle is longer and comprises at least one more synapse. For very fast reactions this seems like a disadvantage and a shorter pathway might be a better fit.

Interestingly, the rotational axes of neck motor neurons originating in the brain and neck motor neurons originating in the prothoracic ganglion are very similar: both ADNMNs and VCNMNs are strongly sensitive for horizontal front-to-back rotations *(Haag et al. 2010; Huston and Krapp 2008*). Thus, there is a direct and an indirect pathway that responds to horizontal optic flow and pulls the head sideward in response. The CNMNs that have been physiologically characterized so far, CNMN6 and CNMN7, are tuned to downward rotations (*Wertz et al. 2012*). Their tuning is reminiscent of the tuning I measured in FNMN2. There are 8 CNMNs altogether, which innervate oblique horizontal muscles (CNMN2), a transverse horizontal muscle (CNMN3), an abductor muscle (CNMN4), ventral longitudinal muscles (CNMN6, CNMN7) and the sclerite retractor and rotator muscles (CNMN1, CNMN5, CNMN8). Like the 8 FNMNs they innervate a variety of different muscles that can rotate the head in many planes. Thus, continuing this idea, CN and FN could also represent two analogous ways, one direct and one indirect, to rotate the head around roll- and pitch-like axes. Like this, the neck motor system could have a fast and mainly visual control system operated by the CN and VCN motor neurons, and a slightly slower but more integrated sensory control system operated by ADN and FN motor neurons: the obvious advantage of a longer pathway is the possibility of multisensory integration in the prothoracic ganglion.

4.4. Outlook

Further investigation of prothoracic neck motor neurons will be a challenging task: they turn out to be highly complex structures. Since the characterization of their response characteristics and visual motion tuning did not clearly reveal neither the shape and size of their receptive fields nor the presynaptic partners that provide visual information, further experiments should focus on cell-cell-connectivity.

Experiments could involve intracellular double-recordings from FNMNs and VS-cells, as well as from FNMNs and the two large diameter descending neurons DNOVS1 and DNOVS2 (*Haag et al. 2007; Wertz et al. 2008*) to unambiguously show the pathways along which visual signals are transported from the lobula plate to the neck motor system. For the ADN, more double recordings between HS-cells and ADNMNs should be conducted to corroborate the observation of a physiological connection. A different possible approach are ablation experiments (see *Farrow et al. 2003 and 2006*): irreversibly shutting down different LPTCs one by one by laser ablation and simultaneously recording visual responses in neck motor neurons could reveal which connections are relevant for the visual computation pathway.

Knowledge about the signal translation from the lobula plate to the neck motor system is an important part of our understanding of the fly visual system. Without this part we can only speculate about the role of the different tuning of LPTCs: as long as we do not know which LPTCs provide visual input for which muscle, it is impossible to evaluate the accuracy of motion tuning for the fly's head turning behavior.

References

Beersma DGM, Stavenga DG, Kuiper JW (1977) Retinal lattice, visual field and binocularities in flies. Dependence of species and sex. J Comp Physiol 119: 207-220.

Bender JA, Dickinson MH (2006) A comparison of visual and haltere-mediated feedback in the control of body saccades in *Drosophila melanogaster*. J Exp Biol 209: 4597-4606.

Blondeau J (1981) Electrically evoked course control in the fly Drosophila melanogaster. J Exp Biol 92: 143-153

Bomphrey RJ, Walker SM, Taylor GK (2009) The typical flight performance of blowflies: measuring the normal performance envelope of *Calliphora vicina* using a novel corner-cube arena. PLoS ONE 4(11): e7852.

Borst A, Haag J (2007) Optic flow processing in the cockpit of the fly. In: Invertebrate Neurobiology. Eds: G North, RJ Greenspan. CSHL-Press, pp 101-122

Borst A, Haag J, Reiff D (2010) Fly motion vision. Annu Rev Neurosci 33:49-70.

Borst A, Weber F (2011) Neural action fields for optic flow based navigation: A simulation study of the fly lobula plate network. PLoS ONE 6: e16303.

Card G, Dickinson MH (2008) Visually guided motor planning in the escape response of *Drosophila*. Curr Biol 18: 1300-1307.

Chiappe ME, Seelig JD, Reiser MB, Jayaraman V (2010) Walking modulates speed sensitivity in *Drosophila* motion vision. Curr Biol 20: 1470–1475.

Coggshall JC, Boschek CB, Buchner SM (1973) Preliminary investigations on a pair of giant fibers in the central nervous system of dipteran flies. Z Naturforsch 28c: 783-784.

Cuntz H, Haag J, Förstner F, Segev 1, Borst A (2007) Robust coding of flow field parameters by axo-axonal gap junctions between fly visual interneurons. Proc Nat Acad Sci USA 104: 10229-10233.

Farrow K, Haag J, Borst A (2003) Input organization of multifunctional motion sensitive neurons in the blowfly. J Neurosci 23: 9805-9811.

Farrow K, Haag J, Borst A (2006) Nonlinear, binocular interactions underlying flow field selectivity in a motion-sensitive neuron. Nat Neurosci 9(10): 1312-1320.

Fotowat H, Gabbiani F (2007) Relationship between the phases of sensory and motor activity during a looming-evoked multistage escape behavior. J Neurosci 27(37): 10047-10059.

Franceschini N (1975) Sampling of the visual environment by the compound eye of the fly: Fundamentals and applications. In: Snyder AW, Menzel R (eds) Photoreceptor optics. Springer, Berlin, Heidelberg. pp 98-125.

Franz MO, Krapp HG (2000) Wide-field, motion-sensitive neurons and matched filters for optic flow fields. Biol Cybern 83: 185-197.

Frye MA, Dickinson MH (2001) Fly flight: A model for the neural control of complex behavior. Neuron 32: 385-388.

Geiger G, Nässel DR (1981) Visually guided orientation behavior of flies after selective laser beam ablation of interneurones. Nature 293: 398-399

Gilbert C, Bauer E (1998) Resistance reflex that maintains upright head posture in the flesh fly *Neobellieria bullata* (Sarcophagidae). J Exp Biol 201: 2735-2744

Gilbert C, Gronenberg W, Strausfeld NJ (1995). Oculomotor control in calliphorid flies: Head movements during activation and inhibition of neck motor neurons corroborate neuroanatomical predictions. J Comp Neurol 361: 285-297.

Gronenberg W, Strausfeld NJ (1990) Descending neurons supplying the neck and flight motor of diptera: Physiological and anatomical characteristics. J Comp Neurol 302:973-991.

Gronenberg W, Strausfeld NJ (1991) Descending pathways connecting the male-specific visual system of flies to the neck and flight motor. J Comp Physiol A 169: 413-426.

Gronenberg W, Milde JJ, Strausfeld NJ (1995) Oculomotor control in calliphorid flies: Organization of descending neurons to neck motor neurons responding to visual stimuli. J Comp Neurol 361: 267-284.

Haag J, Borst A (2004) Neural mechanism underlying complex receptive field properties of motion-sensitive interneurons. Nat Neurosci 7: 628-634.

Haag J, Wertz A, Borst A (2007) Integration of lobula plate output signals by DNOVS1, an identified premotor descending neuron. J Neurosci 27: 1992-2000.

Haag J, Wertz A, Borst A (2010). Central gating of fly optomotor response. Proc Natl Acad Sci 107: 20104-20109.

Haikala V, Joesch M, Borst A, Mauss AS (2013) Optogenetic control of fly optomotor responses. J Neurosci 33(34):13927-34.

Hama H, Kurokawa H, Kawano H, Ando R, Shimogori T, Noda H, Fukami K, Sakaue-Sawano A, Miyawaki A (2011) Sca*l*e: a chemical approach for fluorescence imaging and reconstruction of transparent mouse brain. Nat Neurosci 14: 1481-1488.

Hardie RC (1984) Functional organization of the fly retina. In: Progress in sensory physiology 5 (eds: Autrum H, Ottoson D, Perl ER, Schmidt RF, Shimazu H, Willis WD). Springer Berlin Heidelperg, pp1-79.

Hausen K (1982a) Motion sensitive interneurons in the optomotor system of the fly. I. The horizontal cells: Structure and signals. Biol Cybern 45: 143-156.

Hausen K (1982b) Motion sensitive interneurons in the optomotor system of the fly. II. The horizontal cells: Receptive field organization and response characteristics. Biol Cybern 46: 67-79.

Hausen K (1984) The lobula complex of the fly: Structure, function and significance in visual behavior. In: Ali MA (ed) Photoreception and vision in invertebrates. Plenum Press, New York. pp 523-559

Hausen K and Wehrhahn C (1983) Microsurgical lesion of horizontal cells changes optomotor yaw responses in the blowfly *Calliphora erythrocephala* Proc R Soc Lond B 219: 211-216.

Heisenberg W et al. (1978) optomotor-blind^{H83}- a *Drosophila* mutant of the lobula plate giant neurons. J Comp Physiol A 124: 287-296.

Hengstenberg R (1982) Common visual response properties of giant vertical cells in the lobula plate of the blowfly *Calliphora*. J Comp Physiol A 149: 179-193.

Hengstenberg R (1984) Roll-stabilization during flight of the blowfly's head and body by mechanical and visual cues. In: Varju D (*ed)* Localization and orientation in biology and engineering. Springer, Berlin, Heidelberg. pp 121-134.

Hengstenberg R, Sandeman DC, Hengstenberg B (1986) Compensatory head roll in the blowfly *Calliphora* during flight. Proc R Soc Lond B 227: 455-482.

Hengstenberg R (1991) Gaze control in the blowfly *Calliphora*: a multisensory, two-stage integration process. Sem Neurosci 3: 19-29.

Hengstenberg R (1993) Multisensory control in insect oculomotor systems. In: Miles FA, Wallman J (eds) Visual motion and its role in the stabilization of gaze. Elsevier, Amsterdam. pp285-298

Holmqvist MH, Srinivasan MV (1991) A visually evoked escape response of the housefly. J Comp Physiol A 169: 451-459.

Horstmann W, Egelhaaf M, Warzecha AK (2000) Synaptic interactions increase optic flow specificity. Eur J Neurosci 12(6):2157-65.

Huston SJ, Krapp HG (2008) Visuomotor transformation in the fly gaze stabilization system. PLoS Biol 6: 1468-1478.

Huston SJ, Krapp HG (2009): Nonlinear integration of visual and haltere inputs in fly neck motor neurons. J Neurosci 29: 13097-13105.

Jung SN, Borst A, Haag J (2011) Flight activity alters velocity tuning of fly motion-sensitive neurons. J Neurosci 31: 9231-9237.

Kauer I, Borst A, Haag J (2015) Complementary motion tuning in frontal nerve motor neurons of the blowfly. J Comp Physiol A 201(4):411-26.

Kern R, Egelhaaf M (2000a) Optomotor course control in flies with largely asymmetric visual input. J Comp Physiol A. 186:45-55.

Kern R, Lutterklas M, Egelhaaf M (2000b) Neuronal representation of optic flow experienced by unilaterally blinded flies on their mean walking trajectories. J Comp Physiol A 186 : 467-479.

Kern R, van Hateren JH, Egelhaaf M (2006) Representation of behaviourally relevant information by blowfly motion-sensitive visual interneurons requires precise compensatory head movements. J Exp Biol 209: 1251-1260.

Kirschfeld K (1967) Die Projektion der optischen Umwelt auf das Raster der Rhabdomere im Komplexauge von *Musca*. Exp Brain Res 3: 248-270.

Krapp HG (2009) Ocelli. Curr Biol 19: R435-R437.

Krapp HG, Hengstenberg B, Hengstenberg R (1998) Dendritic structure and receptive-field organization of optic-flow processing interneurons in the fly. J Neurophysiol 79: 1902-1917

Krapp HG, Hengstenberg R (1996) Estimation of self-motion by optic-flow processing in single visual interneurons. Nature 384: 463-466.

Krapp HG, Hengstenberg R, Egelhaaf M (2001) Binocular contributions to optic flow processing in the fly visual system. J Neurophysiol 85:724-734.

Land MF (1999) Motion and vision: why animals move their eyes. J Comp Physiol A 185: 341-352.

Land MF, Eckert H (1985) Maps of the acute zones of fly eyes. J Comp Physiol A Neuroethol Sens Neural Behav Physiol 156:525–538.

Maimon G, Straw AD, Dickinson MH (2010) Active flight increases the gain of visual motion processing in Drosophila. Nat Neurosci 13: 393-399.

Maisak MS, Haag J, Ammer G, Serbe E, Meier M, Leonhardt A, Schilling T, Bahl A, Rubin GM, Nern A, Dickson BJ, Reiff DF, Hopp E, Borst A (2013) A directional tuning map of *Drosophila* elementary motion detectors. Nature 500: 212-218.

Milde JJ, Gronenberg W, Strausfeld NJ (1992) The head-neck system of the blowfly *Calliphora.* II: Functional organization and comparison with the sphinx moth *Manduca sexta*. In Berthoz A, Graf W, Vidal PP (eds): The head-neck sensory motor system. New York Oxford University Press, pp. 65-70.

Milde JJ, Strausfeld NJ (1986) Visuo-motor pathways in arthropods. Giant motion-sensitive neurons connect compound eyes directly to neck muscles in blowflies (*Calliphora erythrocephala*). Naturwissenschaften 73: 151-154.

Milde JJ, Seyan HS, Strausfeld NJ (1987) The neck motor system of the fly *Calliphora erythrocephala*. II. Sensory organization. J Comp Physiol A 160: 225-238.

Nalbach G (1993) The halteres of the blowfly *Calliphora* I. Kinematics and dynamics. J Comp Physiol A 173: 293-300.

Petrowitz R, Dahmen H, Egelhaaf M, Krapp HG (2000) Arrangement of optical axes and spatial resolution in the compound eye of the female blowfly Calliphora. J Comp Physiol A 168:737–746.

Preuss T, Hengstenberg R (1992) Structure and kinematics of the prosternal organs and their influence on head position in the blowfly *Calliphora erythrocephala* Meig. J Comp Physiol A 171: 483-493.

Pringle JWS (1948) The gyroscopic mechanism of the halteres of Diptera. Philos Trans R Soc Lond B 233: 347-385.

Reiser MB, Dickinson MH (2008) A modular display system for insect behavioral neuroscience. J Neurosci Methods 167:127–139.

Rister J, Pauls D, Schnell B, Ting CY, Lee CH, Sinakevitch I, Morante J, Strausfeld NJ, Ito K, Meisenberg M (2007) Dissection of the peripheral motion channel in the visual system of *Drosophila melanogaster*. Neuron 56: 155-170.

Rosner R, Egelhaaf M, Grewe J, Warzecha AK (2009) Variability of blowfly head optomotor responses. J Exp Biol 212: 1170-1184.

Rosner R, Warzecha AK (2011) Relating neuronal to behavioral performance: Variability of optomotor responses in the blowfly. PLoS ONE 6(10): e26886.

Sandeman DC, Markl H (1980) Head movements in flies (*Calliphora*) produced by deflexion of the halteres. J Exp Biol 85: 43-60

Schuppe H, Hengstenberg R (1993) Optical properties of the ocelli of *Calliphora erythrocephala* and their role in the dorsal light response. J Comp Physiol A 173: 143-149.

Srinivasan MV, Zhang S (2004) Visual motor computations in insects. Annu Rev Neurosci 27: 679-696.

Strausfeld NJ, Bassemir UK (1985a). Lobula plate and ocellar interneurons converge onto a cluster of descending neurons leading to neck and leg motor neuropil in *Calliphora erythorcephala*. Cell Tissue Res 240: 617-640.

Strausfeld NJ, Bassemir UK (1985b) The organization of giant horizontal-motion-sensitive neurons and their synaptic relationships in the lateral deutocerebrum of *Calliphora erythrocephala* and *Musca domestica.* Cell Tissue Res 242: 531-550.

Strausfeld NJ, Obermayer M (1976). Resolution of intraneuronal and transynaptic migration of cobalt in the insect visual and central nervous systems. J Comp Phys A 110: 1-12.

Strausfeld NJ, Seyan HS (1985) Convergence of visual, haltere, and prosternal inputs at neck motor neurons of *Calliphora erythrocephala*. Cell Tissue Res 240: 601-615.

Strausfeld NJ, Seyan HS, Milde JJ (1987). The neck motor system of the fly *Calliphora erythrocephala*. I. Muscles and motor neurons. J Comp Physiol A 160: 205-224.

Strausfeld NJ, Kong A, Milde JJ, Gilbert C, Ramaiah L (1995) Oculomotor control in calliphorid flies: GABAergic organization in heterolateral inhibitory pathways. J Comp Neurol 361:298-320.

Strausfeld NJ, Gronenberg W (1990) Descending neurons supplying the neck and flight motor of diptera: Organization and neuroanatomical relationships with visual pathways. J Comp Neurol 302: 954-972.

Taylor GK, Krapp HG (2007) Sensory systems and flight stability: what do insects measure and why? In: J. Casas & S.J. Simpson (eds.) Insect Mechanics and Control. Adv in Insect Physiol 34: 231-316. Academic Press, London.

Van Hateren JH, Schilstra C (1999) Blowfly flight and optic flow. II. Head movements during flight. J Exp Biol 202: 1491-1500.

Wertz A, Borst A, Haag J (2008) Nonlinear integration of binocular optic flow by DNOVS2, a descending neuron of the fly. J Neurosci 28(12): 3131-3140.

Wertz A, Gaub B, Plett J, Haag J, Borst A (2009a) Robust coding of ego-motion in descending neurons of the fly. J Neurosci 29:14993-15000.

Wertz A, Haag J, Borst A (2009b). Local and global motion preferences in descending neurons of the fly. J Comp Physiol A 195:1107-1120.

Wertz A, Haag J, Borst A (2012) Integration of binocular optic flow in cervical neck motor neurons of the fly. J Comp Physiol A 198:655-668.

Yeates DK, Wiegmann BM (2005) Phylogeny and evolution of Diptera: recent insights and new perspectives. The Evolutionary Biology of Flies. Columbia University Press. pp. 14–44

Acknowledgements

I am grateful to everybody who was involved in the creation of this piece of work. First and foremost I thank Alexander Borst for guidance and supervision and for making this thesis possible. I am deeply thankful to Jürgen Haag for his support in almost any issue and for being a reliable supervisor. Numerous people lined my way at the institute: thank you all for your friendship and support, for fun times and a good atmosphere to work in. Last, I thank my family and friends for their unbroken belief in me.

Publications

Kauer I, Borst A, Haag J (2015) Complementary motion tuning in frontal nerve motor neurons of the blowfly. *J Comp Physiol A* 201(4):411-26. doi: 10.1007/s00359-015-0980-0.

Minoli S (co), Kauer I (co), Colson V, Party V, Renou M, et al. (2012) Brief Exposure to Sensory Cues Elicits Stimulus-Nonspecific General Sensitization in an Insect. *PLoS ONE* 7(3): e34141. doi:10.1371/journal.pone.0034141

Versicherung

Eidesstattliche Erklärung

Ich versichere hiermit an Eides statt, dass die vorgelegte Dissertation von mir selbständig und ohne unerlaubte Hilfe angefertigt ist.

Erklärung

Hiermit erkläre ich, dass die Dissertation nicht ganz oder in wesentlichen Teilen einer anderen Prüfungskommission vorgelegt worden ist und dass ich mich anderweitig einer Doktorprüfung ohne Erfolg nicht unterzogen habe.

Isabella Kauer

München, den 21.12.2016